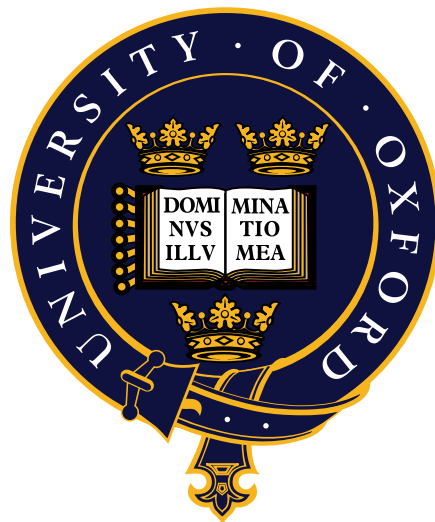


Robust Quantum Phenomena
for
Quantum Information Processing



Tom Close
Oriental College

Thesis submitted for the degree of
Doctor of Philosophy
at the
University of Oxford
Hilary Term 2013

Robust Quantum Phenomena for Quantum Information Processing

Tom Close
Oriel College, University of Oxford
Hilary Term 2013

Abstract of thesis submitted for the degree of Doctor of Philosophy

This thesis is concerned with finding technologically useful quantum phenomena that are robust against real world imperfections. We examine three different areas covering techniques for spin measurement, photon preparation and error correction.

The first research chapter presents a robust spin-measurement procedure, using an amplification approach: the state of the spin is propagated over a two-dimensional array to a point where it can be measured using standard macroscopic state measurement techniques. Even in the presence of decoherence, our two-dimensional scheme allows a linear growth in the total spin polarisation - an important increase over the \sqrt{t} obtainable in one-dimension. The work is an example of how simple propagation rules can lead to predictable macroscopic behaviour and the techniques should be applicable in other state propagation schemes.

The next chapter is concerned with strategies for obtaining a robust and reliable single photon source. Using a microscopic model of electron-phonon interactions and a quantum master equation, we examine phonon-induced decoherence and assess its impact on the rate of production, and indistinguishability, of single photons emitted from an optically driven quantum dot system. We find that, above a certain threshold of desired indistinguishability, it is possible to mitigate the deleterious effects of phonons by exploiting a three-level Raman process for photon production. We introduce a master equation technique for quantum jump situations that should have wide application in other situations.

The final chapter focusses on toric error correcting codes. Toric codes form part of the class of surface codes that have attracted a lot of attention due to their ability to tolerate a high level of errors, using only local operations. We investigate the power of small scale toric codes and determine the minimum size of code necessary for a first experimental demonstration of toric coding power.

Acknowledgements

I would first and foremost like to thank my supervisors, Simon Benjamin and Brendon Lovett. I could not have asked for better supervision or support over the course of my DPhil. I am also incredibly fortunate to have had the input of Erik Gauger, who has in many ways acted as a third supervisor. I thank him for his innumerable valuable contributions. I would also like to thank Kieran Higgins and George Knee both for the part they play in making the office a place I will miss, and also for their assistance with proof-reading chapters of this thesis. For the latter I would also like to thank Victoria Hore.

For financial support, I would like to thank the EPSRC and Oriel College. Furthermore, I would like to thank the CQT at the National University of Singapore for their hospitality.

I would finally like to thank my family and many long-suffering friends - especially Graeme Spence, Peter Inglesby and Richard Wood - who have supported me through the mostly-enjoyable-yet-occasionally-harrowing experience that is undertaking a DPhil.

Contents

1	Introduction	11
2	Quantum Information Processing	15
2.1	The Different Fields of QIP	15
2.1.1	Quantum Computing	15
2.1.2	Quantum Communication	17
2.1.3	Quantum Simulation	19
2.2	Models of Quantum Computing	21
2.2.1	Circuit Model	21
2.2.2	Adiabatic Quantum Computing	21
2.2.3	Measurement Based Quantum Computing	22
2.2.4	Topological Quantum Computing	23
2.3	Entanglement and Distributed Architectures	24
2.3.1	Remote Entanglement Generation	24
2.4	Candidate Quantum Systems	25
2.4.1	Nuclear Magnetic Resonance	25
2.4.2	Silicon based systems	27
2.4.3	Ion Traps	27
2.4.4	Quantum Dots	28
2.4.5	Photonic Systems	29
2.4.6	NV ⁻ Centres	30
2.4.7	Superconducting Devices	30
3	Quantum Dynamics	33
3.1	Closed Quantum Systems	33
3.1.1	State	33
3.1.2	Dynamics	35
3.1.3	Measurements	38
3.2	Open Quantum Systems	39
3.2.1	State	39
3.2.2	Measurement	41
3.2.3	Dynamics	42
3.2.4	Quantum Jump Master Equation	44
3.2.5	Decoherence Master Equation	47

4	Light as a Quantum Field	53
4.1	Quantum Treatment of Light	53
4.1.1	Quantising Light: A toy model	54
4.1.2	Field in Free Space	58
4.1.3	Hong-Ou-Mandel Effect	59
4.2	Light-Matter interactions	62
4.2.1	Atom in a Cavity - Semiclassical Approach	62
4.2.2	Atom in a Cavity: Quantum case	65
4.2.3	Raman procedure	66
4.3	Phonon-matter interactions	68
5	Rapid and Robust Spin Amplification	73
5.1	Review of 1D Model	75
5.2	Extension to 2D Model	77
5.3	Building a Subspace Basis	78
5.4	Rate of Spin Propagation	82
5.5	Extension to 3D	84
5.6	Robustness against Decoherence	84
5.7	Robustness against Imperfect Initialisation	87
5.8	Conclusion and Further Work	88
6	A Reliable, Efficient Source for Indistinguishable Photons	91
6.1	Introduction	91
6.2	Our model	96
6.3	Introducing the Semi-Quantum Master Equation Method	101
6.4	Applying the Semi-Quantum Master Equation Method	105
6.5	Results	110
6.6	Conclusion and Further Work	115
7	The Power of Small Toric Codes	117
7.1	Introduction to the Toric Code	117
7.2	Shor's Code Revisited	118
7.3	Definition of Toric Codespace	121
7.4	Code Variants	123
7.4.1	Classical Toric Code	124
7.4.2	Full Quantum Toric Code	124
7.4.3	Reduced Quantum Toric Code	125
7.5	The Structure of the Code	125
7.6	Error Model	131
7.7	A Precomputed Decoder	132
7.8	Simulation Results	134
7.8.1	Classical Toric Code	134
7.8.2	Reduced Quantum Code	135
7.8.3	Full Quantum Code	136

7.9 An Experimental Suggestion	137
7.10 Conclusion and Further Work	139
Bibliography	141

List of publications

This thesis is based on the following publications:

1. **Towards the experimental realisation of a small toric code.**

T. A. Close, S. C. Benjamin. *In preparation.*

2. **Overcoming phonon-induced dephasing for indistinguishable photon sources**

T. A. Close, E. M. Gauger, B. W. Lovett. *New Journal of Physics* **14** 113004 (2012).

3. **Rapid and robust spin amplification**

T. A. Close, F. A. Fadugba, J. Fitzsimons, and S. C. Benjamin. *Physical Review Letters* **106** 167204 (2011).

Chapter 1

Introduction

The theory of quantum mechanics is arguably the biggest scientific breakthrough of the 20th Century. The seemingly simple postulates that model behaviour of atomic-scale systems give rise to deep-reaching and counter-intuitive consequences. The philosophical implications of quantum mechanics in terms of the apparent lack of determinism in the universe we inhabit, the various interpretations of the quantum superposition and wavefunction collapse, and the apparent paradoxes afforded by phenomenon of quantum entanglement have occupied, and continue to occupy, physicists and philosophers alike.

It is remarkable that a theory provoking such controversy has been such a success experimentally and technologically. When the philosophical implications are put aside and the laws accepted, we are left with an incredibly powerful tool for modelling and reasoning about the behaviour of atomic-scale systems. Many of the key technological advances responsible for shaping our world originated in insights afforded by quantum mechanics: the transistor depends on the quantum mechanical treatment of solid state physics that explains the PN junction; the laser depends both on solid state physics and the quantum mechanical description of light. Without the theory of quantum mechanics, the world we see around us would be unrecognisable.

Quantum Information Processing has the potential to introduce a new wave of technological advances. The theory of the field is well developed and provides powerful new applications of quantum mechanics. The challenge of realising these applications is now largely the challenge of building robust devices that operate on the nanoscale, with an ability to protect information stored in the quantum wavefunction. In this thesis we examine robust techniques for spin measurement, photon preparation and error correction.

We start with a general introduction to Quantum Information Processing in Chapter 2, surveying different areas of research and detailing important recent developments. The next two chapters introduce the theoretical framework and techniques used later in the thesis. Chapter 3 covers relevant parts of the theory of Open Quantum Systems and Chapter 4 contains topics we will use when modelling interactions between matter and light.

In Chapter 5 we present a robust spin-measurement procedure, using an amplification approach: the state of the spin is propagated over a two-dimensional array to a point where it can be measured using standard macroscopic state measurement techniques. The work is an example of how simple propagation rules can lead to predictable macroscopic behaviour and the techniques should be applicable in other state propagation schemes.

Chapter 6 is concerned with the creation of a reliable single photon source in the face of phonon decoherence. We introduce a master equation technique for quantum jump situations that should have wide application in other situations.

Finally, in Chapter 7 we look at toric error correcting codes. The chapter is self contained, starting with an overview and review of the basic toric code and current decoding approaches. We then go on to investigate the power of small scale toric codes and determine the minimum size of code necessary for a first experimental demonstration of toric coding power.

As the research chapters address a rather broad range of different questions in different physical systems, they will each have their own conclusion section in which we summarise key results of the study and discuss interesting remaining questions and avenues for further work.

Chapter 2

Quantum Information Processing

2.1 The Different Fields of QIP

Quantum Information Processing (QIP) is the study of how quantum mechanical systems can be used to perform information processing tasks. In this section we will look at three key fields of QIP: Quantum Computing, Quantum Communication, and Quantum Simulation.

2.1.1 Quantum Computing

The original suggestion that quantum mechanics could be used to improve computing capabilities can be traced back to Feynman [1] in 1981. Feynman made the observation that the exponentially growing number of paths in quantum processes, which make their simulation hard classically, could potentially be exploited for increased computational power. In 1985 Deutsch built upon this work to define the concept, and postulate the existence, of a *universal quantum computer* [2] - a quantum generalisation of the universal Turing machine.

The first quantum algorithm was proposed by Deutsch and Josza [3] in 1992 and was soon followed by several others, including Grover's search algorithm [4, 5].

These early algorithms demonstrated that, in some cases, quantum computers could be used to obtain increased computational power. The most significant contribution to the field of quantum algorithms was made by Shor in 1997 [6]. Shor showed how a quantum computer could be used to factorise a number in polynomial time - a feat thought to be impossible with classical resources. The result attracted widespread attention, not least due to the implications efficient factorisation would have for the RSA algorithm [7], which is widely used to secure communication.

Despite the early interest generated by quantum algorithms, prominent critics, such as Landauer, questioned whether quantum computation could ever be made robust enough to run algorithms at scale [8]. It is important when running a quantum algorithm that the quantum superposition is preserved throughout the calculation [9]. Interactions with external systems can lead to a deterioration in the superposition - a phenomenon known as *decoherence*. The concern was that these effects would make it impossible to practically realise quantum computing power.

An important step towards answering these concerns was made by Shor in 1995, who proposed encoding a single logical qubit using nine physical qubits to allow correction of common errors [10]. Further suggestions for error correcting codes followed from Steane and Laflamme [11, 12, 13] using seven and five qubits respectively. In 1997 Aharonov and Ben-Or proved the *quantum threshold theorem* [14] - that fault tolerant quantum computing is possible if the error per gate can be reduced below a certain (code dependent) threshold. Work by Knill in 2005 [15] demonstrated codes for which this threshold is as high as 3%.

A fully scalable quantum computer has yet to be created but, with robust computing theoretically possible, the challenge is now considered to be one of engineering quantum systems. Since its inception, the field of quantum computing has developed rapidly, with the addition of several new computing paradigms and many competing experimental approaches. We will return to cover these points later in the chapter.

2.1.2 Quantum Communication

The field of cryptography has a long and colourful history [16] in enabling secret communication between two or more parties. The only classical encryption method to be proven to be secure is the ‘one-time pad’, which uses a shared sequence of random numbers to encrypt and decrypt the messages sent between the two parties. All other classical cryptographic algorithms are only computationally secure - the probability of cracking them in a reasonable amount of time using current computational means is very small. The security of such systems therefore depends as much on the computational means as on the algorithm itself; in the face of full-scale quantum computing power, algorithms - such as the RSA algorithm - which were hitherto considered secure can no longer be relied upon.

The main challenge in using a one-time pad as a cryptographic system lies in establishing the shared sequence of random numbers. This sequence, often referred to as a key, is consumed throughout communication and must therefore be continually replenished. *Quantum Key Distribution (QKD)* protocols provide a solution to the key distribution problem. At the heart of these proposals lies one of the core principles of quantum mechanics: the observation of a quantum mechanical system by an observer alters its state. QKD schemes use this principle to establish a shared key in such a way that it is impossible, even in principle, to eavesdrop without disturbing the transmission in a way that can be detected. If we accept that quantum mechanics is valid, QKD is secure.

The first QKD scheme was proposed by Bennett and Brassard in 1984 [17]. The scheme uses the polarisation states of a stream of photons to establish a shared key between the two parties, who we call Alice and Bob. Alice prepares each photon in random state chosen from one of four polarisation states. Bob randomly chooses one of two possible directions to measure for each photon. On average, half of the

time Bob will choose the direction that corresponds to Alice's preparation. In this case he will be able to determine the exact state that Alice prepared. The other half of the time Bob chooses the 'wrong' direction and his measurement outcome will be random. After a measurement has been performed Bob reveals his measurement choice to Alice and she tells him whether he made the 'right' choice. If he did they can use the outcome as a bit of their shared key.

The presence of an eavesdropper will lead to errors in the shared key and can be detected with arbitrarily high probability by comparing (and then discarding) some of the key. This argument relies on the no cloning theorem, which states that the state of a quantum system cannot be copied. If quantum systems could be copied the eavesdropper could simply take copies of the photons and wait until Bob revealed his choices to measure them. The no cloning theorem is fundamental in many areas of QIP and was proven by Wootters and Zurek in 1982 [18].

A more general scheme was proposed by Ekert in 1991 [19]. The scheme is phrased in terms of *entanglement* - a quantum phenomenon involving a superposition of multiple particles. Instead of a stream of photons, pairs of entangled qubits are used as the key resource. Similar to Bennett and Brassard's scheme, measurements are made in a random basis, with basis choices later shared to establish the key. Bell's theorem [20] can be used to test for eavesdropping. The scheme has the benefit that it reduces the communication problem to that of distributing entangled pairs of qubits, which can be done from a central source.

Quantum communication is by far the most experimentally advanced of the QIP fields that we are concerned with [21], in the main part due to the comparatively few requirements it makes of the quantum systems involved. In 2004 a bank transfer in Vienna was secured using QKD [22] and there are at least two commercially available quantum communication systems available on the market [23, 24]. In addition there are a growing number of quantum key distribution networks being created around

the world [25, 26].

In practice there are a few ways in which the system can be vulnerable. One example is the *number splitting attack* [27]: if photons are occasionally emitted in pairs an attacker can split off one of these photons and save it until a time when the basis is revealed, thus being able to reconstruct some portion of the key. This can be prevented with a slight modification to the procedure [28] or with the development of better single photon sources. A more recent example is the *blinding attack* which exploits the specific photon detector design in two commercial QKD systems by constantly bombarding them with photons [29]. It is worth pointing out that both these examples target the deviation of certain real-world systems from the quantum ideal, rather than any inherent weakness in the protocol.

The field continues to progress the ability to establish keys over long distances. QKD was demonstrated between qubits separated by 100km in 2007 and 2008 [30, 31], over a noisy channel in 2012 [32] and more recently between an airplane travelling at 300km/hr and the ground [33]. It looks likely that satellite based quantum communication will be a reality in the near future.

2.1.3 Quantum Simulation

Feynman's initial contributions to quantum computing [1] were phrased in the terms of simulation: the existence of superpositions and entanglement makes it exponentially difficult to exactly simulate quantum systems using classical computers, so Feynman proposed using quantum systems instead. A big advance towards this goal was made by Lloyd, who in 1996 demonstrated the existence of universal quantum simulators for systems with local interactions [34].

The short-term prospects for creating a useful quantum simulator are better than a quantum computer for two reasons [35]. First, quantum simulators appear

to be more tolerant of errors due to decoherence effects: a small amount of noise can render a quantum computation useless whereas a quantum simulator can still give useful insights into the modelled system. Second, the size of system needed to obtain useful results is typically far smaller than for a quantum computer; to run Shor's algorithm for meaningfully large numbers would require thousands of qubits, whereas quantum systems containing a handful of qubits are already difficult to simulate classically.

An important area of application of quantum simulators is to quantum chemistry [36]. Quantum chemistry and band structure calculations currently account for up to 30% of computation time at supercomputing centres [37, 38]. Monte-Carlo and coupled-cluster methods, density functional theory, density renormalisation group theory and others have all been used to successfully solve a wide range of problems, however there are still whole classes of problems that cannot be tackled. Building on the phase estimation approach of Lloyd [39, 40], efficient quantum simulation algorithms for estimating the eigenvalues of many-body systems are known [41, 42].

Quantum simulators have been used to simulate quantum walks [43] with some experimental success [44]. Quantum walk type processes occur in many circumstances including exciton transfer in light harvesting biological systems. Recent experiments have shown the existence of long-lived coherences can exist in biological systems [45, 46, 47] making them a possible simulation target. There has also been some success in simulating in the field of condensed matter such as the simulation of the wavefunction of a frustrated Heisenberg spin system in 2011 [48].

2.2 Models of Quantum Computing

2.2.1 Circuit Model

The circuit model treats quantum computing as a sequence of operations, or gates, applied to qubits - and can therefore be visualised as qubits travelling through a quantum circuit. It was the language in which most of the early work on quantum computing was presented and is still, in many ways, the most natural way to think about and describe most quantum algorithms.

It is possible to construct any quantum operation from a sequence of two-qubit operations: two-qubit gates are universal for quantum computing [49] and are the only gate components we need to construct a circuit. In 2000 DiVincenzo produced five requirements [50] that any candidate quantum computing system must meet. These can be thought of as defining other features of the circuit: in addition to a universal set of gates, we must be able to initialise our system into some given state, and perform individual qubit measurements. It must also be possible to scale our circuits up, and qubit decoherence lifetimes must be longer than the time it takes for the qubit to travel through the circuit.

2.2.2 Adiabatic Quantum Computing

Adiabatic quantum computing involves manipulating qubits into some state that encodes the solution to the problem you wish to solve. Typically it involves using a time dependent Hamiltonian that interpolates between an initial Hamiltonian, whose ground state is easy to prepare, and a final Hamiltonian, whose ground state represents the solution.

The first adiabatic quantum computing algorithm was given by Farhi *et al.* in 2000 [51] to solve instances of the satisfiability problem. The algorithm's speed is

limited by the requirement that the Hamiltonian must change slowly enough that the system remains in its ground state throughout, a process known as adiabatic evolution. The timescale necessary to maintain adiabatic evolution depends on the gap between the ground state and the next highest state - the smaller the gap, the slower the motion must be. In 2007 it was shown that the adiabatic computing model is equivalent in power and resources to the circuit model [52]. A universal set of Hamiltonians requiring only local terms was found in 2008 [53].

2.2.3 Measurement Based Quantum Computing

Measurement based quantum computation (MBQC) [54], or one-way quantum computation, is a computing paradigm proposed by Raussendorf and Briegel in 2001 [55]. The computation is performed by making irreversible measurements on a highly entangled quantum state - an approach with no classical analogues that offers new perspective on the role of entanglement. The approach hinges on the fact that the quantum teleportation-type protocols can be used to construct a universal set of operations for quantum computing [56]. By measuring a specially entangled state in a particular basis and possibly performing a single qubit rotation depending on the outcome we can implement arbitrary operations. In real algorithms it is not necessary to physically perform the rotations - we can instead adapt the measurement basis for future operations. The fact that information from each measurement outcome needs to be fed back into the process introduces a time ordering on the process.

The beauty of this approach is that it separates the computation into two separate stages: the creation of a suitable entangled state and then the implementation of the algorithm by making local measurements on this state. This is both practically and conceptually useful. Practically it separates the creation of entanglement, and

thus the need for multiple qubit interaction, from the running of the algorithm and allows computations to be implemented using spatially separated entangled qubits by removing the requirement to implement two qubit gates. Conceptually it allows us to view entanglement as a resource to be consumed throughout the computation, to ask questions about how to quantify entanglement and to relate this to the computations we can perform.

The procedure relies on a special class of initial entangled state. Building on the initial proposal, Raussendorf, Browne and Briegel detailed how the computation could be performed using a class of states known as *cluster states* [57]. The fundamental issue of which states could serve as universal resources for quantum computing was tackled by Van den Nest *et al.* in 2007 [58]. We will look at how such states can be created in Section 2.3.1.

2.2.4 Topological Quantum Computing

Topological quantum computing began as a new class of quantum error correcting codes, but the area has since developed to the stage where it can now be considered a quantum computing paradigm in its own right. The first codes were introduced by Kitaev [59, 60] arising from an attempt to give simple models of topological order using quantum mechanics. The codes used a large array of physical qubits to encode a pair of logical qubits making use of the two topologically distinct ways to draw a loop that wraps a torus once. Further examples in the class of topological codes soon followed [61, 62].

Focus then turned to how to implement logical operations on encoded qubits. In 2003 Wang, Harrington and Preskill made a suggestion for performing a CNOT gate by extending the code into a third dimension [63], which was followed in 2007 with an approach from Raussendorf and Harrington which used braiding operations

on the code lattices [64, 65]. Both approaches showed error tolerances an order of magnitude higher than standard concatenated codes when only local operations were allowed. Recently the efficient decoding of topological codes has been an active area of research [66, 67, 68, 69].

2.3 Entanglement and Distributed Architectures

The phenomenon of quantum entanglement has played a central role in the development of quantum theory. One of Einstein's objections to the theory of quantum mechanics was the apparent paradox that quantum entanglement effects appeared to require 'spooky', remote interactions [70]. Bell's work in 1964 [20] clarified much of the early confusion and showed that entanglement led to essentially *quantum* correlations that could not be reproduced in classical mechanics. Ekert's communication protocol [19] and the MBQC paradigm [55] show that entanglement can be viewed as a resource for both quantum communication and quantum computing. Entanglement purification schemes [71] serve to strengthen this view showing that small amounts of entanglement can be combined into a more concentrated, useable form.

The characterisation of entanglement as an essential quantum resource has opened up possibilities in the form of distributed quantum systems. By envisaging an entangled network of spatially separated computational nodes, we overcome many of the common barriers to scalability [72]. The problem of scaling the computation is reduced in part to that of entangling remote quantum systems.

2.3.1 Remote Entanglement Generation

Remote entanglement generation involves entangling two spatially separated quantum systems. One standard technique is that of *path erasure* - which, in informal

terms, involves detecting a photon from the two systems and ‘forgetting’ which system it came from, to leave them in an entangled state. Formally, the photon detection performs a projective measurement onto an entangled subspace.

The first path erasure method was proposed by Cabrillo *et al.* [73] in 1999 and involved the detection of a single photon. Photon loss is a problem for this system: if two photons are emitted but only one detected the system is left in a mixed state. More sophisticated path erasure schemes [74, 75, 76, 77] overcome this weakness by requiring that a photon be emitted and detected from both systems. The probability of successful entanglement in any run decreases but in return we can be sure that when both photons are detected the systems are genuinely in an entangled state.

Entanglement creation using such schemes was first demonstrated by Moehring *et al.* in 2007 [78] and was more recently used by Hanson *et al.* to entangle two NV⁻ centres [79]. There have also been theoretical proposals about how to go about using this type of operation to build the entangled network states as required by MBQC proposals [80].

2.4 Candidate Quantum Systems

Many systems exhibit quantum mechanical behaviour of a kind that has the potential to be used for QIP. There are a plethora of different approaches currently under investigation. Here we briefly survey the best known approaches, noting interesting recent advances.

2.4.1 Nuclear Magnetic Resonance

The first physical realisation of simple quantum computational procedures were performed using nuclear magnetic resonance (NMR) techniques. Thanks to the high existing level of expertise available in the area, initial progress in the late 1990s

was quick, following the seminal proposal by Gershenfield and Chuang [81]. By 1998 Chuang *et al.* had demonstrated a simple version of the Deutsch-Josza algorithm [82] and shortly after, in 2001, the same group managed to run Shor's algorithm to factorise the number fifteen [83].

The basic technique involved using electromagnetic pulses of precise frequencies to target particular transitions in order to perform a nuclear spin flip dependent on the position of a second spin. In this manner a two qubit CNOT gate was implemented. Initialisation into the lowest lying energy state was performed by taking a thermal state and equalising the populations in the higher energy states. The resulting mixture has a small excess of the target state, with the signals from the other states cancelling out. This state is said to be a *pseudo-pure state* and was later shown to have no true entanglement [84], calling into question whether early NMR experiments could really be considered quantum computations or whether they should be instead be viewed as simulations of quantum computations. The initialisation procedure also confers an inherent lack of scalability to the scheme; as the system size increases the excess in the target state, and therefore the signal from it, decreases exponentially.

In spite of these difficulties, pure NMR techniques remain at the forefront of what is possible on a quantum computer, as demonstrated by the factorisation of 143 using an adiabatic algorithm in 2012 [85]. However, the majority of the research in this area now focusses on the use of nuclear spins in hybrid systems - for example when coupled with an electronic spin that can be used for manipulation and cooling, as discussed in the next section.

2.4.2 Silicon based systems

There has been renewed interest in silicon based systems in recent years after the original proposal by Kane back in 1998 [86]. Qubits can be realised using the electronic and nuclear spin degrees of freedom in a system of an electron bound to a phosphorous donor. Using such a setup true entanglement was demonstrated in an large, NMR-type ensemble system for the first time in 2011 [87]. Unlike NMR, it is possible to make some measurements on individual spins in a single-shot manner, for example via spin to charge conversion [88].

Due to their weak environmental couplings nuclear spins make excellent candidates for quantum memories. Experiments in 2012 have shown spin coherence times in excess of $200\mu s$ [89, 90] at room temperature, with recent (unpublished) results apparently on the order of hours. It is likely that nuclear spins will play an important role in any solid state quantum computer.

2.4.3 Ion Traps

Ion trap approaches use ions trapped in electrical potentials with qubits often defined using low lying electronic states differentiated by spin, using optical processes for readout. The initial proposal was made by Cirac and Zoller in 1995 [91] and was followed with the implementation of a single qubit gate by Monroe *et al.* later that year [92]. After some theoretical advances [93] there was an implementation of the Deutsch-Josza algorithm in 2003 [94] and a successful quantum simulation using a single trapped atom in 2002 [95]. More recent success includes the demonstration of fourteen qubit entanglement by Blatt in 2011 [96]. Ion traps have also been used for the digital simulation of a range of spin systems using six qubits [97] and a system that can be used to simulate general open quantum system of up to five qubits [98].

Despite these successes the architecture has some weaknesses when it comes to

scaling: nearest neighbour interactions are commonly used to implement two-qubit gates which becomes problematic as the system size grows, with experimentalists forced to investigate approaches as the adiabatic transportation of ions along chip channels [99]. These concerns are less inhibitive in some simulation situations, such as the recent use of a 2D array of hundreds of ions to simulate large Ising systems [100].

2.4.4 Quantum Dots

Quantum dots are formed by confining a quantum particle in all three spacial directions, on a scale similar to its de Broglie wavelength. The resulting system has a series of discrete energy levels and can, to a good approximation, be viewed as an artificial atom. There are several physical systems that exhibit quantum dot behaviour; two of the most relevant systems for QIP are *self-assembled quantum dots* and *surface quantum dots*.

Self-assembled quantum dots are semiconductor structures consisting of a nanoscale region of a low band gap material embedded in higher band gap surroundings, the resulting 3D potential providing the confinement. There are two main approaches to defining qubits in self-assembled quantum dot systems. Spin qubits use the spin of the electronic ground state and have good coherence properties [101, 102] but relatively slow gating times [103]. Excitonic qubits use the existence of an electron-hole pair, or *exciton*, to define the qubit and have very fast gating times [104] but suffer from rapid decoherence due to strong environmental interactions. Some of the more promising proposals seek to combine the desirable features from both these schemes, for example by spin selective creation of an exciton to allow fast manipulation of the spin qubit [105, 106, 107, ?]. There have been several successful demonstrations of initialisation [108, 109], control [110] and measurement [111] of

quantum dot qubits.

Self-assembled quantum dots are hindered by their random nature as optical characteristics vary wildly between dots. Surface quantum dots overcome this problem by using surface electrodes positioned on the surface of a thin semi-conductor film to define the dot. Using such systems, state initialisation, coherent manipulation and measurement via spin-to-charge conversion have been demonstrated [112]. Unlike self-assembled quantum dots, surface quantum dots are not typically optically active, and multiple qubit operations have been a challenge due to the geometrical constraints in placing multiple qubits in close proximity.

2.4.5 Photonic Systems

Due to weak interactions with their environment, photonic qubits show excellent coherence properties. The information can be encoded in various ways, including in the photon's polarisation and also in the 'dual-rail' representation - where the qubit is defined by the absence or presence of a qubit in a given mode [113]. In both these representations single qubit operations can be carried out by well understood linear optical gates [114, 115]. The difficulty with the scheme comes in implementing the two-qubit entangling gates. Non-linear effects, such as the Kerr effect, are very weak, making entanglement generation a challenge [116].

In 2001 Knill, Laflamme and Milburn proposed a system using projective measurements to implement two-qubit gates probabilistically [117]. By using a teleportation type approach these gates can be incorporated into the system with high probability. Combined with theoretical advances to reduce resources [118], the approach has been the basis of some exciting recent developments. In 2009 a team at Bristol managed to implement Shor's algorithm using 4 optical qubits to factorise 15 [119] and then in 2011 used qubit recycling schemes to factorise 21 [120].

Dealing with photon loss is still a key challenge but advances in the fields of efficient photon detectors [121] and sources [122] should go some way to improve the situation.

2.4.6 NV⁻ Centres

NV centers are defects in diamond consisting of a nitrogen and a neighbouring vacancy in the place of two carbon atoms. The NV⁻ system is formed when an additional electron is trapped at the site. The system is optically active and the spin projections of the electron ground state have promising properties for use as a qubit, including good coherence times at room temperature [123, 124].

In 2012 Grover's algorithm was implemented using the degrees of freedom in a single NV⁻ center to define two qubits [125], with gate fidelities of over 90%. There has been much recent progress in generating entanglement between different centers. In 2013 Hanson *et al.* demonstrated the non-deterministic entanglement of an NV⁻ center and a ¹³C atom [79], and Wrachtrup *et al.* demonstrated deterministic entanglement between two neighbouring NV⁻ centres [126]. It has also been shown possible to entangle two NV⁻ centres on different pieces of diamond [127] - a promising step towards a distributed quantum computing architecture.

2.4.7 Superconducting Devices

Superconducting devices represent one of the most attractive systems for quantum computing [128]. A common proposal is to encode the qubit state in the direction of a current flowing in a superconducting ring with non-linear Josephson Junction [129] effects harnessed for two-qubit gates. Other possibilities include using charge or phase properties to define the qubit.

There has been much progress since first implementation of a superconducting

qubit in 1999 [130]. An increase in coherence times [131] has allowed the demonstration of two and three qubits control and entanglement [132, 133]. There have also been successful implementations of quantum computing algorithms, such as a two-qubit versions of the Deutsch-Josza and Grover algorithms in 2009 [134]. It is thought that superconducting qubits can now be made with coherence times approaching those needed for fault tolerant quantum computing [135].

Superconducting devices are also the system of choice of DWave Systems - the only commercial company claiming to offer quantum computing technology. In 2011 DWave published an article in Nature demonstrating the use of their superconducting computing device to find the ground state of an artificial Ising system using a quantum annealing technique [136]. At the time of writing it remains a controversial question exactly to what extent the DWave devices harness true quantum phenomena.

Chapter 3

Quantum Dynamics

3.1 Closed Quantum Systems

We begin by quickly summarising the laws of quantum mechanics as applied to a *closed system*; that is, a system which does not interact in any way with other systems. In practice, it is rare that any given system can truly be considered to be closed, yet the dynamics of closed systems are fundamental to the quantum mechanical description of nature: at the highest level, we can view the universe itself as a closed quantum system which contains all others.

By considering idealised closed systems, we are able to present the purest form of the rules of quantum mechanics: three postulates concerning the system's state, its evolution, and the act of performing measurements on it. In the latter part of this chapter we will generalise the laws stated here to address *open systems*, by first considering the open system as part of a larger closed system to which the postulates apply.

3.1.1 State

The first postulate concerns the description of the state of a system [137]:

Associated to any closed physical system is a Hilbert space known as the *state space* of the system. The system is completely described by its *state vector*, which is a unit vector in the system's state space. The state space of a composite physical system is the tensor product of the state spaces of the component physical systems.

A Hilbert space is a (possibly infinite-dimensional) vector space over the complex numbers, on which an inner product is defined. Note that the postulate does not specify how the correct state space for a given system should be chosen, which is therefore a judgment that must be made when the system is modelled.

In general, when a system can be described using a state vector we say that it exists in a *pure state*. With the state vector specified we have complete knowledge about the system - we know everything that there is to know. We will usually write the state vector using the Dirac bracket notation, $|\psi\rangle$.

In QIP we are often concerned with physical systems where the state space is two-dimensional: the quantum bit or *qubit*. The general state of such a system can be written

$$|\psi\rangle = \alpha |0\rangle + \beta |1\rangle \quad (3.1)$$

where the normalisation condition is imposed by requiring that $|\alpha|^2 + |\beta|^2 = 1$. As an alternative representation we can write

$$|\psi\rangle = \cos \frac{\theta}{2} |0\rangle + e^{i\phi} \sin \frac{\theta}{2} |1\rangle \quad (3.2)$$

where we have used the fact that two states are physically equivalent if they differ by a global phase, $|a\rangle = e^{ik} |b\rangle$, which will become apparent when we look at the measurement postulate. We can use this representation to visualise a qubit as a

point on the surface of a unit sphere, known as the *Bloch sphere*, described by the real 3-vector $(\cos \phi \sin \theta, \sin \phi \sin \theta, \cos \theta)$ (Fig. 3.1).

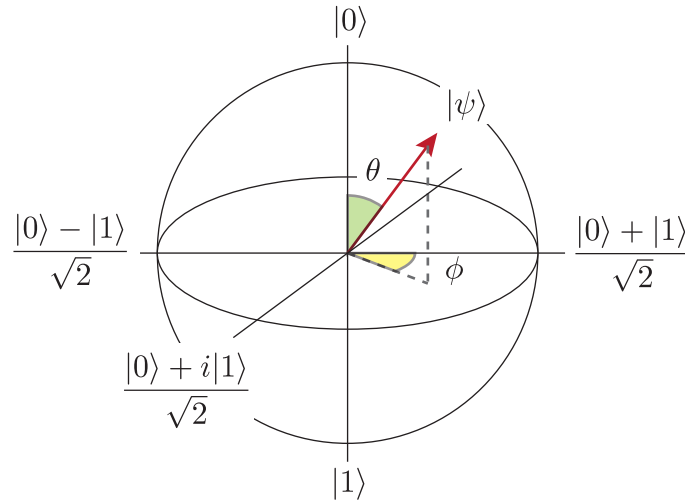


Figure 3.1: The Bloch Sphere: the state $|\psi\rangle = \cos \frac{\theta}{2} |0\rangle + e^{i\phi} \sin \frac{\theta}{2} |1\rangle$ is represented as a vector pointing to a point on a unit sphere, with spherical polar coordinates (θ, ϕ) .

3.1.2 Dynamics

The second postulate concerns the evolution of an isolated quantum system and can be stated [137]:

The time evolution of an isolated quantum system is described by the *Schrödinger equation*,

$$i\hbar \frac{d}{dt} |\psi(t)\rangle = H(t) |\psi(t)\rangle \quad (3.3)$$

where \hbar is a constant, known as *Planck's constant*, and $H(t)$ is a fixed Hermitian operator known as the Hamiltonian of the closed system.

In the rest of this thesis we choose units so as to set $\hbar = 1$, unless stated otherwise.

The Schrödinger equation can be solved in terms of a time evolution operator

$$|\psi(t)\rangle = U(t) |\psi(0)\rangle \quad (3.4)$$

where $U(t)$ is the solution to the differential equation

$$\frac{d}{dt}U(t) = H(t)U(t), \quad U(0) = \mathbf{1} \quad (3.5)$$

As $H(t)$ is Hermitian, $U(t)$ will be unitary. In particular this implies that $U^{-1}(t) = U^\dagger(t)$, so the inverse of $U(t)$ exists and therefore the dynamics of isolated quantum systems are reversible.

As the Hamiltonian is Hermitian we can write it in the form

$$H = \sum_i E_i |\phi_i\rangle \langle \phi_i| \quad (3.6)$$

where E_i are the eigenvalues, which are real, and $|\phi_i\rangle$ are the associated eigenvectors, which can be chosen to be orthogonal. The $|\phi_i\rangle$ are sometimes called stationary states, as they evolve as

$$|\phi_i(t)\rangle = e^{-iE_i t} |\phi_i(0)\rangle \quad (3.7)$$

picking up a phase at rate E_i .

As a simple example of pure state evolution we consider an isolated qubit, under the influence of the *Rabi Hamiltonian*,

$$H = \frac{1}{2} \begin{bmatrix} -\nu & \Omega \\ \Omega & \nu \end{bmatrix}, \quad (3.8)$$

in the $\{|0\rangle, |1\rangle\}$ basis. We diagonalise the Hamiltonian

$$H = E_1 |\phi_1\rangle \langle\phi_1| + E_2 |\phi_2\rangle \langle\phi_2| \quad (3.9)$$

in terms of the eigenvectors and eigenvalues

$$|\phi_1\rangle = \cos \frac{\theta}{2} |0\rangle + \sin \frac{\theta}{2} |1\rangle \quad E_1 = \nu + \sqrt{\nu^2 + \Omega^2} \quad (3.10)$$

$$|\phi_2\rangle = \sin \frac{\theta}{2} |0\rangle + \cos \frac{\theta}{2} |1\rangle \quad E_2 = \nu - \sqrt{\nu^2 + \Omega^2} \quad (3.11)$$

where

$$\theta = \arctan \left(\frac{\Omega}{\nu} \right). \quad (3.12)$$

We can then write the solution to the Schrödinger equation

$$|\psi(t)\rangle = \alpha e^{iE_1 t} |\phi_1\rangle + \beta e^{iE_2 t} |\phi_2\rangle \quad (3.13)$$

$$= \alpha e^{i\Delta t} |\phi_1\rangle + \beta e^{-i\Delta t} |\phi_2\rangle \quad (3.14)$$

where $\Delta = \sqrt{\nu^2 + \Omega^2}$, α and β are constants, and the last equality uses the equivalence of two quantum states differing only by a global phase.

The solution can be visualised as rotation of the initial state vector about the axis connecting the diametrically opposite points relating $|\phi_1\rangle$ and $|\phi_2\rangle$ on the Bloch sphere, at angular speed Δ . The amplitude of the oscillation is proportional to $\sin^2 \theta$, increasing from 0 to 1 as $\theta \rightarrow \pi$. This oscillatory behaviour, known in this case as the *Rabi oscillation*, is a common feature of many quantum systems.

3.1.3 Measurements

The third, and final, postulate concerns itself with measurements performed on isolated quantum systems. We state it in terms of a special class of measurements [137]:

A *projective measurement* is described by an *observable*, M , a Hermitian operator on the system's state space. We can write the operator as

$$M = \sum_m m P_m \quad (3.15)$$

where P_m is the projector onto the eigenspace of M with eigenvalue m . The outcomes of the measurement correspond to the eigenvalues m . When performing a measurement on state $|\psi\rangle$, the probability of obtaining outcome m is

$$p(m) = \langle \psi | P_m | \psi \rangle. \quad (3.16)$$

Given that outcome m occurred, the state of the system immediately after the measurement is

$$\frac{P_m |\psi\rangle}{\sqrt{p(m)}}. \quad (3.17)$$

In fact, projective measurements are not the most general measurement we can make on a closed quantum system. A projective measurement corresponds to making a measurement on the whole system. We could also choose to just measure a part of the system, which would not generally perform a projective measurement on the whole. We state postulate three in terms of projective measurements as they are conceptually simple and it can be shown that the most general types of measure-

ments are always equivalent to a projective measurement on some ancillary system [138]. We visit these more general measurements along with open quantum systems in the next section.

3.2 Open Quantum Systems

In reality, a closed quantum system must be viewed as an idealisation; with the possible exception of the entire universe, the assumption that a system is closed must always be approximate as all physical systems are unavoidably coupled to other physical systems. We could try to rectify the situation by expanding the system we are interested in to include these other systems, but will eventually run into difficulties: when considered together the joint system may be too complex to model given our computational resources, or perhaps we do not have enough knowledge of some of the systems or couplings to make modelling possible. To model real-world situations we must develop the theory of *open quantum systems*.

The subject of open quantum systems is especially important for the field of QIP. Most QIP processes and algorithms are stated in terms of what can be done in principle in ideal systems. All real systems suffer from unwanted interactions with other systems. In assessing a system's suitability as a candidate QIP system, it is important to be able to somehow incorporate these interactions into our model and evaluate the extent of their effect on the system's information processing capacity.

In order to treat open systems we will need to generalise the ideas of state description, evolution and measurement that were introduced in the previous section.

3.2.1 State

When describing the state of closed systems we used the state vector. The state vector represents complete knowledge of the system. When we deal with open

quantum systems, we frequently find ourselves in situations where we do not have this complete knowledge - there is some classical uncertainty in our knowledge of the state. In these cases the state vector is no longer sufficient for giving the best possible representation of the state.

As a simple illustration of this point, consider a pair of qubits in the Bell singlet state, $(|01\rangle - |10\rangle)/\sqrt{2}$. Imagine we only have access to the first qubit and want to provide the best possible description of its state; another party holds the second qubit and there are no restrictions placed on the operations they perform. A first observation is that if we perform a projective measurement described by the Z operator we obtain the outcomes 0 and 1, each with probability $1/2$. The only state vectors with this property take the form $(|0\rangle + e^{i\phi}|1\rangle)/\sqrt{2}$, with $\phi \in [0, 2\pi)$. However, our first qubit also has the property that when measured in the X or Y basis it will also report both possible outcomes with equal probability, which is not the case for any of the state vectors given. A good representation of the state of the first qubit is not possible within the language of state vectors.

Systems where the state is not completely known, and subsystems of composite systems, can be thought of as being in a statistical mixture of pure states. We say these systems exist in a *mixed state*. To describe such states, we introduce the *density matrix*

$$\rho = \sum_i p_i |\psi_i\rangle \langle \psi_i|, \quad (3.18)$$

which represents a statistical mixture of pure states $|\psi_i\rangle$ each with probability p_i . It can be seen immediately that a density matrix must be Hermitian and positive semi-definite (has all eigenvalues ≥ 0), and that $\text{Tr}(\rho) = 1$. It is also true that any matrix satisfying these properties will describe the state of some quantum ensemble.

When we introduced the concept of a mixed state we did not rule out that the

state is also pure, merely that it need not be. We can consider a pure state to be a statistical ‘mixture’ of a single state:

$$\rho = |\psi\rangle\langle\psi|. \quad (3.19)$$

Pure states can be identified by the fact that $\text{Tr}\{\rho^2\} = 1$. In general $\text{Tr}\{\rho^2\}$ can be used as a measure of how pure a state is. A maximally mixed state in a Hilbert space of dimension n has $\rho = \mathbf{1}_n/n$ and $\text{Tr}\{\rho^2\} = 1/n$.

If we have a composite quantum system formed from two systems A and B the density matrix of the joint system is given

$$\rho_{AB} = \rho_A \otimes \rho_B. \quad (3.20)$$

If we are given the density matrix of the joint system, we can find the reduced density matrix of the subsystem A by taking the *partial trace* over B ,

$$\rho_A = \text{Tr}_B\{\rho_{AB}\} = \sum_b \langle b| \rho_{AB} |b\rangle, \quad (3.21)$$

where $\{|b\rangle\}$ is a basis for the Hilbert space of system B .

3.2.2 Measurement

We earlier stated the measurement postulate in terms of projective measurements: a measurement on an isolated quantum system is described by a single operator and the possible measurement outcomes are given by the eigenvalues of that operator. The act of measurement projects the system into the eigenspace of the eigenvalue corresponding to the outcome.

When dealing with non-isolated systems we must extend our measurement frame-

work to *positive operator valued measurements* (POVMs). Neumark's theorem [138] tells us that any POVM on a system is equivalent to a projective measurement on a larger system. For example, a common experimental set-up is to allow a system to interact with an ancilla qubit and then measure the ancilla - in doing so performing a projective measurement onto subspaces defined by the ancilla's state - in order to learn about the system.

A POVM is defined by a set of operators A_k , satisfying

$$\sum_k A_k^\dagger A_k = \mathbf{1} \quad (3.22)$$

Each of the operators A_k corresponds to a different measurement outcome a_k . The probability of outcome a_k is given by $p_k = \text{Tr}\{A_k \rho A_k^\dagger\}$. After a measurement with outcome a_k the system is left in the state

$$\rho \rightarrow \rho' = \frac{1}{p_k} A_k \rho A_k^\dagger \quad (3.23)$$

It is worth noting that, unlike projective measurements, POVMs are not repeatable - performing the same measurement twice in quick succession can give different outcomes.

3.2.3 Dynamics

In the language of density matrices the Schrödinger equation becomes the *von Neumann equation*

$$\frac{d}{dt} \rho = i[\rho, H] \quad (3.24)$$

The von Neumann equation describes the evolution of a closed system in a mixed

state, but the evolution of open systems is far richer than this. In general it may not even be possible to predict the evolution of an open system without also providing a detailed model of all the systems with which it interacts. The study of open quantum systems, and the circumstances under which an interacting system's dynamics can be modelled alone, is a vast subject. Here we will touch on only a small, yet often applicable, corner of it.

In order to set up the theory we first divide the world into two parts: the *system* and the *environment*. We choose the system to be the part that we wish to model and make predictions about. The environment represents everything outside the system. The decision of where to draw the boundary between system and environment in a given case requires much care.

We now look at the important case of *Markovian evolution*: where the current evolution depends only on the system state at the current time, and not on the state of the environment or the history of the system. In practice this evolution will be approximate, but nevertheless provides accurate predictions in many situations. In particular, if the excitations in the environment decay on a much quicker timescale than that of the system dynamics, then the system's evolution is often approximately Markovian.

The most general form [139] of evolution of a Markovian system is given by the *Markovian master equation*

$$\frac{d}{dt}\rho(t) = -i[H, \rho] + \sum_k L_k \rho L_k^\dagger - \frac{1}{2} L_k^\dagger L_k \rho - \frac{1}{2} \rho L_k^\dagger L_k. \quad (3.25)$$

The operators L_k are often referred to as *Lindblad operators* and term involving the sum is often referred to as the *dissipator*, written $D(\rho)$. The H that occurs in the commutator term is not necessarily the free system Hamiltonian, as it may contain corrective terms due to the interaction.

We now look at two situations in which the Markovian master equation arises.

3.2.4 Quantum Jump Master Equation

We first consider a system evolving under continuous measurement. It is important to state carefully what we mean by this to avoid an apparent contradiction: the well known quantum Zeno effect means that any continuous measurement on a quantum system will always give the same outcome. There are two points that allow us to avoid complete Zeno quenching of the systems dynamics: first even ‘continuous’ measurements occur on some timescale over which the measurement outcome can change; and second we look at POVM measurements which act in a weak manner for the majority of the time. A *weak measurement* is one that gives us very little information about the system and correspondingly only slightly perturbs the system’s state. Such measurements occur when the system interacts weakly with an ancilla which is then measured.

We will focus on a specific type of continuous measurement, which can be phrased in terms of isolated detection events. Most of the time the measurement reveals that no event has occurred, behaving like a weak measurement. Occasionally the measurement reveals that an event has occurred and the system changes drastically similar to a projective measurement. In this case we say the system has undergone a *quantum jump*. A good example is photon emission from an atom in a cavity: at any point it is possible that a photon will be emitted and detected, but in most time intervals no emission will occur.

It is important to realise that by placing a system under continuous observation we alter its dynamics even if no detection event occurs. Intuitively, the event of ‘no detection’ increases our knowledge of the system’s state and thus changes it. We say the state follows *no-jump evolution* due to the *back-action* of our observation.

We will now roughly sketch out how this measurement scenario leads back to the Markovian master equation (3.25). The rigorous derivation requires the use of stochastic calculus and a good explanation can be found in [140]. We aim to avoid these complexities whilst still providing some level of intuition for the result.

To put all this on a rigorous footing we will describe our observation using a POVM. For simplicity, we will assume that we look to detect only a single event. We let the detection event operator be A_1 , so that after a detection event the system is in state

$$\frac{A_1 \rho A_1^\dagger}{\text{Tr}\{A_1 \rho A_1^\dagger\}} \quad (3.26)$$

We assume the measurement is weak and that the probability of detecting an event is on the order of ϵ , a ‘weakness parameter’, which we can take to be small. We write $A_1 = \sqrt{\epsilon}L$, in doing so defining L . Currently A_1 represents one outcome of a POVM. To complete our description we must complete the set of measurement outcome operators so that eq. (3.22) is satisfied. We do this by setting $A_0 = \mathbf{1} - \frac{\epsilon}{2}L^\dagger L$ so that

$$A_0^\dagger A_0 + A_1^\dagger A_1 = \left(\mathbf{1} - \frac{\epsilon}{2}L^\dagger L\right)^\dagger \left(\mathbf{1} - \frac{\epsilon}{2}L^\dagger L\right) + \epsilon L^\dagger L = \mathbf{1} + O(\epsilon^2). \quad (3.27)$$

We now consider the measurement to be made over a small time interval, δt , and set $\epsilon \propto \delta t$ so that the probability of detection is proportional to the length of that interval. We absorb any constant factor into our definition of L . We also make the simplifying assumption that the system is stationary apart from the measurement process, so that there are no Hamiltonian terms. Conditional on there being no

jump in the interval the system evolves as

$$\rho(t + \delta t) = \frac{1}{p_0(t, t + \delta t)} \left(\mathbf{1} - \frac{\delta t}{2} L^\dagger L \right) \rho(t) \left(\mathbf{1} - \frac{\delta t}{2} L^\dagger L \right) \quad (3.28)$$

$$= \frac{1}{p_0(t, t + \delta t)} \left(\rho(t) - \frac{\delta t}{2} (L^\dagger L \rho(t) + \rho(t) L^\dagger L) \right), \quad (3.29)$$

where we have normalised the state ρ by dividing by the probability that no jump occurred in the interval, $p_0(t, t + \delta t)$. This normalisation is not ideal as, due to the dependence of $p_0(t, t + \delta t)$ on $\rho(t)$, it introduces a non-linearity into the equation. We can avoid this by simply not performing the normalisation, which has the nice feature that the probability $p_0(t, t + \delta t)$ is now encoded in the trace of the density matrix. As the outcomes of measurements in different time intervals are independent, the probabilities multiply, and so the trace of the density matrix $\rho(t)$ will represent the cumulative probability there has been no jump by time t .

We can use this equation to deduce the continuous conditional no-jump dynamics of the system by allowing $\delta t \rightarrow dt$. Strictly speaking we need to be careful here, as by taking δt to be infinitesimal we risk running into quantum Zeno effects. What we mean is that we take δt to be far smaller than the timescale of the system's dynamics, so that the motion we observe is approximately continuous according to the differential equation:

$$\frac{d}{dt} \rho(t) = -\frac{1}{2} (L^\dagger L \rho(t) + \rho(t) L^\dagger L). \quad (3.30)$$

This makes precise the earlier statement that the act of not detecting an event has a tangible effect on the physical system.

In a similar fashion to before we can look at what happens if we do detect an event in the interval δt . Conditional on an event being detected the system evolves

as

$$\rho(t + \delta t) = L\rho(t)L^\dagger, \quad (3.31)$$

where we have chosen not to normalise, so that the trace of $\rho(t + \delta t)$ records the probability that an event was detected.

If we average over these two possible outcomes we obtain the equation

$$\frac{\rho(t + \delta t) - \rho(t)}{\delta t} = L\rho(t)L^\dagger - \frac{1}{2} (L^\dagger L\rho(t) + \rho(t)L^\dagger L). \quad (3.32)$$

By allowing $\delta t \rightarrow dt$ we recover the Markovian master equation (3.25).

Such an averaging procedure would be justified if, for example, we performed the measurement but forgot to look at the outcome. Perhaps a better way of viewing it is that Nature measured the system. The result is in principle recorded in the environment but we do not have access to it. In this way we can interpret decoherence processes, as described by the Markovian master equation, in terms of information leaking from the system into the environment.

It also allows us to view the Markovian master equation as an averaging over all possible trajectories of the system. It is sometimes useful to think in terms of *unravelling* a master equation into the different trajectories. A simple example would be to pull out the no-jump component that we derived above, to partially unravel the evolution into no-jump and at-least-one-jump processes.

3.2.5 Decoherence Master Equation

We have so far presented the general form of a Markovian Master Equation and seen how such an equation can be interpreted as the average over the different observation histories of a continuously observed quantum system. We now approach the master

equation from a different direction by deriving it directly from Hamiltonian for a weakly interacting, time independent system-environment. In doing so we visit some of the common assumptions made to cast the system into Markovian form.

We begin by separating the Hamiltonian into terms acting solely on the system, terms acting solely on the environment, and terms involving both the system and environment (the interaction terms):

$$H = H_S + H_E + H_I. \quad (3.33)$$

Up until this point we have viewed system evolution in terms of a state evolving with respect to fixed operators representing the system's observables. This view is commonly known as the *Schrödinger picture*. The only truly physical features of the system are given by the observables, which are a combination of both the system operators and the system state. It is therefore physically equivalent to consider system evolution as evolving operators with respect to a fixed state, or even somewhere in between. In order to simplify our description of the system evolution, we change to the *interaction picture*: we let $U(t) = \exp(i(H_S + H_E)t)$ and transform operators as $\tilde{A}(t) = U(t)A(t)U^\dagger(t)$. The von Neumann equation is transformed to

$$\frac{d}{dt}\tilde{\rho}(t) = -i \left[\tilde{H}_I(t), \tilde{\rho}(t) \right] \quad (3.34)$$

By switching to the interaction picture we move to a basis which follows the natural, independent evolution of both the system and environment. The natural motion of the system and environment have thus been absorbed into our description of the states, and so the terms H_S and H_E are eliminated from the Hamiltonian.

Our best description of the state of the system S is given by taking the partial

trace of the overall density matrix over the environment E :

$$\tilde{\rho}_S(t) = \text{Tr}_E \{ \tilde{\rho}(t) \}. \quad (3.35)$$

We now look to find the master equation for the system, S , which will be an expression for the rate of change of $\tilde{\rho}_S$ in terms of $\tilde{\rho}_S$. To this end, we formally solve eq. (3.34) to find an equation for $\tilde{\rho}$ in integral form

$$\tilde{\rho}(t) = \tilde{\rho}(0) + -i \int_0^t [\tilde{H}_I(s), \tilde{\rho}(s)] ds \quad (3.36)$$

and then substitute this back into eq. (3.34) and apply eq. (3.35) to get

$$\frac{d}{dt} \tilde{\rho}_S(t) = - \int_0^t \text{Tr}_E \left\{ [\tilde{H}_I(t), [\tilde{H}_I(s), \tilde{\rho}(s)]] \right\} ds \quad (3.37)$$

where we have assumed that $\text{Tr}_E[\tilde{H}_I(t), \tilde{\rho}(0)] = 0$.

This isn't yet in a closed form as the RHS still contains $\tilde{\rho}(t)$, the density matrix of the whole system. To begin rectifying this we first make the Born approximation by letting $\tilde{\rho}(s) \approx \tilde{\rho}_S(s) \otimes \tilde{\rho}_E$. When doing this we envisage a system that is weakly coupled to a large environment. We expect the influence of the system on the environment to be small enough that the state remains approximately separable throughout. Excitations from the system are allowed to enter the environment, but we assume there is a sufficiently large continuum of frequencies that the excitations dissipate on a timescale that is small with respect to the timescale over which the system evolves.

After the Born approximation the RHS of eq. (3.37) no longer depends on the history of the environment, but still depends on the system state at previous times. To remove this dependence we make the first part of the *Markov approximation* by

setting $\rho(s) = \rho(t)$

$$\frac{d}{dt}\tilde{\rho}_S = -i \int_s^t \text{Tr}_E \left\{ \left[\tilde{H}_I(t), \left[\tilde{H}_I(s), \tilde{\rho}_S(t) \otimes \tilde{\rho}_E \right] \right] \right\} ds. \quad (3.38)$$

This equation is known as the Redfield equation. We can justify the Markov approximation by noting that we have already assumed that excitations entering the environment decay on a timescale that is short in comparison to system dynamics; the terms in the integrand will oscillate, averaging to zero, for values of s away from t . Following this argument we can remove the Redfield equation's reference to the initial time $t = 0$, by changing the direction of the integral in time:

$$\frac{d}{dt}\tilde{\rho}_S(t) = -i \int_s^\infty \text{Tr}_B \left\{ \left[\tilde{H}_I(t), \left[\tilde{H}_I(t-s), \tilde{\rho}(t) \right] \right] \right\} ds. \quad (3.39)$$

It is important to reiterate that timescales are important here: the *Born-Markov approximation* is suitable for modelling the system on a timescale larger than the typical environmental decay time. We make this notion more precise when we later write the equation in terms of the environmental correlation functions. It can be shown [141] that the Born-Markov approximation is equivalent to keeping second order commutator terms in a formal expansion of the solution to eq. (3.34).

We now look to get the equation into a form where we can perform the integral by examining the form of the Hamiltonian. We begin by returning to the Schrödinger picture Hamiltonian and writing

$$H_I = \sum_{\alpha} A_{\alpha} \otimes B_{\alpha}, \quad (3.40)$$

where A_{α} and B_{α} act on the system and environment respectively. We have assumed here that the system-environment interaction is linear.

To find the time dependence of $\tilde{H}_I(t)$ we further split the A_α into operators

$$A_\alpha(\omega) = \sum_{\epsilon' - \epsilon = \omega} \Pi(\epsilon) A_\alpha \Pi(\epsilon'), \quad (3.41)$$

where $\Pi(\epsilon)$ is a projector onto the eigenspace of energy ϵ . This gives us that

$$[H_S, A_\alpha(\omega)] = -\omega A_\alpha(\omega) \quad (3.42)$$

$$[H_S, A_\alpha^\dagger(\omega)] = +\omega A_\alpha^\dagger(\omega). \quad (3.43)$$

The $A_\alpha(\omega)$ are eigenoperators of the Hamiltonian with frequencies $\pm\omega$.

Returning to the interaction picture we have

$$\tilde{A}(\omega, t) = e^{iH_S t} A_\alpha(\omega) e^{-iH_S t} = e^{-i\omega t} A_\alpha(\omega), \quad (3.44)$$

so that

$$\tilde{H}_I(t) = \sum_{\alpha, \omega} e^{-i\omega t} A_\alpha(\omega) \otimes \tilde{B}_\alpha(t) = \sum_{\alpha, \omega} e^{i\omega t} A_\alpha^\dagger(\omega) \otimes \tilde{B}_\alpha^\dagger(t). \quad (3.45)$$

If we substitute this back into the Redfield eq. (3.39) we are able to perform the integration

$$\frac{d}{dt} \tilde{\rho}_S(t) = \sum_{\omega, \omega'} \sum_{\alpha, \beta} e^{i(\omega' - \omega)t} \Gamma_{\alpha\beta}(\omega) (A_\beta(\omega) \tilde{\rho}_S(t) A_\alpha^\dagger(\omega') - A_\alpha^\dagger(\omega') A_\beta(\omega)) + \text{H.c.}, \quad (3.46)$$

where the reservoir correlations functions are defined by

$$\Gamma_{\alpha\beta}(\omega) = \int_0^\infty ds e^{i\omega s} \text{Tr}_E \{ \tilde{B}_\alpha^\dagger(t) \tilde{B}_\beta(t-s) \rho_E \}. \quad (3.47)$$

We have assumed that ρ_E is a stationary state of the environment, so that $\text{Tr}_E\{\tilde{B}_\alpha^\dagger(t)\tilde{B}_\beta(t-s)\rho_E\} = \text{Tr}_E\{\tilde{B}_\alpha^\dagger(s)\tilde{B}_\beta(0)\rho_E\}$ and thus $\Gamma_{\alpha\beta}(\omega)$ has no time dependence. We have also dropped any terms involving AA and $A^\dagger A^\dagger$, as the associated correlation functions will be zero.

We now make the *secular approximation* or *rotating wave approximation* (RWA): we eliminate any terms from eq. (3.46) where $\omega' \neq \omega$. We justify this by again thinking about the timescales involved: terms involving $e^{i(\omega'-\omega)t}$ will average to zero on a characteristic timescale of $1/(\omega' - \omega)$. If this is small compared to the timescale of system evolution we can perform the approximation to give

$$\frac{d}{dt}\tilde{\rho}_S(t) = \sum_{\omega} \sum_{\alpha,\beta} \Gamma_{\alpha\beta}(\omega) (A_\beta(\omega)\tilde{\rho}_S(t)A_\alpha^\dagger(\omega) - A_\alpha^\dagger(\omega)A_\beta(\omega)) + \text{H.c.} \quad (3.48)$$

We now have a Markovian evolution equation and all that is left is to massage it into the form of the Markovian master equation (3.25). To this end we write

$$\Gamma_{\alpha\beta}(\omega) = \frac{1}{2}\gamma_{\alpha\beta}(\omega) + iS_{\alpha\beta}(\omega). \quad (3.49)$$

and return to the Schrödinger picture to recover

$$\frac{d}{dt}\rho_S(t) = -i[H_S + H_{LS}, \rho_S(t)] + D(\rho_S(t)), \quad (3.50)$$

where

$$D(\rho) = \sum_{\omega} \sum_{\alpha,\beta} \gamma_{\alpha\beta}(\omega) \left(A_\beta(\omega)\rho A_\alpha^\dagger(\omega) - \frac{1}{2}\{A_\alpha^\dagger(\omega)A_\beta(\omega), \rho\} \right). \quad (3.51)$$

Note that the system Hamiltonian has picked up the Lamb shift contribution H_{LS} , from the terms $S_{\alpha\beta}$. It can be shown [142] that the matrix $\gamma_{\alpha\beta}$ is positive, so that we can diagonalise it to recover the Master Equation form in eq. (3.25).

Chapter 4

Light as a Quantum Field

4.1 Quantum Treatment of Light

The quest to define the nature of light occupies an important place in the history of physics. Much of the debate has focussed on whether light should be modelled as a particle or as a wave. Newton favoured the particular description, which formed the basis for his many fundamental contributions to optics, while his contemporary Huygens believed in a wave description. Young's famous split experiment demonstrated that light exhibited interference effects and when Maxwell introduced his unifying equations for the electric field, the problem was thought to be settled: in a vacuum Maxwell's equations for the electric field, \mathbf{E} , and magnetic field, \mathbf{B} , reduce to:

$$\nabla \times \mathbf{B} = \frac{1}{c^2} \frac{\partial \mathbf{E}}{\partial t} \quad (4.1)$$

$$\nabla \times \mathbf{E} = -\frac{\partial \mathbf{B}}{\partial t} \quad (4.2)$$

$$\nabla \cdot \mathbf{B} = 0 \quad (4.3)$$

$$\nabla \cdot \mathbf{E} = 0, \quad (4.4)$$

which lead to the wave equation for $\mathbf{E}(\mathbf{r}, t)$:

$$\nabla^2 \mathbf{E} - \frac{1}{c^2} \frac{\partial^2 \mathbf{E}}{\partial t^2} = 0, \quad (4.5)$$

where c is the speed of light.

At the beginning of the 20th century physicists were forced to return to the question in order to explain the photoelectric effect and ‘ultraviolet catastrophe’ of black body radiation. These problems were overcome, by Einstein [143] and Planck [144] respectively, by assuming that light could only be absorbed and emitted in discrete units of energy. The results were fundamental in the early development of the field of quantum mechanics. The modern description of light, capable of producing both wave and particle phenomena, is largely based on proposals from Dirac in the late 1920s [145].

4.1.1 Quantising Light: A toy model

The modern approach to quantising the electromagnetic field involves working with the electromagnetic vector potential and is fairly technical due to the relativistic nature of light and continuous spectrum of modes. We aim to avoid these technical complexities while still providing an overview of the key stages by looking at a toy model of light: an electromagnetic field in a one dimensional cavity. We later state the results for the quantisation of the full field.

We begin by taking a one dimensional cavity occupying the interval $[0, L]$ on the z axis. We assume that our electric field is linearly polarised in the x direction, so that solving the wave equation (4.5) gives the only non-zero components of \mathbf{E} and

\mathbf{B} to be

$$E_x = \sum_j \sqrt{\frac{2\omega_j^2}{\epsilon_0 L}} q_j(t) \sin(k_j z) \quad (4.6)$$

$$B_y = \sum_j \frac{1}{k_j \mu_0} \sqrt{\frac{2\omega_j^2}{\epsilon_0 L}} q_j(t) \cos(k_j z), \quad (4.7)$$

where $\omega_j = ck_j = \pi j/L$ for $j \in \{1, 2, \dots\}$ and ϵ_0 and μ_0 are constants that satisfy $\epsilon_0 \mu_0 = 1/c^2$. The discrete set of values ω_j arise from applying the boundary conditions at either end of the cavity. We know from the wave equation that

$$\ddot{q}_j = -\omega_j^2 q_j \quad (4.8)$$

which has solutions

$$q_j = Ae^{-i\omega_j t} + Be^{i\omega_j t} = ae^{-i\omega_j t} + a^* e^{i\omega_j t}, \quad (4.9)$$

where in the last equality we have enforced that $q_j(t)$ must be real.

We now write the standard electromagnetic field Hamiltonian in terms of q :

$$H = \frac{\epsilon_0}{2} \int_0^L |\mathbf{E}|^2 + c^2 |\mathbf{B}|^2 dz = \frac{1}{2} \sum_j (\omega_j q_j^2 + p_j^2), \quad (4.10)$$

where $p_i = \dot{q}_i$, the conjugate momentum for q . The Hamiltonian now takes the same form as the Hamiltonian for the simple harmonic oscillator. We proceed with quantisation by analogy with the harmonic oscillator by promoting p and q to operators satisfying the commutation relations

$$[\hat{q}_i, \hat{p}_j] = i\delta_{ij} \quad (4.11)$$

$$[\hat{q}_i, \hat{q}_j] = [\hat{p}_i, \hat{p}_j] = 0. \quad (4.12)$$

Since \hat{p} and \hat{q} satisfy the Heisenberg commutation relations, so will \hat{E}_x and \hat{B}_y . As a consequence \hat{E}_x and \hat{B}_y will obey the Heisenberg uncertainty principle, so it is not possible to simultaneously have a well defined electric field and magnetic field. It is convenient to introduce operators \hat{a} and \hat{a}^\dagger so that

$$\hat{q}_i = \sqrt{\frac{\hbar}{2\omega_i}} \left(\hat{a}_i e^{-i\omega_i t} + \hat{a}_i^\dagger e^{i\omega_i t} \right) \quad (4.13)$$

$$\hat{p}_i = -i\sqrt{\frac{\hbar\omega_i}{2}} \left(\hat{a}_i e^{-i\omega_i t} - \hat{a}_i^\dagger e^{i\omega_i t} \right) \quad (4.14)$$

$$\hat{H} = \sum_k \hbar \left(\omega_k \hat{a}_k^\dagger \hat{a}_k + \frac{1}{2} \right). \quad (4.15)$$

The commutation relations for \hat{q}_i and \hat{p}_i imply the following commutation relations:

$$[\hat{a}_i^\dagger, \hat{a}_j] = \delta_{ij} \quad (4.16)$$

$$[\hat{a}_i^\dagger, \hat{a}_j^\dagger] = [\hat{a}_i, \hat{a}_j] = 0 \quad (4.17)$$

$$[H, \hat{a}_k] = -\hbar\omega_k \hat{a}_k \quad (4.18)$$

$$[H, \hat{a}_k^\dagger] = \hbar\omega_k \hat{a}_k^\dagger \quad (4.19)$$

It is interesting to compare equations (4.9) and (4.13). By analogy it appears that the operator \hat{a}_k^\dagger is in some way connected to the amplitude. It turns out that the operators \hat{a}_k and \hat{a}_k^\dagger are incredibly useful in the quantum treatment of the electromagnetic (and other) fields, so we will now spend a bit of time investigating some of their properties. In what follows we will deal with a generic mode with frequency ω and corresponding operators \hat{a} and \hat{a}^\dagger .

Suppose we have a state $|n\rangle$ which is an eigenstate of the Hamiltonian with energy E_n . By using the commutation relations for H and \hat{a} we see that

$$H\hat{a}|n\rangle = (E_n - \hbar\omega)\hat{a}|n\rangle, \quad (4.20)$$

so $\hat{a}|\psi\rangle$ is also an eigenstate of the Hamiltonian with energy $E - \hbar\omega$. Similarly $\hat{a}^\dagger|\psi\rangle$ is an eigenstate with energy $E + \hbar\omega$. The operators \hat{a} and \hat{a}^\dagger are known as *annihilation operators* and *creation operators* respectively. They can be thought of as respectively removing and adding excitations to the system.

We now let

$$|n-1\rangle = k_{n-1}\hat{a}|n\rangle \quad (4.21)$$

where k_{n-1} is a normalisation constant. By repeatedly applying a we can create a ladder of states at an energy spacing of $\hbar\omega_k$. In order for the system to have a lowest energy level E_0 this process must terminate somehow. If $|0\rangle$ is an eigenstate of H with energy E_0 we must have $a|0\rangle = 0$, or otherwise $a|0\rangle$ would be an eigenstate with energy lower than E_0 . We can use $|0\rangle$, which we call the *vacuum state*, to construct the states $|n\rangle$ explicitly:

$$|n\rangle = \frac{(\hat{a}^\dagger)^n |0\rangle}{\sqrt{n!}}. \quad (4.22)$$

We then have that $E_n = (n + 1/2)\hbar\omega$. Note that $E_0 = \hbar\omega/2$, so that the ground energy state is not zero - a signature of the vacuum fluctuations of the electromagnetic field.

The states $|n\rangle$ are commonly known as *Fock states* and form a basis for the excitation states of the mode. If we introduce the *number operator*,

$$N = \hat{a}^\dagger\hat{a}, \quad (4.23)$$

we have that $N|n\rangle = n|n\rangle$. We interpret the number operator as counting the number of excitations in the mode and see that the Fock state $|n\rangle$ can be interpreted as having n excitations.

We can return to the classical expression for the electric field (4.6) and promote it to a quantum field by writing in terms of creation and annihilation operators:

$$\hat{E}_x = \sum_j \left(\hat{a}_k e^{-i\omega_k t} + \hat{a}_k^\dagger e^{i\omega_k t} \right) \sin(k_j s). \quad (4.24)$$

Note that $\langle n | \hat{E}_x | n \rangle = 0$ for all n , so that for a state with a definite number of excitations the expected value of the electric field at any point is zero. If we instead introduce states

$$|\alpha\rangle = e^{|\alpha|/2} \sum_n \frac{\alpha^n |n\rangle}{\sqrt{n!}} \quad (4.25)$$

for complex number $\alpha = p + iq$, we find that

$$\langle \alpha | \hat{E}_x | \alpha \rangle = (p \cos \omega t + q \sin \omega t) \sin(k_j z). \quad (4.26)$$

The states $|\alpha\rangle$ are known as *coherent states* and are the closest quantum analogue to the classical states of radiation.

4.1.2 Field in Free Space

We now present the corresponding results for the full electromagnetic field in free space. It will be useful to give the results for both the classic and quantum states, as we will use both at later points in this thesis. Classically the state of the electromagnetic field can be decomposed into plane waves

$$\mathbf{E}(\mathbf{r}, t) = \sum_{\lambda=1}^2 \int d\mathbf{k} a_\lambda(\mathbf{k}) \boldsymbol{\epsilon}_\lambda(\mathbf{k}) u(\mathbf{k}; \mathbf{r}, t) + \text{c.c.}, \quad (4.27)$$

where $a_\lambda(\mathbf{k})$ gives the amplitude of the wave with polarisation $\boldsymbol{\epsilon}_\lambda(\mathbf{k})$, $\{\boldsymbol{\epsilon}_1(\mathbf{k}), \boldsymbol{\epsilon}_2(\mathbf{k})\}$ are a basis for the space perpendicular to \mathbf{k} and the modes $u(\mathbf{k}; \mathbf{r}, t)$ describe plane

waves with definite momentum \mathbf{k} ,

$$u(\mathbf{k}; \mathbf{r}, t) = \frac{e^{i\mathbf{k}\cdot\mathbf{r} - i\omega_{\mathbf{k}}t}}{\sqrt{(2\pi)^3 2\omega_{\mathbf{k}}}}. \quad (4.28)$$

It is worth noting that this expression allows for circularly polarised light, for example by taking $\epsilon_{\lambda}(\mathbf{k})$ to have complex components (or similar).

After quantisation we obtain the expression

$$\hat{\mathbf{E}}(\mathbf{r}, t) = \sum_{\lambda} \int d\mathbf{k} \sqrt{\frac{\hbar\omega_{\mathbf{k}}}{2(2\pi)^3\epsilon_0}} \hat{a}_{\lambda}(\mathbf{k}) \epsilon_{\lambda} + \text{H.c.}, \quad (4.29)$$

where $\hat{a}_{\lambda}(\mathbf{k})$ and $\hat{a}_{\lambda}^{\dagger}(\mathbf{k})$ are the annihilation and creation operators for excitations of the mode $u(\mathbf{k}; \mathbf{r}, t)$, which satisfy

$$[\hat{a}_{\lambda}(\mathbf{k}), \hat{a}_{\lambda'}^{\dagger}(\mathbf{k}')] = \delta_{\lambda\lambda'} \delta^3(\mathbf{k} - \mathbf{k}') \quad (4.30)$$

$$[\hat{a}_{\lambda}(\mathbf{k}), \hat{a}_{\lambda'}(\mathbf{k}')] = 0 \quad (4.31)$$

$$[\hat{a}_{\lambda}^{\dagger}(\mathbf{k}), \hat{a}_{\lambda'}^{\dagger}(\mathbf{k}')] = 0. \quad (4.32)$$

The modes $u(\mathbf{k}; \mathbf{r}, t)$ are not physical, as the plane wave solutions cannot be normalised, but nevertheless the operators $\hat{a}_{\lambda}(\mathbf{k})$ and $\hat{a}_{\lambda}^{\dagger}(\mathbf{k})$ are very convenient when formulating the theory.

In terms of these operators, the Hamiltonian for the free field is given by

$$H = \sum_{\lambda} \int d\mathbf{k} \frac{\hbar\omega_{\mathbf{k}}}{2} [\hat{a}_{\lambda}^{\dagger}(\mathbf{k}) \hat{a}_{\lambda}(\mathbf{k}) + \hat{a}_{\lambda}(\mathbf{k}) \hat{a}_{\lambda}^{\dagger}(\mathbf{k})]. \quad (4.33)$$

4.1.3 Hong-Ou-Mandel Effect

The Hong-Ou-Mandel effect is a demonstration of two photon interference. If two photons with identical wavepackets enter the two ports of a 50:50 beam splitter

simultaneously, they bunch together and exit on the same port. The effect is important as, as discussed later, it can be used to provide a quality measure for a single photon source. It also be thought of as a demonstration of the bosonic nature of photons.

A beam splitter is an optical device that reflects some of the incident light while allowing the rest to pass through. If a_1 and a_2 describe the two modes that cross at the beam splitter, the beam splitter performs the transformation B where

$$B(\hat{a}_1^\dagger) = \frac{1}{\sqrt{2}} (\hat{a}_1^\dagger + \hat{a}_2^\dagger) \quad (4.34)$$

$$B(\hat{a}_2^\dagger) = \frac{1}{\sqrt{2}} (\hat{a}_1^\dagger - \hat{a}_2^\dagger). \quad (4.35)$$

If both modes contain a single excitation on the input side of the beam splitter we get

$$B(\hat{a}_1^\dagger \hat{a}_2^\dagger) = \frac{1}{2} (\hat{a}_1^\dagger + \hat{a}_2^\dagger) (\hat{a}_1^\dagger - \hat{a}_2^\dagger) = \frac{1}{2} (\hat{a}_1^\dagger \hat{a}_1^\dagger - \hat{a}_2^\dagger \hat{a}_2^\dagger), \quad (4.36)$$

so on the output side we only see states where both excitations are in the same modes.

As already discussed, single mode excitations are not physical - in real systems excitations will have finite extent in space and time and must be expressed as a superposition of excitations of different modes. We can write a the state of a single photon in the form

$$\hat{b}^\dagger |0\rangle = \int f(k) \hat{a}^\dagger(k) dk |0\rangle, \quad (4.37)$$

where we require that $\int f(k)^* f(k) dk = 1$. We consider \hat{b}^\dagger to be the creation operation of a photon, so that our input state can be written $\hat{b}_1^\dagger \hat{b}_2^\dagger |0\rangle$. To find the output

state we must act on this with the beamsplitter operation:

$$|\psi_{\text{out}}\rangle = B(\hat{b}_1^\dagger \hat{b}_2^\dagger) |0\rangle \quad (4.38)$$

$$= \int \int f_1(k) f_2(k') B(\hat{a}_1^\dagger(k) \hat{a}_2^\dagger(k')) dk dk' \quad (4.39)$$

$$= \int \int f_1(k) f_2(k') \left(\hat{a}_1^\dagger(k) + \hat{a}_2^\dagger(k) \right) \left(\hat{a}_1^\dagger(k') - \hat{a}_2^\dagger(k') \right) dk dk' \quad (4.40)$$

$$(4.41)$$

The probability of detecting the two photons in different arms of the detector is given by

$$C = \langle \psi_{\text{out}} | \int \int \hat{a}_1^\dagger(k) \hat{a}_1(k) \hat{a}_2^\dagger(k') \hat{a}_2(k') dk dk' | \psi_{\text{out}} \rangle. \quad (4.42)$$

Calculating this for our output state gives

$$C = \frac{1}{2} - \frac{1}{2} \int \int f_1(k) f_1^*(k') f_2(k') f_2^*(k) dk dk'. \quad (4.43)$$

If $f_1 = f_2$ then $C = 0$: perfectly identical photon wavepackets demonstrate perfect bunching at a beam splitter.

The Hong-Ou-Mandel effect can be used as a diagnostic tool for single photon sources. We can compare the photon output from two different sources, or from the same source at different times by using a delay circuit. The coincidence rate, C - the probability of detecting the photons on different arms, will be ideally be zero. This will be the case if the two photons are indistinguishable and both emitted in a pure state. In order for the photon wavepacket to be in a pure state it is necessary that the photon have no correlations with the source - there should be no information left in the source that could add to our description of the photon. Having indistinguishable photons in a pure state is important for a lot of quantum computing uses, including

remote entanglement generation and linear optical quantum computing.

Showing good Hong-Ou-Mandel interference is not the only important measure of a good photon source. In some applications, notably in quantum communication devices, it is vital that exactly one photon, and not more, is emitted. It is possible to test for this using the Hanbury-Brown-Twiss experiment (e.g. [146]). Another important measure of the source is the efficiency - what proportion of the time a photon is emitted when requested - which can be measured by gathering statistics.

4.2 Light-Matter interactions

4.2.1 Atom in a Cavity - Semiclassical Approach

We begin our section on light-matter interactions by looking at the semiclassical theory an atom interacting with electromagnetic modes in a cavity. The semiclassical approach treats the light field classically and the atom quantum mechanically, and is appropriate for coherent states of light with high photon number. We treat the cavity as an idealised system where only certain modes can exist, which allows us to ignore many of the complexities due to coupling to the full electromagnetic spectrum. Cavities are also incredibly important in quantum technologies due to their ability to filter and enhance emission into a given mode.

An atom will couple to an electromagnetic field due to its charge configuration. It is convenient to use the dipole approximation to the coupling, taking the interaction Hamiltonian $H_d = -\mathbf{d} \cdot \mathbf{E}(t)$ where $\mathbf{d} = -e\mathbf{r}$ for the charge e and the position operator \mathbf{r} from the atom's center of mass, which we assume to be at the origin. The dipole approximation can be obtained by keeping the first order terms of an expansion of \mathbf{E} about the origin and is a good approximation when the wavelength of the radiation is bigger the spacial extent of the atom. In quantum optics we

do not usually use frequencies about the UV spectrum, $\lambda > 100\text{nm}$, which when compared with typical atomic radii of the order of 0.1nm makes the approximation valid. We also assume that, although we treat the atom quantum mechanically, we can treat its center of mass classically, so that the operator \mathbf{r} really does correspond to a vector operator from the origin.

We model our atom as a two level system with Hamiltonian

$$H_S = -\frac{\omega_0}{2} |g\rangle \langle g| + \frac{\omega_0}{2} |e\rangle \langle e|. \quad (4.44)$$

In doing this we assume there is some specific transition we wish to target and that all other transitions will be far off resonance from the cavity mode. We call $|g\rangle$ the ground state and $|e\rangle$ the excited state.

In order to calculate the dipole interaction term H_d we need to know about the electric field, \mathbf{E} , and the position operator, \mathbf{r} . Classically the electric field is given by

$$\mathbf{E} = E_0(\boldsymbol{\epsilon} \exp(i[\omega t - \mathbf{k} \cdot \mathbf{r}]) + \boldsymbol{\epsilon}^* \exp(-i[\omega t - \mathbf{k} \cdot \mathbf{r}])), \quad (4.45)$$

where \mathbf{k} is the wavevector, ω is the frequency, $\boldsymbol{\epsilon}$ is the polarisation and E_0 is a constant of correct dimension. We now need to write the position operator, \mathbf{r} , in terms of our system basis $\{|g\rangle, |e\rangle\}$. As \mathbf{r} has odd parity the diagonal elements $\langle g|H_d|g\rangle$ and $\langle e|H_d|e\rangle$ must both vanish. As the Hamiltonian is Hermitian there is only one element left to specify:

$$\langle e|H_d|g\rangle = \langle g|H_d|e\rangle^* = E_0 \mathbf{r}_{eg} \cdot (\boldsymbol{\epsilon} \exp(i\omega t) + \boldsymbol{\epsilon}^* \exp(-i\omega t)), \quad (4.46)$$

where $\mathbf{r}_{eg} = \langle e|\mathbf{r}|g\rangle$.

Substituting these values into $H = H_S + H_d$ leaves us with the overall Hamiltonian

$$H = \begin{bmatrix} -\omega_0/2 & eE_0\mathbf{r}_{eg}^* \cdot (\boldsymbol{\epsilon}^* \exp(-i\omega t) + \boldsymbol{\epsilon} \exp(i\omega t)) \\ eE_0\mathbf{r}_{eg} \cdot (\boldsymbol{\epsilon} \exp(i\omega t) + \boldsymbol{\epsilon}^* \exp(-i\omega t)) & +\omega_0/2 \end{bmatrix}. \quad (4.47)$$

To remove some of the time dependency we make a unitary transformation into a basis that rotates with the electromagnetic field:

$$U(t) = \begin{bmatrix} e^{i\omega t/2} & 0 \\ 0 & e^{-i\omega t/2} \end{bmatrix}, \quad (4.48)$$

The Hamiltonian transforms as $\hat{H} = UHU^{-1} + iU'U^{-1}$, to give

$$\hat{H} = \begin{bmatrix} -(\omega_0 - \omega)/2 & eE_0\mathbf{r}_{eg}^* \cdot (\boldsymbol{\epsilon}^* + \boldsymbol{\epsilon} \exp(2i\omega t)) \\ eE_0\mathbf{r}_{eg} \cdot (\boldsymbol{\epsilon} + \boldsymbol{\epsilon}^* \exp(-2i\omega t)) & +(\omega_0 - \omega)/2 \end{bmatrix}. \quad (4.49)$$

We now make the rotating wave approximation, neglecting the fast rotating terms $e^{2i\omega t}$ and $e^{-2i\omega t}$ on the basis that they will be far off-resonance and their contribution will average to zero over time. This leaves us with

$$\hat{H} = \begin{bmatrix} -(\omega_0 - \omega)/2 & eE_0\mathbf{r}_{eg}^* \cdot \boldsymbol{\epsilon}^* \\ eE_0\mathbf{r}_{eg} \cdot \boldsymbol{\epsilon} & +(\omega_0 - \omega)/2 \end{bmatrix} \quad (4.50)$$

which is of the form of the Rabi Hamiltonian (3.8). The system will undergo oscillations between the ground state, $|g\rangle$, and excited state, $|e\rangle$, driven by the electromagnetic field.

4.2.2 Atom in a Cavity: Quantum case

In many cases the semiclassical approach is sufficient, however if we want to look at the emission and absorption of single photons we must instead use the fully quantised field. We can either rederive the dipole approximation from the quantised Hamiltonian, in terms of the vector potential A (e.g. [141]), or appeal to the correspondence principle.

Quantum mechanically an electric field operator for a field with a single mode and definite polarisation is given

$$\hat{\mathbf{E}} = E_0(\boldsymbol{\epsilon}\hat{a} + \boldsymbol{\epsilon}^*\hat{a}^\dagger). \quad (4.51)$$

with \mathbf{r}_{eg} defined as before we write the dipole interaction term in the system basis:

$$H_d = E_0 e \mathbf{r}_{eg} \cdot (\boldsymbol{\epsilon}\hat{a} + \boldsymbol{\epsilon}^*\hat{a}^\dagger)\sigma_+ + E_0 e \mathbf{r}_{eg}^* \cdot (\boldsymbol{\epsilon}\hat{a} + \boldsymbol{\epsilon}^*\hat{a}^\dagger)\sigma_-, \quad (4.52)$$

where we have used spin language to describe atomic transitions, $|e\rangle\langle g| \equiv \sigma_+$ and $|g\rangle\langle e| \equiv \sigma_-$. We use this to rewrite the total Hamiltonian (ignoring the vacuum energy contribution)

$$H = \frac{\hbar\omega_0}{2}\sigma_z + \hbar\omega\hat{a}^\dagger\hat{a} + g\hat{a}\sigma_+ + g^*\hat{a}^\dagger\sigma_- + \gamma\hat{a}\sigma_- + \gamma^*\hat{a}^\dagger\sigma_+, \quad (4.53)$$

where $g = E_0 e \mathbf{r}_{eg} \cdot \boldsymbol{\epsilon}$ and $\gamma = E_0 e \mathbf{r}_{eg}^* \cdot \boldsymbol{\epsilon}$. The middle two terms on the RHS correspond to exchanging excitations between the system and electromagnetic field. If the field mode is on resonance with the atomic transition these processes will be energy conserving. The last two terms involve adding or removing excitations from both atom and field at the same time. If we have that $\omega \approx \omega_0$ these terms will be

highly off-resonant; ignoring them is equivalent to making the RWA and gives

$$H = \frac{\hbar\omega_0}{2}\sigma_z + \hbar\omega\hat{a}^\dagger\hat{a} + g\hat{a}\sigma_+ + g^*\hat{a}^\dagger\sigma_-. \quad (4.54)$$

This is the well known *Jaynes-Cummings Hamiltonian* (e.g. [141]). If we consider a basis of *dressed states*, where we let $|g, n\rangle = |g\rangle \otimes |n\rangle$ and similarly for $|e, n\rangle$, we find that the Jaynes-Cummings Hamiltonian looks like the Rabi Hamiltonian on closed subspaces $\{|g, n\rangle, |e, n-1\rangle\}$ - the joint system oscillates between a state where it is relaxed and a state where it is excited but the mode contains one fewer excitation.

4.2.3 Raman procedure

We now consider a three level system $\{|0\rangle, |1\rangle, |e\rangle\}$ where the transitions $|0\rangle \leftrightarrow |e\rangle$ and $|1\rangle \leftrightarrow |e\rangle$ are optically active. Using the semiclassical approach, as at the beginning of the previous section, we can write the Hamiltonian

$$H = \hbar \begin{bmatrix} 0 & 0 & \Omega_1 \cos \omega_1 t \\ 0 & \delta & \Omega_2 \cos \omega_2 t \\ \Omega_1 \cos \omega_1 t & \Omega_2 \cos \omega_2 t & \omega \end{bmatrix}, \quad (4.55)$$

where we have assumed for simplicity that for both optically active transitions we have that $\boldsymbol{\epsilon} \cdot \mathbf{r}_{eg} = \boldsymbol{\epsilon}^* \cdot \mathbf{r}_{eg} = \Omega$ for some real Ω , so that we can write the oscillatory behaviour in terms of a single cosine.

We next move to the rotating frame with the transformation

$$U(t) = \begin{bmatrix} 1 & 0 & 0 \\ 0 & e^{i(\omega_1 - \omega_2)t} & 0 \\ 0 & 0 & e^{i\omega_1 t} \end{bmatrix}, \quad (4.56)$$

so that the Hamiltonian becomes

$$\tilde{H} = \frac{\hbar}{2} \begin{bmatrix} 0 & 0 & \Omega_1(1 + e^{2i\omega_1 t}) \\ 0 & 2(\delta + \omega_2 - \omega_1) & \Omega_2(1 + e^{2i\omega_2 t}) \\ \Omega_1(1 + e^{2i\omega_1 t}) & \Omega_2(1 + e^{2i\omega_2 t}) & 2(\omega - \omega_1) \end{bmatrix}. \quad (4.57)$$

After we make the RWA to eliminate the off-resonant $e^{\pm 2i\omega_2 t}$ terms, we are left with

$$\tilde{H} = \frac{\hbar}{2} \begin{bmatrix} 0 & 0 & \Omega_1 \\ 0 & 2(\nu_1 - \nu_2) & \Omega_2 \\ \Omega_1 & \Omega_2 & 2\nu_1 \end{bmatrix}. \quad (4.58)$$

We then restrict to the case where $\nu_1 = \nu_2 =: \Delta$, which corresponds to tuning the frequencies ω_1 and ω_2 so they are both detuned from resonance by the same amount. We spectrally decompose the Hamiltonian

$$\tilde{H} = \lambda_d |d\rangle \langle d| + \lambda_+ |+\rangle \langle +| + \lambda_- |-\rangle \langle -|, \quad (4.59)$$

where the eigenvalues are given

$$\lambda_d = 0 \quad (4.60)$$

$$\lambda_{\pm} = \Delta \pm \sqrt{\Delta^2 + \Omega_1^2 + \Omega_2^2} \quad (4.61)$$

and we write the eigenvectors

$$|d\rangle = \cos \theta |0\rangle - \sin \theta |1\rangle \quad (4.62)$$

$$|+\rangle = \sin \phi \sin \theta |0\rangle + \sin \phi \cos \theta |1\rangle + \cos \phi |e\rangle \quad (4.63)$$

$$|-\rangle = \cos \phi \sin \theta |0\rangle + \cos \phi \cos \theta |1\rangle - \sin \phi |e\rangle \quad (4.64)$$

in terms of the parameters

$$\theta = \arctan\left(\frac{\Omega_1}{\Omega_2}\right) \quad (4.65)$$

$$\phi = \arctan\left(\frac{\Omega_1^2 + \Omega_2^2}{\lambda_+}\right). \quad (4.66)$$

The state $|d\rangle$ lies in the subspace spanned by $\{|0\rangle, |1\rangle\}$ and is not optically active.

For this reason it is often referred to as a *dark state*.

In the limit where $\Delta \gg \{\Omega_1, \Omega_2\}$ we get $|+\rangle \approx |e\rangle$ and $|-\rangle \approx \sin\theta|0\rangle + \cos\theta|1\rangle$, so if the system starts in the space spanned by $\{|0\rangle, |1\rangle\}$ it will stay there. In terms of this reduced basis the Hamiltonian becomes

$$H \approx \Delta \left(1 - \sqrt{1 + \frac{\Omega_1^2 + \Omega_2^2}{\Delta^2}}\right) |-\rangle \langle -| \quad (4.67)$$

$$\approx -\frac{1}{4\Delta} \begin{bmatrix} \Omega_1^2 & \Omega_1\Omega_2 \\ \Omega_1\Omega_2 & \Omega_2^2 \end{bmatrix}, \quad (4.68)$$

which has the same form as the Rabi Hamiltonian (3.8). Oscillation with angular frequency $\Delta = (\Omega_1^2 + \Omega_2^2)/4\nu$ between the states $|0\rangle$ and $|1\rangle$ is induced via the third state.

4.3 Phonon-matter interactions

Solid state systems contain a large number of quantum degrees of freedom, some of which are suitable for exploiting in QIP, some of which are not. When dealing with solid state systems a major source of decoherence is due to interaction with lattice vibrations. In this section we aim to present a quantum description of the lattice vibrations and model their interaction with a simple optical system, as a first step to mitigating their deleterious effects.

Following a similar pattern to the quantisation of the electromagnetic field, we can quantise the vibrational modes of a lattice, in terms of *phonons*, quanta of vibrational energy, giving Hamiltonian

$$H_E = \sum_{\alpha} \omega_{\alpha} \hat{b}_{\alpha}^{\dagger} \hat{b}_{\alpha}, \quad (4.69)$$

where \hat{b}^{\dagger} and \hat{b} are creation and annihilation operators, satisfying the familiar commutation relations: like photons, phonons are bosonic in nature. In a finite crystal there exist a discrete set of vibrational modes, but in practice in bodies of large extent the spectrum becomes approximately continuous. In any case, we choose to write the set of modes as a sum over discrete modes, mostly out of convenience. We usually assume that the phonon bath exists in a thermal state

$$\rho_E = \frac{1}{Z_{\beta}} e^{-\beta H_E} \quad (4.70)$$

where $\beta = 1/(kT)$ and Z_{β} is a normalisation factor (the partition function from statistical mechanics).

Phonons couple to any states of our system that lead to a distortion in the atomic lattice. We restrict ourselves to looking at relatively low-energy states, coupling only to long-wavelength, acoustic phonons. There are two dominant coupling mechanisms in this case: *deformation potential* coupling, D , and *piezoelectric coupling*, P , [147] leading to the interaction Hamiltonian

$$H = \sum_{\mathbf{q}} \sqrt{\frac{\hbar}{2\mu V \omega_{\mathbf{q}}}} (D|\mathbf{q}| + iP) \hat{g}(\mathbf{q}) \left(\hat{a}_{\mathbf{q}} + \hat{a}_{-\mathbf{q}}^{\dagger} \right). \quad (4.71)$$

As a concrete example we look at the Raman process from the previous section. We envisage that we have a lambda system embedded in some solid state system in

such a way phonons couple only to the excited state $|e\rangle$. This would be appropriate in a quantum dot system where $|0\rangle$ and $|1\rangle$ correspond to low lying spin states and $|e\rangle$ is an exciton state with considerably different charge configuration. In this case the interaction Hamiltonian becomes

$$H = |e\rangle \langle e| \sum_{\mathbf{q}} g_{\mathbf{q}} \left(\hat{a}_{\mathbf{q}} + \hat{a}_{-\mathbf{q}}^{\dagger} \right). \quad (4.72)$$

We have also used that in quantum dot systems the deformation potential dominates [148, 149, ?, ?].

Following the technique given in chapter 3 we move to the interaction picture and decompose the system part of the interaction Hamiltonian, $|e\rangle \langle e|$ into eigenoperators of the system Hamiltonian:

$$\tilde{H} = \left(P_0 + P_{\Lambda} e^{-i(2\Delta+\Lambda)t} + P_{\Lambda}^{\dagger} e^{-i(2\Delta-\Lambda)t} \right) \sum_{\mathbf{q}} g_{\mathbf{q}} \left(\hat{a}_{\mathbf{q}} e^{-i\omega_{\mathbf{q}}t} + \hat{a}_{\mathbf{q}}^{\dagger} e^{i\omega_{\mathbf{q}}t} \right) \quad (4.73)$$

where P_0 and P_{Λ} are given in terms of the eigenvectors from the previous section

$$P_0 = \cos^2 \phi |+\rangle \langle +| + \sin^2 \phi |-\rangle \langle -| \quad (4.74)$$

$$P_{\Lambda} = -\sin \phi \cos \phi |-\rangle \langle +|. \quad (4.75)$$

and $\Lambda = \lambda_+ - \lambda_-$. By comparing with eq. (3.40) we identify

$$B_0(t) = \sum_{\mathbf{q}} g_{\mathbf{q}} \left(\hat{a}_{\mathbf{q}} e^{-i\omega_{\mathbf{q}}t} + \hat{a}_{\mathbf{q}}^{\dagger} e^{i\omega_{\mathbf{q}}t} \right) \quad (4.76)$$

$$B_{\Lambda}(t) = e^{-i2\Delta t} \sum_{\mathbf{q}} g_{\mathbf{q}} \left(\hat{a}_{\mathbf{q}} e^{-i\omega_{\mathbf{q}}t} + \hat{a}_{\mathbf{q}}^{\dagger} e^{i\omega_{\mathbf{q}}t} \right). \quad (4.77)$$

$$\Gamma_{\alpha\beta}(\omega) = \frac{1}{\hbar^2} \int_0^\infty ds e^{i\omega s} \langle B_\beta^\dagger(t) B_\alpha(t-s) \rangle \quad (4.78)$$

In the thermal state we can calculate the correlation functions explicitly

$$\langle \hat{b}_i \hat{b}_j \rangle = 0 \quad (4.79)$$

$$\langle \hat{b}_i^\dagger \hat{b}_j^\dagger \rangle = 0 \quad (4.80)$$

$$\langle \hat{b}_i \hat{b}_j^\dagger \rangle = \delta_{ij} (N(\omega_i) + 1) \quad (4.81)$$

$$\langle \hat{b}_i^\dagger \hat{b}_j \rangle = \delta_{ij} N(\omega_i) \quad (4.82)$$

where

$$N(\omega) = \frac{1}{e^{\beta\omega} - 1} \quad (4.83)$$

is the occupation of state i . This allows us to define the Lindblad coefficients

$$\gamma_\alpha(\omega) = \begin{cases} J(\omega) (N(\omega) + 1) & \text{if } \omega > 0 \\ J(\omega) N(\omega) & \text{if } \omega \leq 0 \end{cases} \quad (4.84)$$

where the *spectral density* is given by

$$J(\omega) = 2\pi \sum_{\mathbf{q}} |g_{\mathbf{q}}|^2 \delta(\omega - \omega_{\mathbf{q}}) \quad (4.85)$$

and depends both on the number of modes with frequency ω and our system's coupling affinity to them.

We end up with the phonon dissipator term

$$D_{\text{ph}}(\rho) = J(\Lambda) \left[(N(\Lambda) + 1)D[P_{\Lambda}]\rho + N(\Lambda)D[P_{\Lambda}^{\dagger}]\rho \right], \quad (4.86)$$

where $D[L]\rho = L\rho L^{\dagger} - 1/2(L^{\dagger}L\rho + \rho L^{\dagger}L)$. The dissipator terms correspond to a jump from $|+\rangle$ to $|-\rangle$ with emission of energy into the phonon bath, and a jump from $|-\rangle$ to $|+\rangle$ with the corresponding absorption of energy from the the phonon bath. The transition rate is proportional to the spectral density, which encapsulates all the information about the physical system that we need to supply. What is more, we only sample the spectral density at the given frequency Λ , which can be adjusted using other system paramaters allowing us to minimise the phonon decoherence effects.

Chapter 5

Rapid and Robust Spin

Amplification

The standard approach to implementing a quantum technology is to identify a physical system that can represent a qubit: it must exhibit two (or more) stable states, it should be manipulable through external fields and possess a long decoherence time. Provided that the system can controllably interact with other such systems, then it may be a strong candidate. Electron and nuclear spins, within suitable molecules or solid state structures, can meet these requirements. However the drawback with spin qubits is that they have not been directly measured through a detection of the magnetic field they produce. The magnetic moment of a single electron spin is orders of magnitude too weak to be detected by standard ESR techniques and even the most sensitive magnetometers still fall short of single spin measurement [150] - meanwhile the situation with nuclear spins is worse still. In a few special systems it is possible to convert the spin information into another degree of freedom. For example, a spin-dependent optical transition allow spin to photon conversion in some crystal defects [124, 151, 88], self-assembled semiconductor quantum dots [152, 153], and trapped atoms held in a vacuum [154]. Alternatively, spin to charge conversion is an

established technology in lithographic quantum dots [155]. However, the majority of otherwise promising spin systems do not have such a convenient property [156] and therefore cannot be measured directly.

One suggested solution is to ‘amplify’ a single spin, by using a set of ancillary spins that are (ideally) initialised to $|0\rangle$. We would look for a transformation of the form

$$|0\rangle|0\rangle^{\otimes n} \rightarrow |0\rangle|0\rangle^{\otimes n} \quad |1\rangle|0\rangle^{\otimes n} \rightarrow |1\rangle|1\rangle^{\otimes n}, \quad (5.1)$$

the idea being that the n ancillary spins constitute a large enough set that state of the art magnetic field sensing technologies can detect them. Note that the transformation need not be unitary or indeed even coherent: since the intention is to make a measurement of the primary spin, it is not necessary to preserve any superposition (that is, we need not limit ourselves to transformations that take $\alpha|0\rangle|0\rangle^{\otimes n} + \beta|1\rangle|0\rangle^{\otimes n}$ to a cat state like $\alpha|0\rangle^{\otimes n+1} + \beta|1\rangle^{\otimes n+1}$).

This is a rather broadly defined transformation and there are a number of ways that one might perform it. Clearly one would like to find the method that is the least demanding experimentally. Previous authors have proposed schemes using a strictly one-dimensional (1D) homogeneous lattice with continuous global driving [157], and an inhomogeneous three-dimensional (3D) lattice with alternating timed EM pulses [158]. The former result has the advantage of simplicity but the rate at which amplification occurs will inevitably be limited by the single dimension of the array; moreover such a system must be highly vulnerable to imperfect initialisation (i.e. finite temperature).

In this chapter we present an amplification procedure using a homogeneous two-dimensional (2D) square lattice. We show that a continuous global EM field can drive an amplification process that succeeds at finite temperatures (imperfect initialisation of the ancilla spins) and in the presence of decoherence. By bringing the

global EM field onto resonance with certain transitions, we are able to create a set of rules that govern locally how spins propagate over the lattice. We then look at the rate of increase in the total number of flipped spins as a measure of quality of the scheme. While our focus is on the 2D case, we are also able to predict the performance of the amplification protocol for a homogeneous 3D lattice with continuous driving.

5.1 Review of 1D Model

The case of a 1D lattice has been studied in detail by Lee and Khitrin [157]. Before moving to the 2D spin lattice that will form the core of the chapter, we first recall how to simplify the description of this (semi-infinite) 1D spin chain, with nearest neighbour Ising (ZZ) interactions. Under a microwave driving field of frequency ω , the Hamiltonian is given by

$$\mathcal{H} = \sum_{i=1}^{\infty} \epsilon_i \sigma_z^i + J_i \sigma_z^i \sigma_z^{i+1} + 2\Omega_i \sigma_x^i \cos(\omega t) \quad (5.2)$$

ϵ_i is the on-site Zeeman energy of spin i , and J_i is the magnitude of the coupling between spins i and $i + 1$. Ω describes the coupling of spin i and the microwave field. In this case, spin $i = 1$ is the one whose state is supposed to be amplified. We assume that the chain is uniform, such that $\Omega_i = \Omega$, $\epsilon_i = \epsilon$ and $J_i = J$, and that Ω is weak. Following the same procedure as in Section 4.2.1, we move into a frame rotating at frequency ω and make a rotating wave approximation, setting $\omega = \epsilon$:

$$\mathcal{H} = \sum_{i=1}^{\infty} J \sigma_z^i \sigma_z^{i+1} + \Omega \sigma_x^i. \quad (5.3)$$

In order to understand the dynamics of the system, it is instructive to explicitly separate all terms that involve a particular spin k :

$$\mathcal{H} = J(\sigma_z^{k-1} + \sigma_z^{k+1})\sigma_z^k + \Omega\sigma_x^k + \sum_{i \neq \{k, k-1\}} \Omega\sigma_x^i + J\sigma_z^i\sigma_z^{i+1} + \Omega\sigma_x^{k-1} \quad (5.4)$$

Choosing a driving field such that $\Omega \ll J$ means that spin k will only undergo resonant oscillations when the first term in Eq. 5.4 goes to zero - i.e. when the two spins neighbouring spin k are oriented in opposite directions. In any other configuration the Ising coupling takes the spin k off resonance with the microwave and no appreciable dynamics are expected.

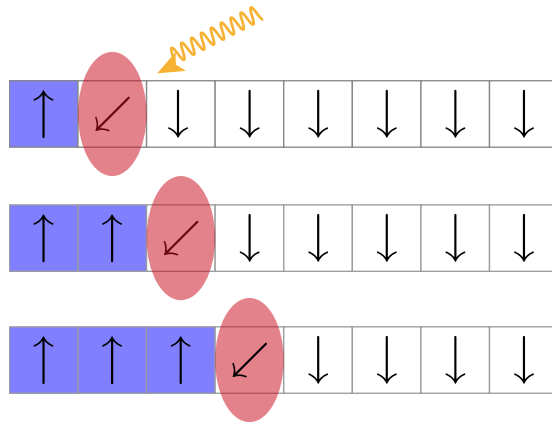


Figure 5.1: States of the 1D chain: only spins with one neighbour \uparrow and the other neighbour \downarrow are on resonance.

Let us now define a subset of states S that exist in the spin chain Hilbert space, $|n\rangle$, which have the first n spins of the chain in state $|\uparrow\rangle$ with the rest $|\downarrow\rangle$. If the rule we just derived holds exactly, these states define a closed subspace. We may then write a very simple isolated Hamiltonian for this subspace:

$$\mathcal{H}_S = \Omega \sum_{n=1}^{\infty} |n\rangle \langle n+1| + |n+1\rangle \langle n|. \quad (5.5)$$

The Hamiltonian couples states with n up-spins to those with $n - 1$ and $n + 1$, with coupling strength Ω .

5.2 Extension to 2D Model

With this simplification of the 1D Hamiltonian in mind, we progress now to a semi-infinite square spin lattice with nearest-neighbour ZZ interactions. For this case we have

$$\mathcal{H} = \sum_{i=1}^{\infty} \sum_{j=1}^{\infty} \epsilon \sigma_z^{i,j} + J \sigma_z^{i,j} \sigma_z^{i+1,j} + J \sigma_z^{i,j} \sigma_z^{i,j+1} + 2\Omega \sigma_x^{i,j} \cos(\omega t). \quad (5.6)$$

By again considering the terms affecting a particular spin in the main body of the lattice ($k(> 1), l(> 1)$ say) we find for $\omega = \epsilon$ and after moving to a rotating frame and making the rotating wave approximation:

$$\mathcal{H} = J \sigma_z^{k,l} (\sigma_z^{k+1,l} + \sigma_z^{k,l+1} + \sigma_z^{k-1,l} + \sigma_z^{k,l-1}) + \dots \quad (5.7)$$

where we do not explicitly write out terms not involving spin (k, l) . The microwave is now only resonant for spin (k, l) if it has two neighbour spins in each orientation. For a spin on the edge of the lattice there are an odd number of neighbours so resonance cannot be achieved in this case. However, applying a second microwave with $\omega = \epsilon - J$ allows resonant flips on the edge if two neighbours are down and one up - and this second field has no effect on the bulk spins.

The spin to be measured is the corner spin ($i = j = 1$) and so would form part of a wider computational apparatus. We may therefore assume that it is a different species with a unique resonant frequency. The dynamics of the whole lattice may then be summarised by three rules (in order of precedence):

1. The corner (test) spin is fixed.
2. An edge spin can flip if it has one of its neighbours up and two down.

3. A body spin can flip if it has two of its neighbours up and two down.

We begin by supposing all spins are initialised in the ‘down’ state apart from the test spin, which is located in the upper left hand corner of our lattice. We can describe this initial state by choosing two basis elements: $|0\rangle$ when the test spin is down, and $|1\rangle$ when the test spin is up. Using our heuristic rules we can see that these two states do not couple to each other - that $\langle 0|H|1\rangle = 0$. In fact $|0\rangle$ does not couple to any other state, so if we start in the $|0\rangle$ state no amplification occurs, as desired.

5.3 Building a Subspace Basis

We will now seek to construct a basis for the subspace containing our system evolution, by looking at states connected by our Hamiltonian. It will be convenient to represent these states on the nodes of a graph, using the edges to represent non-zero elements of the Hamiltonian.

Our starting point is the state $|1\rangle$, with just the corner spin ‘up’. From this position our rules allow two possibilities: either the spin to the right of the corner flips, or the spin below it flips (see Fig. 5.2). In each case, the magnitude of the transition matrix element is Ω . As we continue this procedure, we notice that the states that arise for each excitation number can be characterised by a non-increasing sequence of integers that represent the number of ‘up’-spins in each column of the lattice (see Fig. 5.2). Such sequences can also be used to define partitions of an integer: ways of splitting an integer up into a sum of other integers, e.g. $3 = 3 = 2 + 1 = 1 + 1 + 1$. In fact, the states that arise are in 1-to-1 correspondence with such partitions; we call these states ‘partition states’ and denote them with standard partition notation (see Fig. 5.2). The graph we have just described is depicted in Fig. 5.2 is known as ‘Young’s lattice’ and arises in areas of pure mathematics, such

construct the state $|k+1\rangle$ by eliminating the k -dimensional subspace with $k+1$ excitations, to which $|k\rangle$ does not couple.

Let $|\psi\rangle = \sum_{j \in P(k+1)} \alpha_j |\psi_j\rangle$ and consider the states $|\psi\rangle$ such that

$$0 = \langle k | H | \psi \rangle = \sum_{i \in P(k)} \sum_{j \in P(k+1)} c_i^* \alpha_j \langle \psi_i | H | \psi_j \rangle$$

but $\langle \psi_i | H | \psi_j \rangle = \Omega$ if i is a *parent* of j (a state connect to j , in the lattice row above it), and 0 otherwise, so

$$0 = \langle k | H | \psi \rangle = \sum_{j \in P(k+1)} \alpha_j \sum_{i \in \text{parents}(j)} c_i^*.$$

This is the equation of a hyperplane in $|P(k+1)|$ dimensions, defining the states that are not coupled to $|k\rangle$ through the Hamiltonian. There is a unique single state orthogonal to this hyperplane, $\beta_j = \sum_{i \in \text{parents}(j)} c_i$, to which $|k\rangle$ couples. So the only state with $k+1$ ‘up’-spins that $|k\rangle$ couples has coefficients proportional to β_j . After normalisation, we call this state $|k+1\rangle$.

Unfortunately there is no easy way to write down the partition states and weights for the n th row of the lattice. Fortunately, for our purposes, we only need to know that the states $|k\rangle$ exist and what the coupling between them is. To find this coupling, consider

$$\begin{aligned} g_{n-1,n} &= \langle n | H | n-1 \rangle \\ &= \frac{1}{N_{n-1} N_n} \sum_{i \in P(n)} \sum_{j \in P(n-1)} c_i^* c_j \langle \psi_i | H | \psi_j \rangle \\ &= \frac{1}{N_{n-1} N_n} \Omega \sum_{i \in P(n)} c_i^* \sum_{j \in \text{parents}(i)} c_j \\ &= \frac{1}{N_{n-1} N_n} \Omega \sum_{i \in P(n)} |c_i|^2 = \Omega \frac{N_n}{N_{n-1}} \end{aligned} \tag{5.8}$$

To find the N_n we need the sum of the squares of the weights of partitions in a given row. A standard result about Young's lattice immediately gives us this sum: $n!$ [159].

This result can be taken straight from the representation theory of the symmetric group: it can be shown that the nodes and their weights represent the irreducible representations and their dimensions. Given that the dimension of each representation is its multiplicity in the regular representation (with dimension $|S_n| = n!$), by dimension counting the result follows. However, for our purposes it is more enlightening to focus on a differential poset approach, which uses particular combinatorial features of the lattice to produce the result. Here we give a brief overview of the approach detailed by Sagan in [160].

Let L be an operator that takes a partition state to a sum of its children, and R take a state to the sum of its parents. For example

$$\begin{aligned} L|\psi_1\rangle &= |\psi_{1,1}\rangle + |\psi_2\rangle \\ R|\psi_{2,1}\rangle &= |\psi_{1,1}\rangle + |\psi_2\rangle \end{aligned}$$

We add a state $|\emptyset\rangle$ such that $L|\emptyset\rangle = |\psi_1\rangle$ and $R|\emptyset\rangle = 0$. Then

$$L^n|\emptyset\rangle = \sum_{i \in P(n)} c_i |\psi_i\rangle \quad (5.9)$$

and

$$R^n L^n |\emptyset\rangle = \sum_{i \in P(n)} |c_i|^2 \quad (5.10)$$

We then need to use two facts about the structure of the lattice: that each element has one more child than it does parents, and each pair of elements either share both

a single parent and a single child, or neither. The first of these properties is easy to see: each child corresponds to adding a square at a concave corner of the diagram, and each parent corresponds to removing a convex corner. These corners alternate along the boundary of the shape, starting and ending with concave ones, and so there is always one more child than parents. The second property requires more work, but is roughly because two elements share a parent if, when placed on top of one another they differ by precisely two squares. Taking the union of these shapes you can find the unique child that they also both share.

These properties imply the commutation relation $RL - LR = I$, so

$$R^n L^n |\emptyset\rangle = R^{n-1} L^n R |\emptyset\rangle + n R^{n-1} L^{n-1} |\emptyset\rangle = \dots = n! |\emptyset\rangle \quad (5.11)$$

and so, $n! = \sum_{i \in P(n)} |c_i|^2$.

Referring back to Eq. (5.8), and using $N_i = \sqrt{i!}$, we see that

$$\mathcal{H} = \Omega \sum_n \sqrt{n} (|n-1\rangle \langle n| + |n\rangle \langle n-1|). \quad (5.12)$$

In essence we have established a linear sequence of states, each coupled to the next analogously to the states on a 1D chain 5.5. However, each of our states is in fact a superposition of many configurations of the 2D array, and crucially the effective coupling from each state to the next increases along the sequence.

5.4 Rate of Spin Propagation

It has been shown (e.g. [161]) that a quantum state released at the end of a semi-infinite chain of states, with constant couplings, will travel ballistically: the average position of the state along the chain is proportional to the time passed, and inversely proportional to the coupling strength. Since, in the one-dimensional case, the posi-

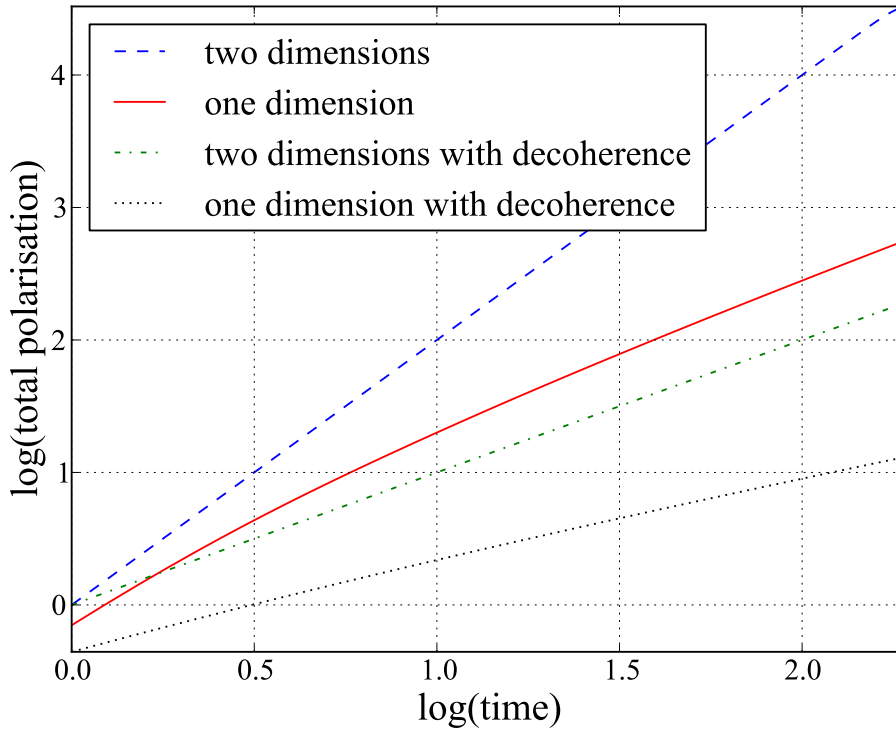


Figure 5.3: Expected total polarisation against time. Time in units of $\frac{1}{\Omega}$, dephasing rate $\Gamma = 1$. The gradient of the ‘one dimension with decoherence’ line tends to $\frac{1}{2}$ asymptotically.

tion is proportional to the number of spins that have flipped, we have that the total polarisation will increase linearly with time.

We can establish the rate of propagation in the 2D case using the ansatz that the time taken to travel between two neighbouring nodes is inversely proportional to the strength of the coupling between them. The total time is then $t_{2D} \propto \sum_{i=1}^n \frac{1}{\sqrt{i}} \simeq n^{\frac{1}{2}}$. As in the one-dimensional case, the position along the chain corresponds to the number of spins that have flipped, and so we would expect the total polarisation to be proportional to t^2 . This prediction of a quadratic speed-up of signal going from 1D to 2D is the central result of the chapter, and was confirmed by simple numerical simulations of Eq. (5.12) (Fig. 5.3).

5.5 Extension to 3D

Unfortunately the mapping from 2D to 1D is not readily extendible to 3D. However, our results so far could have been anticipated using simple dimensional arguments; if one postulates that the rate of spin propagation is proportional to the boundary of the region, one can predict the correct scaling behaviour. In 1D the boundary size is independent of the region size; no matter how many spins have flipped, it still has size one. The coupling strength between states $|n\rangle$ is constant. In the 2D case, the boundary size scales with the square root of the area, and the coupling goes with \sqrt{n} . In 3D, the boundary scales like the cube root of the volume squared, and so we expect the coupling to scale as $n^{\frac{2}{3}}$. Following similar logic to that used in 2D case: $t_{3D} \propto \sum_{i=1}^n \frac{1}{i^{\frac{2}{3}}} \simeq n^{\frac{1}{3}}$, and so $n \sim t^3$.

5.6 Robustness against Decoherence

We now consider the effect of decoherence. Much of the early work on continuous time quantum random walks looked at the speedup they afforded over their classical counterparts [162], but didn't make any statement about the conditions under which we would expect the quantum walk to exhibit classical behaviour, as we might expect in a regime of suitably heavy dephasing, say.

We begin by considering a collective noise operator: $L = \sum_n n |n\rangle \langle n|$. This represents noise that applies uniformly to the whole lattice: global fluctuations in the magnetic field, for example. As the effect of this type of noise depends only on the number of 'up' spins, the system remains in the reduced basis of number states calculated earlier, with only the coherences between these states affected.

Our starting point is the Lindblad master equation

$$\dot{\rho} = i[\rho, H] + \frac{1}{2}\Gamma(2L\rho L^\dagger - L^\dagger L\rho - \rho L^\dagger L). \quad (5.13)$$

We proceed by splitting up the equation into diagonal and off-diagonal terms

$$\dot{\rho}_{ii} = i \sum_{k=\pm i} (\rho_{ik}g_{ki} - \rho_{ki}g_{ik}) = -2 \sum_{k=\pm i} \text{Re} [\rho_{ik}g_{ki}] \quad (5.14)$$

$$\dot{\rho}_{ij} = i \left(\sum_{k=\pm j} \rho_{ik}g_{kj} - \sum_{k=\pm i} \rho_{kj}g_{ik} \right) - \Gamma \rho_{ij} \quad (5.15)$$

where g_{ij} is the coupling between states i and j . In the limit of heavy dephasing ($\Gamma \gg g$), we have a process similar to adiabatic following, and we can make the approximation

$$\Gamma \rho_{ij} \approx i \left(\sum_{k=\pm j} \rho_{ik}g_{kj} - \sum_{k=\pm i} \rho_{kj}g_{ik} \right).$$

We consider the ρ_{ij} as a set of $\frac{n(n-1)}{2}$ variables and solve for them in terms of the ρ_{ii} . Neglecting terms that are second order in $\frac{g}{\Gamma}$, and substituting back into Eq. (5.14) gives

$$\dot{\rho}_{ii} = - \sum_{j=i\pm 1} \frac{2|g_{ij}|^2}{\Gamma} (\rho_{ii} - \rho_{jj}).$$

Our quantum chain formally reduces to a classical Markov chain on the same statespace, with transition rates proportional to the coupling squared.

In one-dimension $g_{ij} = 1$ and we are reduced to a simple random walk on a semi-infinite line. By analogy with simple diffusion we expect that the resulting distribution is roughly Gaussian, with the expected number of flipped spins going with \sqrt{t} : the rate of spin propagation drops from t to \sqrt{t} . This result was confirmed numerically - although (Fig. 5.3) appears to show something closer to a $t^{\frac{2}{3}}$ dependence, (Fig. 5.4) shows that the \sqrt{t} value is recovered as time increases.

In the two-dimensional case $g_{ij} = \sqrt{j}$, $j = i + 1$: We get a random walk with increasing transition rates. Numerically (Fig. 5.3), we find that the rate of spin propagation drops from t^2 to t - still an encouraging scaling.

So far we considered a collective noise scenario, using a single Lindblad operator,

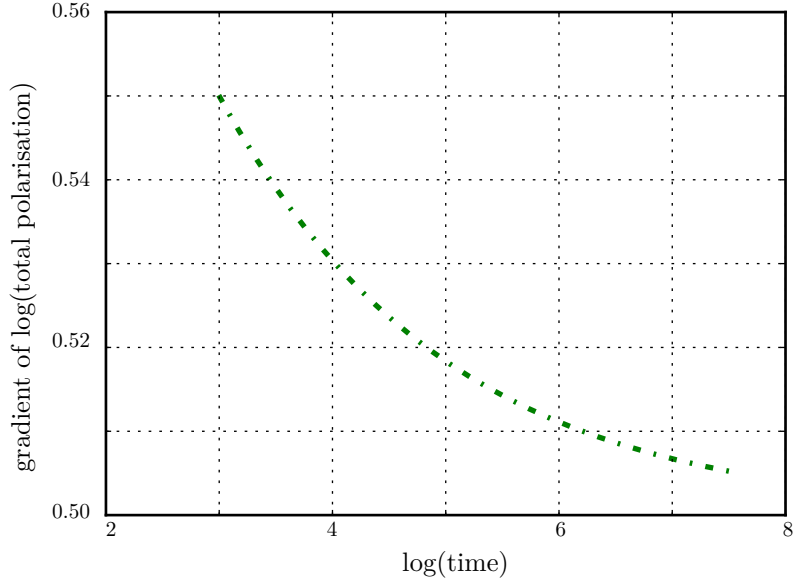


Figure 5.4: The gradient of the ‘one dimension with decoherence’ line tends to $\frac{1}{2}$ asymptotically.

$L = \sum_n n |n\rangle \langle n|$. This is convenient to analyse for our system, as the system remains in the subspace covered by our basis of number states. A more realistic model involves treating the noise occurring at each site as independent. In this case we have Lindblad operators of the form

$$L_i = \sigma_z^i \quad (5.16)$$

for lattice sites i . Following a similar procedure to before we find the equivalent classical chain to be

$$\dot{\rho}_{ii} = - \sum_{j \in P(i)} \frac{2|g_{ij}|^2}{\Gamma} (\rho_{ii} - \rho_{jj}) \quad (5.17)$$

where, crucially, the index now runs over all the partition states, rather than our basis of accessible states. In fact, in the 1D case these states are one and the same, and so the spin propagation goes as \sqrt{t} , as found in the collective noise case. In the 2D case, we are now performing a continuous-time classical random walk on Young’s

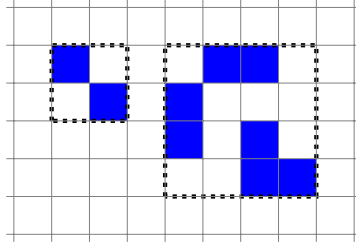


Figure 5.5: Maximum extent of propagation of initialisation imperfections in the lattice - due to propagation rules imperfections are unable to grow beyond the dotted bounding boxes.

lattice. We are able to use the property that each node always has one more child than parents, to predict that the rate of spin propagation will be proportional to t - the same as the collective noise case.

5.7 Robustness against Imperfect Initialisation

Finally we consider imperfect initial polarisation (i.e. finite temperature) - a property exhibited by any real experimental system. A fortuitous consequence of the propagation rules is that our system is particularly robust against this source of error; it is difficult for imperfections in the centre of the lattice to spread (Fig. 5.5).

To estimate an upper bound for our initialisation threshold we took a randomly initialised lattice, with given imperfection probability, and evolved it using purely deterministic rules, to see whether the imperfections grew to cover over half the lattice. We expect this to give a loose upper bound for the quantum case, as quantum imperfections will both grow and shrink, making it less likely that they will compound in the same manner as deterministic growth. Fig 5.6 shows the results of these simulations; below 4% the probability of growing to cover the majority of the lattice is negligible.

This threshold places our protocol well within experimental capabilities; for ex-

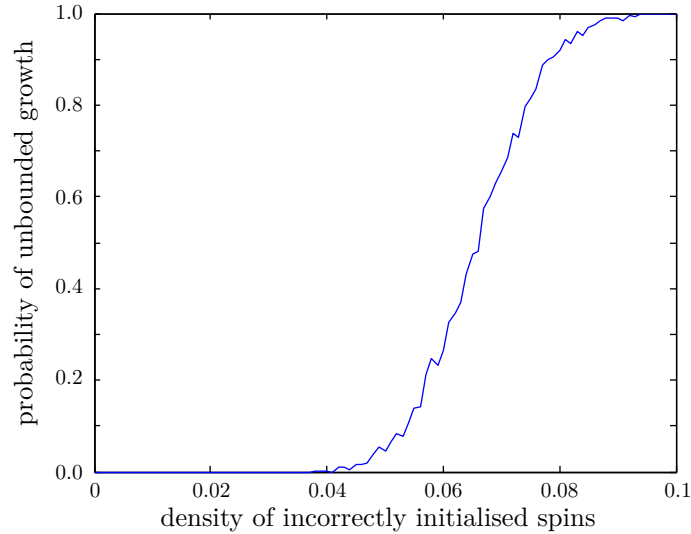


Figure 5.6: Probability that imperfections at given density will deterministically grow to cover over half the lattice.

ample for an array placed in a standard W-band electron spin resonance system (100 GHz) and cooled using liquid 4He to 1.4 degrees Kelvin, only 3.1% of electron spins will be in the ‘up’ state.

5.8 Conclusion and Further Work

Electron and nuclear spins have been employed in many of the early demonstrations of quantum technology but applications in real world QT are limited by the difficulty of measuring single spins. In this chapter we have shown that it is possible to rapidly and robustly amplify a spin state using a lattice of ancillary spins. The model we have employed corresponds to an extremely simple experimental system: a homogenous Ising-coupled spin lattice in one, two or three dimensions, driven by a continuous microwave field. We have constructed a natural basis for the problem and used this to assess the rate of amplification, both ideally and in the presence of environmental noise. We establish that the process can operate at finite temperature (imperfect initial polarisation) and under the effects of various forms of decoherence.

There are several directions in which the work presented in this paper could be extended. As noted, our strategy for the construction of the Hamiltonian for the reduced system does not transfer directly into the 3D case. It could be that further study of the system would yield a closed form, which would allow us to verify our claims about the rate of spin propagation in a 3D system.

There is also potential to develop the ideas discussed here to provide an experimental test for the regularity of a lattice structure: the ability to perform a controlled expansion, and later contraction, of the lattice polarisation would provide evidence of a uniform structure. Further theoretical work could focus on characterising the possible signatures of semi-regular array structures.

Chapter 6

A Reliable, Efficient Source for Indistinguishable Photons

6.1 Introduction

Single photon sources are an essential component of many quantum information processing (QIP) protocols, from quantum key distribution (QKD) protocols [17, 19] to linear optical quantum computing (LOQC) schemes [163, 164, 165]. As described in Section 2.3.1, optical schemes using path erasure can be used to generate long-range entanglement between physically separated systems [76, 166, 167, 168]. Such procedures can be repeated on many different pairs of systems and so create a distributed cluster state [169, 165], which is the key resource required for implementation of measurement based quantum computing (Section 2.2.3).

In order to be useful in these applications, a photon source must be of a high quality in two respects: it must reliably produce a single photon on demand, and the photons produced must be indistinguishable from one another.

To be perfectly indistinguishable, photons must have the same pulse width, bandwidth, polarization, arrival time at the detector, and carrier frequency. Indistin-

guishability is vital if photons are to exhibit high quality quantum interference, and its consideration is therefore critical when designing photon sources for LOQC and path erasure entanglement generation. If photons can be distinguished even in principle, this can lead directly to imperfect LOQC gates, or to a lessening of the degree of entanglement generated in distributed cluster states. In QKD, indistinguishability is less important as interference effects are not required, but it is of paramount importance that no more than one photon is emitted on demand; multiple photon emission leads to security loopholes [165].

As a measure of indistinguishability we exploit the Hong-Ou-Mandel (HOM) effect [170], which relies on the bunching behaviour of identical photons when they are incident on a beam splitter with the same temporal profile. As explained in Section 4.1.3, if the photons are indistinguishable, they will always emerge in and be detected in the same output arm (Fig. 6.1). The number of same-arm detection events are usually plotted as a function of arrival time of the two photons - and hence a ‘dip’ at a time difference of zero is an indicator of indistinguishability. The

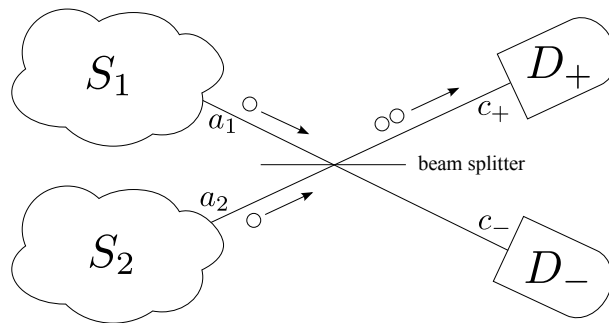


Figure 6.1: Hong-Ou-Mandel effect: a pair of photons from two sources S_1 and S_2 incident on a beam splitter exhibit perfect bunching behaviour if they are completely indistinguishable. In this case the detectors D_+ and D_- will never click simultaneously.

degree of distinguishability can be given by the Hong-Ou-Mandel visibility, v_{HOM} , which is the proportion of same-arm detections, over many runs of the experiment.

It is worth noting that this definition of v_{HOM} differs from the Hong-Ou-Mandel dip commonly measured in experiments: the typical experimental setup involves continuously pumped systems, and looks for an absence of simultaneous detections in different detector arms; we consider an on-demand photon pair, and look at the probability that the two detections are in the same arm *over the complete run of the experiment*.

As mentioned above, besides indistinguishability an essential characteristic of a good photon source is that it will consistently produce a single photon, but never more than one, on demand [171]. A laser source can be attenuated so that it gives zero or single photons most of the time. However, photons from classical laser sources obey Poissonian statistics so that in order to keep the two-photon event rate low the probability of a single photon may become unworkably small for many applications. In addition to this, Poissonian sources are unsuitable for two-photon interference experiments since the rate of two photon production from a single source is similar to that for a single photon from each source [165]. It is worth noting that perfect efficiency should never be a requirement in any realistic optical QIP scheme, as these schemes must always be tolerant to photon loss within other parts of the apparatus. However, a good photon source must be reasonably efficient to be useful, and we should not be forced to trade efficiency for other desirable characteristics.

The use of low-dimensional quantum systems as single photon sources avoids the efficiency problems of Poissonian sources. Successful experimental implementations have been realised in a number of different systems including atom-cavity schemes [172, 173, 174, 175], quantum dots [176, 177] and diamond colour centres [178, 179, 180]. While the majority of the work has been focussed on the efficient production of a single photon, recent experiments in NV centres [179, 180] and quantum dots [181, 182] have demonstrated two-photon interference effects from different sources, albeit sacrificing efficiency by filtering out undesired frequencies. It has been suggested

that cavities could be used in these systems, to enhance the emission into the target mode, reducing the need for filtering [183].

In order to improve the characteristics of a photon source, it is not sufficient to simply consider the material parameters of the system being used: one should also consider the approach used to control the system. Perhaps the simplest strategy is to excite the system first optically, either coherently or incoherently, and wait for the system to relax into its ground state, emitting a photon in the process; we will henceforth refer to this as the ‘pulse-relax’ technique. This approach makes minimal resource demands on the system and, due to its simplicity, is the technique proposed in some remote entanglement generation schemes [76, 167]. The pulse-relax approach is problematic in systems where the excited state is sensitive to decoherence, which will degrade the photon’s indistinguishability [184, 185, 76, 186]. These effects can be reduced, for example by exploiting the Purcell effect to enhance the emission rate into the desired photon mode [187, 188] or by using temporal post-selection of emitted photons [186]. However with experimental limits on cavity couplings both of these inevitably lead to lower efficiency as the proportion of emissions that are utilized falls [189].

A fundamentally different approach is to use more elaborate QED schemes to release a photon from the system in a controlled manner. In particular single photon sources using a Raman approach have been analysed [184, 185] and experimentally realised [172]. The approach places more demands on the system, requiring a three level system with a Λ -system configuration. Each arm is coupled to either a classical or a quantum light field; in Fig 6.2 we show the situation when one arm is driven classically, with a coupling Ω , and the other arm is coupled to a cavity mode with strength h . By detuning both arms of the Λ -system by the same amount ν , population is transferred from one arm to the other, whilst suppressing population in the top state. Provided that the coupling strengths are small in comparison to

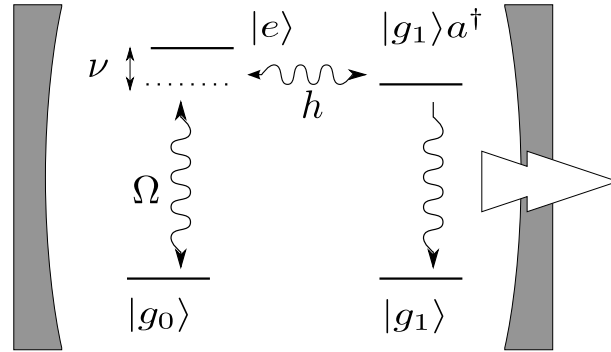


Figure 6.2: Effective level structure of a driven Λ -system inside an optical cavity. Here, Ω is the amplitude of an external (laser) driving field, h the optical dipole-cavity-coupling, and ν the shared detuning of the laser and the cavity transition frequency from the excited state. The system can decay into state $|g_1\rangle$ and in doing so emit a photon into a well-defined external mode.

the detuning, $\Omega \ll \nu$ and $h \ll \nu$, we induce an effective coupling between the two low-lying states, which causes oscillations with Rabi frequency $h\Omega/4\nu$. The population in the excited state remains small at all times, and so any decoherence that arises due to environmental coupling to this excited state may be reduced using this strategy. In particular, a common realisation of a single photon source is a quantum dot, in which the excited state typically has a different charge configuration to the ground state. This causes local lattice distortions, which in turn locally alter the electronic bandgap, thus inducing a coupling to acoustic phonons [190, 191] that can act as a noise source.

In this chapter we provide a detailed and realistic analysis of the effects of the lattice vibrations for single photon emitters based on (self-assembled) semiconductor quantum dots. By comparing a standard pulse-relax approach with the aforementioned Raman technique, we find that the latter can offer considerable improvements in terms of both photon indistinguishability and source efficiency. Our results extend and complement a previous study [185] which considered generic pure dephasing noise. However, here we also show that the precise choice of control parameters

is important if phonon-induced decoherence is to be successfully suppressed.

6.2 Our model

For convenience of notation we consider the Λ -system detailed in Fig. 6.2 for both the pulse-relax and the Raman approach. In both cases one arm of the system is coupled to the cavity with detuning ν . In the Raman scheme, the other arm is driven with strength Ω by a laser with a matching detuning ν , and the system starts in state $|g_0\rangle$. By contrast, we model the pulse-relax approach by setting $\Omega = \nu = 0$ and starting in state $|e\rangle$, ignoring the details of the excitation process. The fact that we are neglecting the excitation step in this simplified picture will slightly favour the pulse-relax approach in terms of production rate, but is largely justified on the assumption that the initial excitation process takes place quickly compared with other system dynamics. Our framework thus allows us to consider the pulse-relax approach as a special case of the master equation we will now derive for the Raman approach.

We split the Hamiltonian into contributions from the emitter system and cavity (sys), the driving laser (dr), the unperturbed phonon bath (ph) and interaction terms between the system and phonon bath ($sys - ph$), system and target external mode ($sys - mod$), and system and other external modes ($sys - ext$):

$$H = H_{sys} + H_{dr} + H_{ph} + H_{sys-ph} + H_{sys-mod} + H_{sys-ext} . \quad (6.1)$$

The $H_{sys-mod}$ and $H_{sys-ext}$ terms are well understood, and we will treat these by adding in the appropriate Lindblad terms to our final master equation. In the following, we shall describe the rest of these terms separately.

Using the standard Jaynes-Cummings Hamiltonian (Section 4.2.2), the Λ -system

coupled to a cavity mode with strength h and detuning ν from resonance can be described by the following Hamiltonian:

$$H_{sys} = (\omega + \nu) |e\rangle \langle e| + \omega a^\dagger a + \frac{h}{2} (|g_1\rangle \langle e| a^\dagger + \text{h.c.}) , \quad (6.2)$$

where h.c. denotes the Hermitian conjugate. ω is the cavity mode frequency.

We can restrict ourselves to one or zero cavity photons since the Jaynes-Cummings model preserves excitation number and after photon emission we assume that the emitter system remains in state $|g_1\rangle$ - i.e. we make the approximation that once a photon has escaped re-excitation does not occur - at least until an appropriate reset step (such as thermal relaxation) which we assume happens on a much longer timescale than the photon emission dynamics. This allows us to replace $|g_1\rangle a^\dagger$ with a new combined atom-photon state $|g_a\rangle$ and $a^\dagger a$ with $|g_a\rangle \langle g_a|$.

The term H_{dr} describes a laser driving the transition $|g_0\rangle \leftrightarrow |e\rangle$ with coupling strength Ω , and whose frequency is detuned from resonance by the same ν parameter, yielding

$$H_{dr} = \Omega \cos(\omega t) (|e\rangle \langle g_0| + \text{h.c.}) . \quad (6.3)$$

After performing the rotating wave approximation, assuming that $\omega \gg \nu, h, \Omega$, we are left with

$$H_{sys} + H_{dr} = \nu |e\rangle \langle e| + \frac{1}{2} (h |g_a\rangle \langle e| + \Omega |e\rangle \langle g_0|) + \text{h.c.} \quad (6.4)$$

for the total system Hamiltonian.

We model the phonons as a bath of harmonic oscillators with creation and an-

annihilation operators, b_q^\dagger and b_q , as in Section 4.3:

$$H_{ph} = \sum_q \omega_q b_q^\dagger b_q, \quad (6.5)$$

which couple to the exciton state $|e\rangle$ through the deformation coupling with coupling constants $f_q = D|q|$ in the usual way [191]:

$$H_{sys-ph} = |e\rangle \langle e| \sum_q f_q (b_q^\dagger + b_q). \quad (6.6)$$

The effect of the phonon bath on a driven quantum dot can be described using a Lindblad master equation [192, ?], where the Lindblad operators induce phonon-assisted transitions between the dressed system eigenstates [193]. We follow the derivation from Section 4.3. To derive the master equation we must first diagonalise the system Hamiltonian, $H_{sys} + H_{dr}$. We find that the eigenvalues are

$$\begin{aligned} \lambda_0 &= 0, \\ \lambda_\pm &= \frac{\nu \pm \sqrt{\nu^2 + \Omega^2 + \hbar^2}}{2}, \end{aligned} \quad (6.7)$$

with corresponding eigenvectors

$$\begin{aligned} |\psi_0\rangle &= n_0 (h |g_0\rangle - \Omega |g_a\rangle), \\ |\psi_\pm\rangle &= n_\pm (\Omega |g_0\rangle + h |g_a\rangle + 2\lambda_\pm |e\rangle). \end{aligned} \quad (6.8)$$

n_0 and n_\pm are appropriate normalisation factors. We now make the Born and Markov approximations which lead to the master equation [194] in standard Lindblad form:

$$\dot{\rho} = i [\rho, H] + D_{ph}(\rho) \quad (6.9)$$

with the phonon dissipator given by

$$D_{ph}(\rho) = J(\Lambda) \left[(N(\Lambda) + 1) D[P_\Lambda] \rho + N(\Lambda) D[P_\Lambda^\dagger] \rho \right] \quad (6.10)$$

where $D[L]\rho = L\rho L^\dagger - 1/2(L^\dagger L\rho + \rho L^\dagger L)$, $\Lambda = \lambda_+ - \lambda_-$, and $P_\Lambda = -|\psi_-\rangle\langle\psi_+|$. Note that the phonons only induce transitions between the two optically bright system eigenstates and do not couple to the dark $|\psi_0\rangle$. In the above equation $N(\Lambda)$ is the bosonic mode occupation number:

$$N(\omega) = \frac{1}{e^{\beta\omega} - 1} \quad (6.11)$$

$\beta = (k_B T)^{-1}$ and we shall henceforth consider all systems at room temperature, $T = 298$ K. The spectral density function $J(\omega)$ represents the electron-phonon coupling weighted by the density of phonon modes [194]. The quantum dot system we consider is well described by taking [192]

$$J(\omega) = \alpha\omega^3 e^{-\left(\frac{\omega}{\omega_c}\right)^2}. \quad (6.12)$$

We take $\alpha = 0.0027$ ps⁻¹ and $\omega_c = 2.2$ ps⁻¹, values that agree well with experiments on self-assembled quantum dots [190, 195].

We absorb the rates in (6.10) into the Lindblad operators to obtain following decoherence operators:

$$U_+ = \sqrt{J(N+1)} |\psi_-\rangle\langle\psi_+| \quad (6.13)$$

$$U_- = \sqrt{JN} |\psi_+\rangle\langle\psi_-| \quad (6.14)$$

where we have taken $J = J(\Lambda)$ and $N = N(\Lambda)$. Note that if non-Markovian dynamics are taken into account [196] this can lead to effects on the ultra-short

timescale, but these are in general much shorter than typical dynamics studied here.

As a measure of the degree of indistinguishability of the photons produced in the emission process, we consider the HOM visibility, which is the normalised probability of same arm detections obtained over many runs of the experiment,

$$v_{\text{HOM}} = \frac{p_{\text{same}} - p_{\text{diff}}}{p_{\text{same}} + p_{\text{diff}}}, \quad (6.15)$$

where $p_{\text{same}} = p(D_+ \cap D_+) + p(D_- \cap D_-)$ and $p_{\text{diff}} = p(D_+ \cap D_-) + p(D_- \cap D_+)$ with $p(D_x \cap D_y)$ being the probability of obtaining a click in detector D_y followed by a click in detector D_x . Note that HOM visibility, v_{HOM} , as described here is not the standard HOM dip figure from the literature: the HOM visibility measures the similarity of two single-photon wave packets, not two incoherently pumped sources. We assume that both systems start their evolution at the same time, so that the wavepackets coincide on the beam splitter.

In order to calculate v_{HOM} we thus need to consider photons emitted from two copies of the system S_1 and S_2 , one for each input arm of the beam splitter interferometer. The joint state of the system then inhabits the space $S = S_1 \otimes S_2$ (Fig. 6.1). We label the two cavity modes using annihilation operators a_1 and a_2 . Using the input-output formalism (e.g [115]) and neglecting incoming light, we can describe the modes outside the cavities as $a_{i,\text{out}} = \sqrt{\kappa}a_{i,\text{in}}$, where κ is the cavity leakage rate. The modes corresponding to detection in D_{\pm} are labelled c_{\pm} respectively. Due to the transformation performed by the beam splitter, c_{\pm} can be written in terms of a_1 and a_2 as follows:

$$c_+ = \sqrt{\kappa} \frac{1}{\sqrt{2}} (a_1 + a_2), \quad (6.16)$$

$$c_- = \sqrt{\kappa} \frac{1}{\sqrt{2}} (a_1 - a_2). \quad (6.17)$$

We assume that the field in the mode outside the cavity is directly related to the field inside, neglecting the process of escape from the cavity. The effect on the system $S = S_1 \otimes S_2$ of a detection in the plus or minus output mode is then described by the projection operators

$$C_{\pm} = |g_1\rangle \langle g_a| \otimes \mathbf{1} \pm \mathbf{1} \otimes |g_1\rangle \langle g_a|. \quad (6.18)$$

We could now simulate many trajectories of this system and build up an estimate of v_{HOM} by averaging these [197]. Instead we introduce a technique that we call the *semi-quantum master equation* method, which will allow us to find v_{HOM} in a single run of a master equation acting on a slightly larger Hilbert space.

6.3 Introducing the Semi-Quantum Master Equation Method

We are often interested in ‘observable events’ in quantum systems, such as the emission of a photon. When an event is observed the system undergoes a transition due to wave function collapse. During a period when no event is observed the system evolves according to a conditional master equation, reflecting the fact if events could be observed but are not, then this also informs our knowledge of the state. In order to answer questions about the probabilities and time distributions of events or chains of events, one approach is to use a quantum jump master equation to generate individual trajectories of the system. In each time step we decide probabilistically whether an event should occur. If it does occur then the system collapses according to a quantum jump; if it does not occur then the system evolves conditioned on no jump occurring. Statistics about the quantities of interest are built up as many trajectories are created.

Here we look at a different approach to calculating the quantities relating to events that occur in such systems. Instead of simulating multiple trajectories of the system, we efficiently increase the size of the statespace to record the information of interest. This allows us to calculate the desired system properties, and their time evolution, by solving a single master equation.

Consider a system that can exist in a number of different states. Let a movement between these states constitute an event, and assume that each kind of event happens at a given rate. Such a system is heavily reminiscent of a classical continuous time Markov chain (CTMC), which can be represented as a graph with the states as nodes and the edges events weighted by the transition rates (Fig. 6.3). Given an

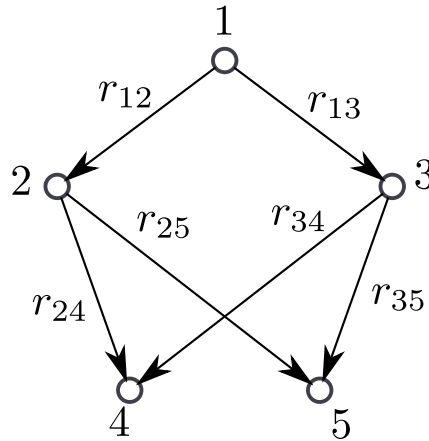


Figure 6.3: A classical continuous-time Markov chain, with statespace $W = \{1, 2, 3, 4, 5\}$. The edge weight, r_{ij} , represents the transition rate from state i to state j . If $\rho_i(t)$ is the population in state i at time t , the system is governed by the rate equations $\dot{\rho}_i = \sum_{j \in W} r_{ji} \rho_j$.

initial state i in a chain of size n , we can calculate the probability that at a later time t the chain is in state j , by solving the rate equations - a set of n ordinary differential equations.

Quantum systems differ from classical continuous-time Markov chains due to quantum superposition. We are not able to simply record the population in each

quantum state as inter-state coherences are also important. Using a Markov chain to model the whole quantum system is not possible by definition - systems that can be modelled in this way do not exhibit quantum behaviour.

In what follows it is helpful to explain carefully what we mean by ‘state’. In quantum systems a state is usually a vector in the Hilbert space of the system. We shall call this a quantum-state. We can also refer to the ‘state’ of the overall process, considering for example a system that has emitted a photon to be in a different process-state to one which has not. A system changes process-state when an event is observed.

Whereas thinking in terms of the CTMC is not useful when considering quantum-states, it is an effective way to think about process-states. As process-states are separated by an observed event, no coherences can exist between the two histories, making a CTMC approach feasible. Of course, process-states alone are not enough to model the whole system. Each process-state needs its own copy of the system attached to it. We can think of a Markov chain with a copy of our system at each node, where the transition rates are determined by the jump Lindblad operators corresponding to the events. Another way of thinking about this is that we extend our overall space with a set of process-states, to allow us to record events in the system.

Formally, we take a set of process-states S_P , transitions between which correspond to our observable jump events described by jump operators $J_Q^{(i)}$. We extend the Hilbert space of our quantum system S_Q by forming the tensor product:

$$S = S_Q \otimes S_P. \quad (6.19)$$

The new Hamiltonian is given by

$$H = H_Q \otimes \mathbf{1}. \quad (6.20)$$

If event $J_Q^{(i)}$ causes a transition from system state a to b we say it is of type (a, b) .

Its action on the extended system S is described by

$$J^{(i)} = J_Q^{(i)} \otimes |b\rangle \langle a|. \quad (6.21)$$

For any other Lindblad operators acting on the system $L_Q^{(i)}$, we need to create a set of size $|S_P|$ Lindblad operators - one to operate on each subspace independently:

$$s(L_Q^{(i)}) = \left\{ L_Q^{(i)} \otimes |j\rangle \langle j|, j \in S_P \right\}. \quad (6.22)$$

At first glance it might appear that we have increased a system of size $m = |S|$ to size mn , where $n = |S_P|$. Whilst this is true, the situation is not as bad as it seems at first, because the coherences between the different subsystems are unimportant – instead of a density matrix of size $(nm)^2$ we can use a system of size nm^2 , an increase linear in the number of system states. In practice we can often do better than this by eliminating unnecessary states from some of the subsystems.

As a simple concrete example, consider a resonantly driven two-level system $S_Q = \{|g\rangle, |e\rangle\}$, with Hamiltonian

$$H_Q = \Omega (|g\rangle \langle e| + |e\rangle \langle g|). \quad (6.23)$$

Suppose that it is also possible for the system to spontaneously emit from state $|e\rangle$

into the environment - a transition described by the jump operator

$$J_Q = |g\rangle \langle e|. \quad (6.24)$$

We are interested in knowing about the time distribution of the first time a photon is emitted. We add the two process-states 0 and 1, indicating whether the event has occurred or not. Our new system is described by:

$$S = \{|g0\rangle, |e0\rangle, |g1\rangle, |e1\rangle\} \quad (6.25)$$

$$H = \Omega (|g0\rangle \langle e0| + |e0\rangle \langle g0| + |g1\rangle \langle e1| + |e1\rangle \langle g1|) \quad (6.26)$$

$$J_1 = |g1\rangle \langle e0| \quad (6.27)$$

$$J_2 = |g1\rangle \langle e1|. \quad (6.28)$$

The population in the 1 subspace at time t will give us the probability a photon has been emitted by this time.

If we only cared about this distribution, we could reduce the size of the system by replacing the states $|g1\rangle$ and $|e1\rangle$ with a single state $|1\rangle$ to keep track of the cumulative jump probability over time. We would need to remove the last two terms from the Hamiltonian as well as J_2 , and set $J_1 = |1\rangle \langle e0|$. Figure 6.4 shows the cumulative jump probability for this system, showing agreement between the SQME results and Monte Carlo simulations with increasing numbers of runs.

6.4 Applying the Semi-Quantum Master Equation Method

When calculating v_{HOM} we must consider events in which photons trigger either detector, and events in which photons are spontaneously emitted into the environ-

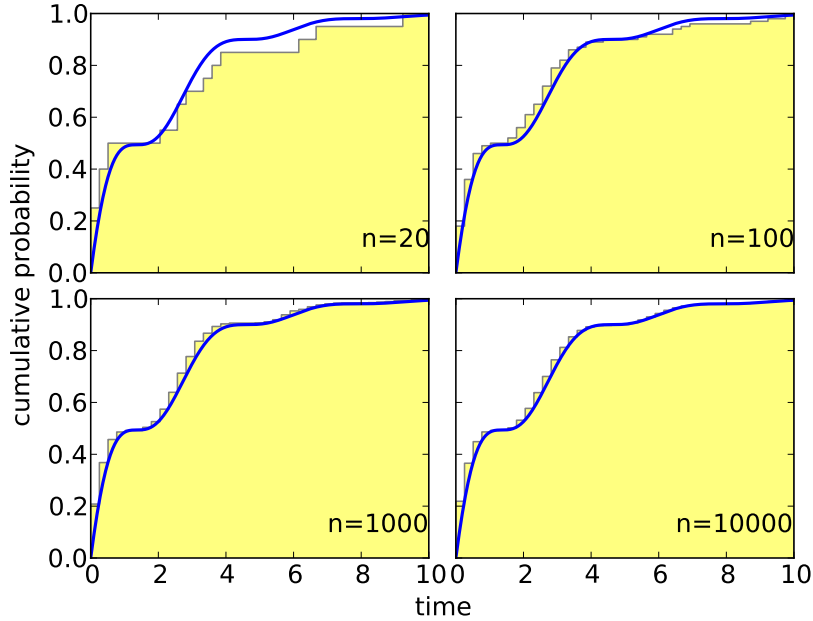


Figure 6.4: Comparison of semi-quantum master equation approach with Monte Carlo simulations of $n=20$, 100, 1000, and 10000 runs, for the system described by 6.25- 6.28. For the cumulative histogram plots we used horizontal binning with 40 bins, which explains why the horizontal resolution does not improve further for the larger values of n .

ment. We introduce a set of process-states to record and labels these event classes (Fig. 6.5):

$$S_P = \{P_0, P_+, P_-, P_S, P_D, P_E\}. \quad (6.29)$$

The process-state starts as P_0 and remains there until an event of interest occurs. $P_{+/-}$ represents the process-state after a single photon has been detected in the $D_{+/-}$ detectors respectively. After a second photon has been detected the process-state becomes $P_{S/D}$ depending on whether the second photon was detected in the same or different detector as the first. If at any point a photon is emitted into the environment the process moves to state P_E . When calculating the indistinguishability

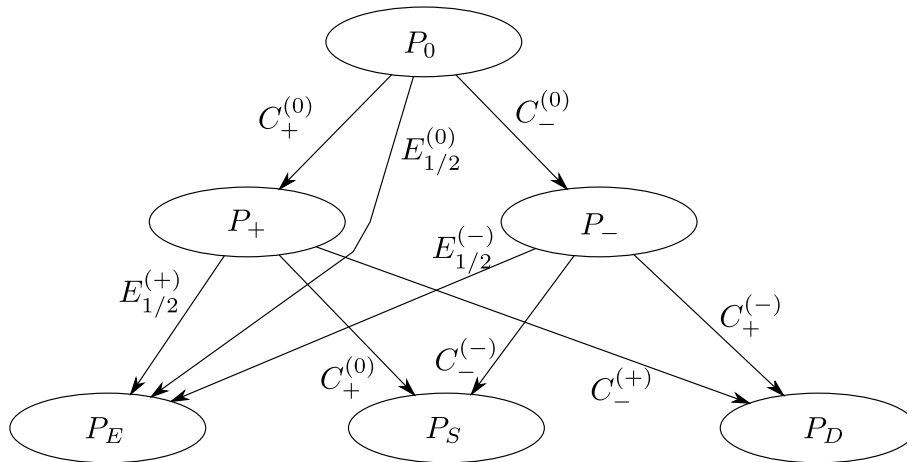


Figure 6.5: The system jump-space: On the first jump the system moves to P_+/P_- depending on the arm in which the photon is detected. After the second jump the system moves to state P_S/P_D depending on whether the second photon was detected in the same or different arm to the first. At any point the system can undesirably spontaneously emit into the environment, moving to the junk state P_E .

bility we can then ignore any population in state P_E , but we must include it when considering the overall efficiency of the process.

We must also identify the operators that cause the movement between the process-states. Before doing this we extend the state-space S of the system to include the process-states:

$$S = S_1 \otimes S_2 \otimes S_P. \quad (6.30)$$

The detection operators are then given by

$$C_+^{(0)} = C_+ \otimes |P_+\rangle \langle P_0| \quad (6.31)$$

$$C_+^{(+)} = C_+ \otimes |P_S\rangle \langle P_+| \quad (6.32)$$

$$C_+^{(-)} = C_+ \otimes |P_D\rangle \langle P_-| \quad (6.33)$$

$$C_-^{(0)} = C_- \otimes |P_-\rangle \langle P_0| \quad (6.34)$$

$$C_-^{(-)} = C_- \otimes |P_S\rangle \langle P_-| \quad (6.35)$$

$$C_-^{(+)} = C_- \otimes |P_D\rangle \langle P_+| \quad (6.36)$$

where for example $C_+^{(-)}$ is the jump operator representing a second detection in the D_+ detector, when the first detection was in D_- . The spontaneous emission operators are given similarly:

$$E_1^{(0)} = |g_1\rangle \langle e| \otimes \mathbf{1}_S \otimes |P_E\rangle \langle P_0| \quad (6.37)$$

$$E_2^{(0)} = \mathbf{1}_S \otimes |g_1\rangle \langle e| \otimes |P_E\rangle \langle P_0| \quad (6.38)$$

$$E_1^{(+)} = |g_1\rangle \langle e| \otimes \mathbf{1}_S \otimes |P_E\rangle \langle P_+| \quad (6.39)$$

$$E_2^{(+)} = \mathbf{1}_S \otimes |g_1\rangle \langle e| \otimes |P_E\rangle \langle P_+| \quad (6.40)$$

$$E_1^{(-)} = |g_1\rangle \langle e| \otimes \mathbf{1}_S \otimes |P_E\rangle \langle P_-| \quad (6.41)$$

$$E_2^{(-)} = \mathbf{1}_S \otimes |g_1\rangle \langle e| \otimes |P_E\rangle \langle P_-| \quad (6.42)$$

where here $E_1^{(+)}$ represents a emission from S_1 acting after the first photon was detected in the D_+ detector.

Finally we must modify our phonon decoherence operators. The subspaces corresponding to different process-states, are classically separated by observable events. These classically separated branches cannot exhibit interference, and we can there-

fore take the decoherence processes to occur independently on each branch:

$$U_{+,1}^{(0)} = \sqrt{J(N+1)} |\psi_{-}\rangle \langle \psi_{+}| \otimes \mathbf{1}_S \otimes |P_0\rangle \langle P_0| \quad (6.43)$$

$$U_{-,1}^{(0)} = \sqrt{JN} |\psi_{+}\rangle \langle \psi_{-}| \otimes \mathbf{1}_S \otimes |P_0\rangle \langle P_0| \quad (6.44)$$

$$U_{+,1}^{(+)} = \sqrt{J(N+1)} |\psi_{-}\rangle \langle \psi_{+}| \otimes \mathbf{1}_S \otimes |P_{+}\rangle \langle P_{+}| \quad (6.45)$$

$$U_{-,1}^{(+)} = \sqrt{JN} |\psi_{+}\rangle \langle \psi_{-}| \otimes \mathbf{1}_S \otimes |P_{+}\rangle \langle P_{+}| \quad (6.46)$$

$$U_{+,1}^{(-)} = \sqrt{J(N+1)} |\psi_{-}\rangle \langle \psi_{+}| \otimes \mathbf{1}_S \otimes |P_{-}\rangle \langle P_{-}| \quad (6.47)$$

$$U_{-,1}^{(-)} = \sqrt{JN} |\psi_{+}\rangle \langle \psi_{-}| \otimes \mathbf{1}_S \otimes |P_{-}\rangle \langle P_{-}| \quad (6.48)$$

with similar operators acting on the second system. We do not need decoherence operators acting on the P_S , P_D or P_E , since we are only concerned with populations in, and not coherences between, these states. Moreover, we only really need to keep track of the total population in each of these subspace, and not the populations of each state that make up each subspace - a fact that we exploit to reduce the dimension of our problem for the numerical simulations.

We form a Lindblad master equation using these 24 Lindblad operators:

$$\dot{\rho} = i[\rho, H] + \sum_i \gamma_i \left(L_i \rho L_i^\dagger - 1/2(L_i^\dagger L_i \rho + \rho L_i^\dagger L_i) \right). \quad (6.49)$$

The γ_i are the rates for each process. As noted earlier for the $U_{\pm,i}^{(j)}$ this rate is 1, as the rates have been incorporated into the Lindblad operators. For the $C_{\pm}^{(i)}$ we need $\gamma = \kappa$, the cavity leakage rate, which we take to be $3h$, a choice that allows for a reasonable enhancement of photon emission from the emitter system into the desired mode outside of the cavity, whilst preventing cavity photons being reabsorbed by the emitter system. For the $E_i^{(j)}$ we take $\gamma = 0.005ps^{-1}$, assuming a radiative lifetime of 200 ps. Our model allows only for spontaneous emission directly from the excited state $|e\rangle$; we assume that there is no loss from the cavity to modes

other than the target waveguide mode, and that all photons that are emitted into the target mode are detected. For similar cavities we expect these effects to impact the two approaches to equal extent.

The dimension of this extended space S is $4 \times 4 \times 6 = 96$. In fact we can reduce this by eliminating some unnecessary states from the subspaces. By carefully considering the basis states accessible in each the subspace corresponding to each process, we can reduce the number of system states to $9 + 6 + 6 + 1 + 1 + 1 = 24$. For our simulation we will need to calculate the density matrix for this system. As noted in the previous section, no coherences can exist between the different process-state subspaces. This reduces the number of density matrix elements we need to track to $9^2 + 6^2 + 6^2 + 1 + 1 + 1 = 116$.

6.5 Results

Fig. 6.6 shows the HOM visibility obtained from, and spectral density used in, simulations of the pulse-relax technique. At low coupling strengths the phonon spectral density is small, and so phonon decoherence is largely avoided giving high indistinguishability. As described earlier, we have fixed κ , the cavity leakage rate, to be $3h$ so the effective coupling to the the target mode is proportional to the Purcell factor $h^2/\kappa \sim h$. This means that, for small h , the rate of photon emission into the cavity mode is slow and thus spontaneous emission into environmental optical modes is a problem. To take account of this effect, we define the ‘combined HOM visibility’, which is the product of success probability and bare HOM visibility, which approaches zero as $h \rightarrow 0$. Taking large coupling strengths allows one to access the region to the higher frequency side of the hump in the phonon spectral density and so could avoid this problem, but is unrealistic given the cavity parameters currently obtainable experimentally. In the experimentally feasible region ($h < 1$) [198] we

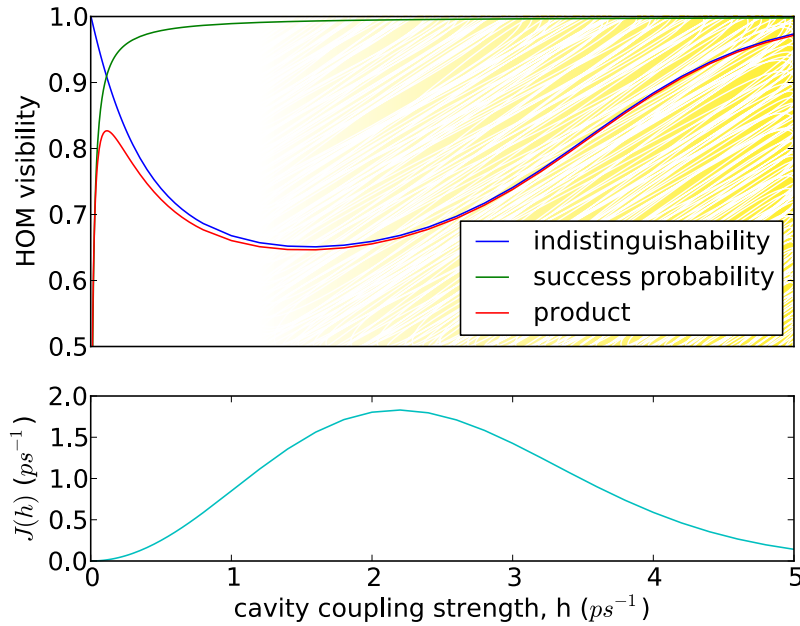


Figure 6.6: Pulse-relax technique: calculations are performed as a function of the cavity coupling strength. Upper panel: at realistic coupling strengths ($h < 1$) increased HOM indistinguishability necessarily entails a decrease in efficiency (success probability), with the product of the two (blue curve) approaching zero. Here the spontaneous emission rate is $\Gamma = 0.005 \text{ ps}^{-1}$. For overcoming phonon-induced decoherence and achieving a high success probability, we must move into a region of unrealistically high h , represented by the increasing level of shading of this plot. The lower panel shows the phonon spectral density, Eq. 6.12, evaluated at the cavity coupling strength h , giving a rate that is directly proportional to phonon-induced dephasing during the pulse-relax process.

must therefore trade indistinguishability for efficiency.

In contrast, the Raman procedure (Fig. 6.7) avoids this trade-off. For small detuning the visibility is low, but this is because we do not get a proper Raman ground state transition unless $\nu \gg h$. If this condition is not met, the system simply undergoes a non-optimal detuned pulse-relax transition. Once we reach a detuning of around $\nu = 12h (= 6 \text{ ps}^{-1})$ the indistinguishability and efficiency both increase. Our choice of detuning size is limited in that it must be small in comparison with the original energy gap between the ground and excited states, and that it avoids any

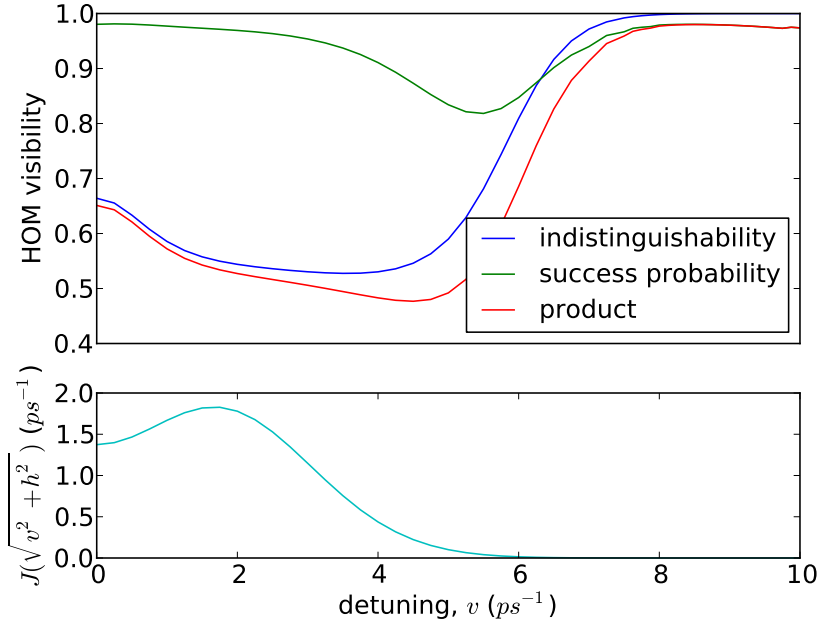


Figure 6.7: Raman technique, $h = 0.5$: by choosing a detuning to move beyond the region of high phonon spectral density we can achieve near-perfect indistinguishability. The efficiency in this region is high enough for a feasible photon source.

nearby excited states. This leaves us some freedom to use large detunings to push to frequencies above the region of high phonon spectral density. As the detuning is increased the efficiency saturates below unity. In this region both the time taken for the Raman process and the average excited state lifetime scale with the detuning squared, the two effects cancelling one another.

In many applications where photons are used, the product of efficiency and indistinguishability may not be the most useful metric for characterising the performance of the source; often photon escape errors can be accounted for, and the indistinguishability of photons that are detected is the important figure of merit. We therefore also calculate the rate of production of pairs of photons of a given

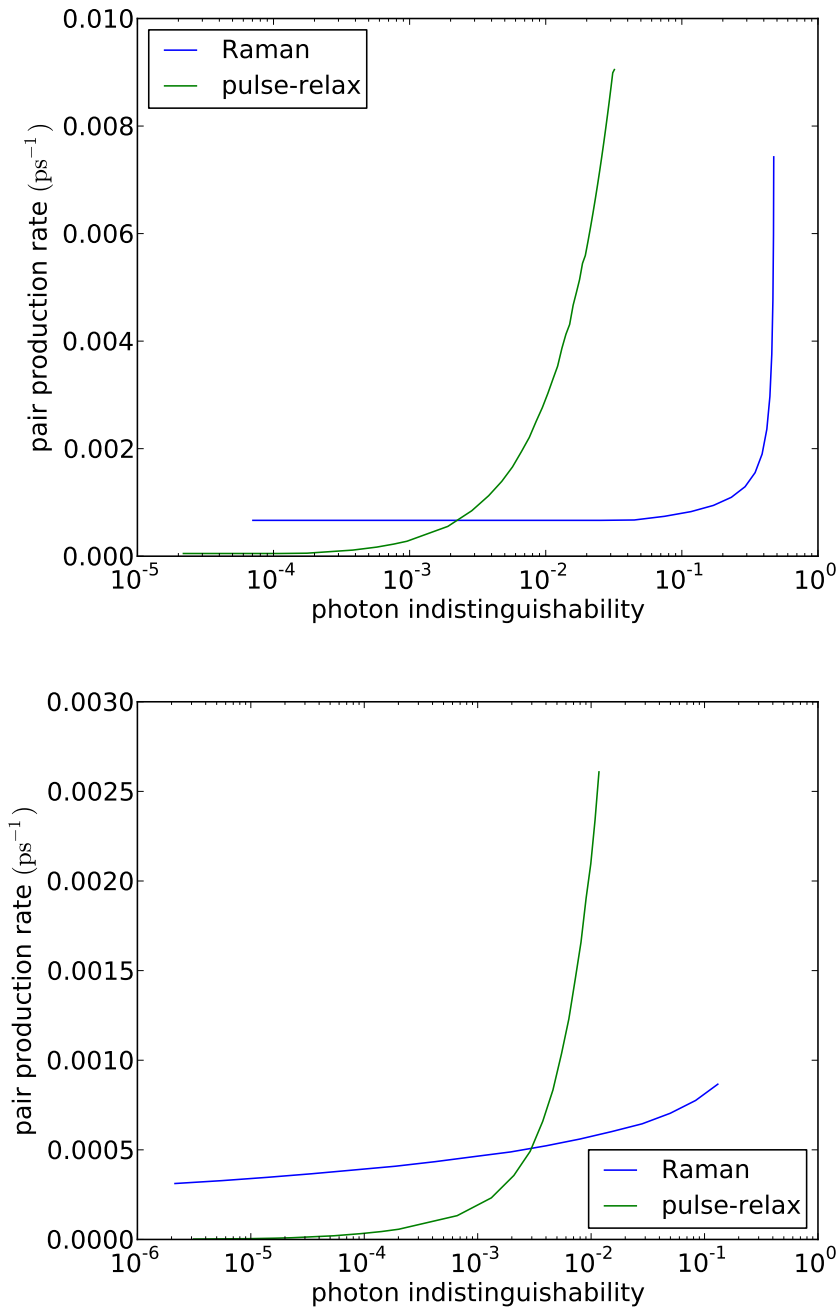


Figure 6.8: Rate of photon pair production: with no spontaneous emission (upper), and spontaneous emission with an excited-state lifetime of 200 ps (lower)

indistinguishability using each approach (Fig. 6.8). For our production rate we take

$$r_f = \frac{e_f}{t_f} \quad (6.50)$$

where e_f is the efficiency and t_f is the time taken for 99% of the runs to have completed (possibly unsuccessfully), for parameters (h in the pulse-relax scheme, and ν in the Raman scheme) chosen to obtain a given indistinguishability, f . This figure is somewhat approximate as it takes no account of how successful runs (where two photons are emitted into the correct modes) and unsuccessful runs are distributed within the process run time, and no allowance is made for time taken to reset the system in the event of a failure. The effect of the former is minor since in our model spontaneous emission can occur uniformly at any point of the process. We will revisit the effect of the latter shortly.

Even in the absence of spontaneous emission (Fig. 6.8, upper panel), the Raman procedure is quicker than the pulse-relax process at generating photons of a sufficiently high level of indistinguishability. With the dephasing parameters chosen in our model this occurs for indistinguishability of greater than 99.9%. In our model, spontaneous emission is the only process degrading the efficiency – without it we have perfect efficiency and so neither of the potential shortcomings discussed in the previous paragraph apply.

When spontaneous emission is added, we see a similar pattern but the indistinguishability threshold is very slightly lower. This is an upper bound, as here the reset time becomes important. The efficiency of the Raman procedure remains fixed at about 80%, requiring on average 1.25 runs per pair. In contrast, the efficiency of the pulse-relax procedure heads towards zero, meaning that many attempts will be needed to produce a pair. If the time taken to reset the system (to the excited state $|e\rangle$ in which we have assumed the pulse-relax system starts) is large, the Raman procedure will become advantageous at a far lower threshold.

6.6 Conclusion and Further Work

To conclude, we have developed a realistic and microscopically justified model of the impact of phonons on solid state single photon sources. We used a modified, ‘semi-quantum’, master equation method for the efficient calculation of coincidence rates, without having to resort to a quantum Monte-Carlo simulation approach.

Our physical results are best summarised by considering the following scenario: suppose you are working with a system where phonon dephasing and spontaneous emission are the dominant loss channels, where you have some control over the cavity parameters (\hbar and κ), and that you are tasked with building a high indistinguishability, efficient, on-demand photon source. In this scenario, we find that a Raman technique is preferable to the pulse-relax approach. In particular, in addition to producing superior production rates at a given indistinguishability, the Raman approach we have taken only requires varying of the detuning - by tuning the cavity mode, and driving field - whilst leaving the other cavity properties fixed. This is in contrast in to the pulse-relax approach that we used for comparison where we allowed the cavity coupling strength itself to be varied within a realistic range of values.

An interesting extension of this work would be to apply the methods developed here to other solid state systems by modifying our phonon interaction model. The basic idea of tuning the procedure to avoid harmful dephasing effects should be applicable in a wide range of systems.

The master equation techniques presented allow for modest yet important reductions in the system size required in a number of quantum jump processes. It would be useful to extract the core code implementing the technique from the specific system code, in order to create a package that could be used by the community at large.

Chapter 7

The Power of Small Toric Codes

7.1 Introduction to the Toric Code

The ability to correct and recover from errors is important for any quantum computing scheme. The discovery of the first error correcting quantum codes by Shor and Steane [10, 11, 12] was vital for demonstrating that quantum computing was theoretically viable. The toric code is an error correcting code proposed by Kitaev [59, 60], arising from work using quantum mechanics to provide simple models of topological order. It can be regarded as the simplest and most elegant in the class of such codes, collectively known as surface codes [61, 62].

One of the key advantages of surface codes is their local nature - the codes can be implemented on a two-dimensional lattice of qubits using only nearest neighbour interactions. In this realistic experimental scenario, surface codes can tolerate per-operation error rates of up to 1% [199, 200], compared with rates in of the order of 10^{-4} for the early error correcting codes [201].

In this chapter we look towards an experimental realisation of the toric code and study the code for small values of n . We pre-compute a decoding library, an approach that quickly becomes intractable for values of n above those considered

here, but has the advantage that we obtain a provably optimum decoding success rate. We use our pre-computed decoder to assess the *encoding power* of the code: we say the code has positive encoding power if the encoded qubits exhibit a lower error rate than the same number of unencoded qubits subjected to the same noise.

7.2 Shor's Code Revisited

Before moving on to the toric code, we first look at a simple example of an error correcting code in order to introduce some of the notation and concepts that we use later. For this purpose we pick the first stage of Shor's code [10]. The full code uses nine qubits to protect against general errors; the code we analyse here uses only three qubits and protects only against a single error channel. We describe the code by specifying how to encode a general qubit:

$$\alpha |0\rangle + \beta |1\rangle \rightarrow \alpha |000\rangle + \beta |111\rangle. \quad (7.1)$$

The idea here is very simple: each logical qubit is encoded into three physical qubits. Shor constructed a circuit such that if there was a bit-flip error - interchanging $|0\rangle \leftrightarrow |1\rangle$ - on any one of the three qubits, the state would automatically be corrected. The system basically implements a 'majority vote' error correction scheme.

We now develop a different description of the code, which will directly translate to our treatment of the toric code later in the chapter. In order to do this we first introduce the standard qubit operators:

$$Z = |0\rangle \langle 0| - |1\rangle \langle 1| \quad (7.2)$$

$$X = |0\rangle \langle 1| + |1\rangle \langle 0| \quad (7.3)$$

$$Y = |0\rangle \langle 1| - |1\rangle \langle 0| = ZX. \quad (7.4)$$

State	Z_1Z_2	Z_2Z_3	Z_1Z_3	Z_1
$ 000\rangle$	+1	+1	+1	+1
$ 001\rangle$	+1	-1	-1	+1
$ 010\rangle$	-1	-1	+1	+1
$ 100\rangle$	-1	+1	-1	-1
$ 110\rangle$	+1	-1	-1	-1
$ 101\rangle$	-1	-1	+1	-1
$ 011\rangle$	-1	+1	-1	+1
$ 111\rangle$	+1	+1	+1	-1

Table 7.1: The eigenvalues of the operators on their simultaneous eigenstates

In what follows we will need to apply these operators to states of multiple qubits. To do this we will introduce subscripts to the operators, so that, for example, Z_1 is the Z operator acting on the first qubit. Operators acting on different qubits can be seen to commute with one another.

We will start by considering a state of three qubits and the set of operators $S = \{Z_1Z_2, Z_2Z_3, Z_1Z_3\}$. As these operators commute with one another it is possible to find states that are simultaneous eigenstates of all three. For the set S that we have chosen, the simultaneous eigenstates can be taken to be the Z basis vectors, as shown in Table 7.1. Note that the set of eigenvalues vary with the state, but the third column is the product of the first two. The operators we have chosen are not actually independent as

$$(Z_1Z_2)(Z_2Z_3) = Z_1Z_3. \quad (7.5)$$

To break the degeneracy in the eigenstates we introduce a fourth operator Z_1 that commutes with the elements of S , but cannot be written as a product of them. There are many other operators that we could have chosen here, for example Z_2 , Z_3 , or $Z_1Z_2Z_3$.

We say that the set $T = \{Z_1Z_2, Z_2Z_3, Z_1\}$ is an *independent* set of commuting

operators. The eigenvalues of these operators uniquely define the basis states. We say that the set T stabilises the state $|000\rangle$, as $t|000\rangle = |000\rangle$ for all $t \in T$. Similarly $\{Z_1Z_2, -Z_2Z_3, Z_1\}$ stabilises $|001\rangle$. We call T the *stabiliser representation* of the state $|000\rangle$; by specifying three independent, binary-outcome operators in a Hilbert space of dimension 2^3 we have uniquely defined the state.

We can also use the stabiliser representation to define a subspace of the Hilbert space. The set $\{Z_1Z_2, Z_2Z_3\}$ uniquely defines a subspace spanned by the states $\{|000\rangle, |111\rangle\}$, which is precisely the codespace defined in Eqn. (7.1). If we were to perform measurements corresponding to the operators Z_1Z_2 and Z_2Z_3 on our encoded state we would expect the outcome $+1$ in both cases, no matter how many times the measurement was repeated. We can consider a measurement of the operator Z_1 as a measurement of the encoded logical qubit.

Following Shor's approach, we model the introduction of errors as the X and Z operations acting on one or more of the qubits. To take a concrete example consider the error represented by X_1 acting on the state:

$$X_1(\alpha|000\rangle + \beta|111\rangle) = \alpha|100\rangle + \beta|011\rangle. \quad (7.6)$$

If we evaluate the stabilisers now we find $Z_1Z_2 \rightarrow -1$ and $Z_2Z_3 \rightarrow +1$. We can see from the stabiliser outcomes, or *syndrome*, that we are no longer in the codespace and that an error has occurred. You will notice that the error was visible only in the outcome of the stabiliser that anti-commuted with the error operator: $(Z_1Z_2)X_1 = -X_1(Z_1Z_2)$.

Although we can tell that an error occurred, we do not know if it was X_1 or X_2X_3 , because both these errors would have given rise to the same syndrome. In Shor's scheme we correct the most likely. A different way of looking at this is that we can return to the codespace by applying X_1 : if the error was actually X_1 , the

logical qubit will be intact, but if the error was X_2X_3 the overall operation will be $X_1X_2X_3$ and there will be an error on the logical qubit.

If we instead have a phase flip Z_1 we will not be able to detect the error, as Z_1 commutes with all the stabilisers and will go unseen. In Shor's original paper he fixes this by expanding the codespace.

We have introduced the stabiliser notation to describe Shor's code and have seen how by measuring stabiliser operators we can detect certain errors. We have an operator that completes the commuting set and that defines an operation on the logical qubit. We can detect errors provided they do not commute with all of the stabilisers. We then correct the most likely error consistent with the error syndrome that the code produces. We will now use this language to introduce the toric code.

7.3 Definition of Toric Codespace

The toric $2n$ -code (Fig. 7.1) uses $2n^2$ physical qubits to encode two logical qubits. The codespace is most elegantly described using the stabiliser formalism. In particular we shall specify a set of $2n^2 - 2$ independent stabilisers to give a codespace of dimension four.

To describe the code, it is useful to picture the $2n^2$ physical qubits positioned on the odd diagonals of a $2n \times 2n$ lattice (i.e. in the positions with coordinates (i, j) , where $i+j$ is odd). On the sites (i, j) where i and j are both even we construct an X -stabiliser, s_k^X , by taking the product of X operators of qubits on the neighbouring squares. Although Fig. 7.1 depicts a flat surface, in fact the left-most column is taken to be adjacent to the right-most, and similarly for the top and bottom rows. In identifying the opposite edges in this way we define a torus, hence the 'toric' nature of the code. On the sites (i, j) where i and j are both odd, we define the Z -stabilisers, s_k^Z , in a similar manner.

s_0^X	q_0	s_1^X	q_1
q_2	s_0^Z	q_3	s_1^Z
s_2^X	q_4	s_3^X	q_5
q_6	s_2^Z	q_7	s_3^Z

Figure 7.1: Qubit lattice for the 4-code. s_k^X and s_k^Z are X - and Z -stabilisers represented by the sites respectively. q_i are qubits. By way of example, $s_0^X = X_0X_2X_1X_6$ and $s_0^Z = Z_3Z_4Z_2Z_0$.

We let $S_X = \{s_k^X\}$. There are n^2 elements in S_X , but only $n^2 - 1$ independent elements, as the final element is the product of all the others. We similarly define $S_Z = \{s_k^Z\}$. We will later use the sets S_X and S_Z to define the stabilisers of the codespace. Practically we will make measurements of these operators to check whether the state is still in the codespace.

Just as in Shor's code, to fully define a state we will need to add additional independent, commuting operators to our set of stabilisers. We now construct a set of operators that will be used for this purpose. We define X_h (horizontal X) to be the product of X_i s acting on qubits in an even row, X_v (vertical X) the product of X_i s acting on qubits in an even column, and similarly, Z_h to be Z_i s on an odd row, and Z_v to be Z_i s on an odd column. We will use the pairs, $\{X_v, Z_h\}$ and $\{X_h, Z_v\}$, to define the two logical qubits: each pair shares exactly one physical qubit and because of this it is possible to show that the operators anti-commute, as qubit operators should. Any of the remaining pairs $\{X_v, X_h\}$, $\{X_v, Z_v\}$, $\{Z_v, Z_h\}$, and $\{Z_h, X_h\}$ can be used to initialise our two qubits, and suffice to fully define the state. We call this set the *logical operators*, $L = \{X_v, X_h, Z_v, Z_h\}$, on our pair of independent *logical qubits*.

We will now turn to how errors are detected in the toric code. As with the treatment of the Shor code we will consider an error to be a set of individual X and Z errors applied to a subset of the physical qubits. An X -error on a single physical qubit will flip the eigenvalue of the neighbouring Z -stabilisers, but commutes with the X -stabilisers and will not be detected by them. This can be verified by checking the commutation relation of the operators for the stabiliser and physical error. We say that an X -error causes the neighbouring Z -stabiliser sites to *fire*. Similarly, a Z error will be detected by the X -stabilisers and not the Z -stabilisers, and a Y will be detected by both sets. Additional errors will cause the stabiliser eigenvalues to toggle. If errors occur sequentially they will be detected by the stabilisers at either end of the chain (see Fig. 7.2).

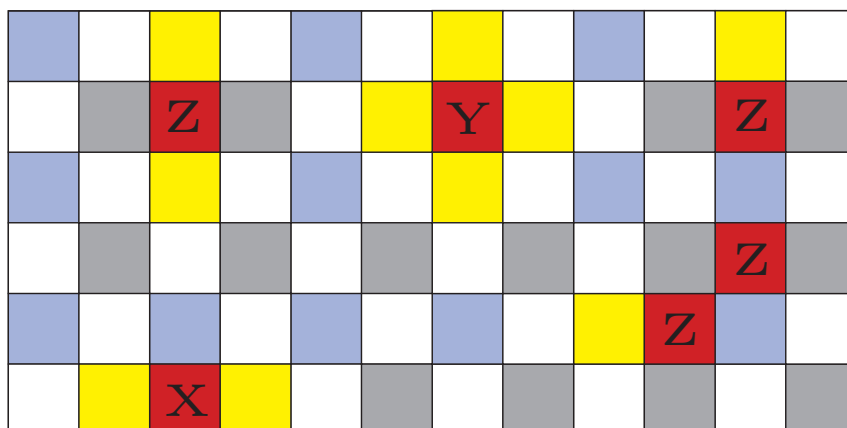


Figure 7.2: Error detection of isolated Z -, X -, Y -errors and a chain of Z -errors. Error qubits are shown in red and firing stabilisers in yellow.

7.4 Code Variants

In the rest of the chapter, we will consider three variants of the toric code, that we refer to as the *classical toric code*, the *reduced quantum toric code* and the *full quantum toric code*.

7.4.1 Classical Toric Code

In the classical toric code we completely ignore the phase of each qubit, concerning ourselves only with the outcomes of measurements on the logical qubits in the Z -basis. To define the codespace we take our set of code stabilisers S to be the set S_Z and the set of logical operators $L = \{Z_h, Z_v\}$. We have the same geometry and number of physical qubits as described but only measure a reduced set of stabilisers. The codespace is massively degenerate but any state in it will be sufficient for our purposes.

We simplify the analysis by considering only X_i errors on the individual qubits, as these are the only ones that can affect the measurement outcomes we are interested in. We define the complete set of error operators, E , to be the set generated by the individual physical qubit X_i operators - that is the set of all products of such operators. As the $2n^2$ individual qubit operators, X_i , commute with one another and as $X_i^2 = \mathbf{1}$ we can show that $|E| = 2^{2n^2}$.

We also introduce the set of *syndromes*, A - the possible outcomes when the code stabilisers S are measured. When each stabiliser measurement outcome is $+1$ we say we have obtained the *zero-syndrome*, which we denote by the element $a_0 \in A$. If we obtain the zero-syndrome we know that we are in the codespace. In the classical toric code we have that $|A| = 2^{n^2-1}$, as each of the n^2 elements of S can report ± 1 , but the last outcome is fixed by the others.

7.4.2 Full Quantum Toric Code

For the full quantum toric code, we aim to fully protect our encoded qubits against all sources of error. We take a full set of code stabilisers, $S = S_X \cup S_Z$, and the full set of logical operators $L = \{Z_h, Z_v, X_h, X_v\}$. The complete set of errors is generated by the set of all individual qubit operators $\{X_i, Z_i\}$, so that $|E| = 4^{2n^2}$.

Following similar reasoning to the classical toric code we can deduce the size of the set of syndromes, A : the outcomes of each of the $2n^2 - 2$ independent stabilisers in S completely define a syndrome, so that $|A| = 2^{2n^2-2}$.

7.4.3 Reduced Quantum Toric Code

The reduced quantum toric code is slightly more subtle than the previous two cases. We take the full set of stabilisers $S = S_X \cup S_Z$ and logical operators $L = \{Z_h, Z_v, X_h, X_v\}$, but aim only to protect against individual qubit Y_i errors. As previously, it is straightforward to show that $|E| = 2^{2n^2}$. It is more difficult to determine the size of A in this case, as not all syndromes are possible from the errors that we consider. It is possible to show that $|A| = 2^{2n(n-1)}$ but this requires a deeper understanding of the structure of the code - which we will now develop.

7.5 The Structure of the Code

We now describe the structure of the set of errors, E , and how they relate to the syndromes, A , and logical errors, L . We take the definition of E from the previous section: each ‘error’ in E is actually a set of Pauli operations of the physical qubits. We begin by defining the function

$$\text{synd} : E \rightarrow A \tag{7.7}$$

that maps an error onto its associated syndrome. We are then able to define

$$E_a = \{e \in E : \text{synd}(e) = a\}, \tag{7.8}$$

the set of all possible errors corresponding to a syndrome a . For convenience we define $E_0 = E_{a_0}$ to be the set of errors corresponding to the zero-syndrome, a_0 . If an error in E_0 occurs it will go undetected by the code. This error has mapped a legitimate code state either onto itself or onto another legitimate code state; in the latter case inducing a logical error. We define a function to act on the set E_0 ,

$$\text{lerr} : E_0 \rightarrow L, \quad (7.9)$$

taking an error to the corresponding logical error on the encoded qubits. The possible logical errors on the logical qubits are precisely the same as the logical operators L that we defined earlier. Finally we define the set

$$E_{0,l} = \{e \in E_0 : \text{lerr}(e) = l\}. \quad (7.10)$$

It is easy to see that each $E_{0,l}$ contains at least one element, as l itself is a member: Our code contains the ability to perform logical operations on our code state. These operations could happen in an error sequence and so $l \in E_{0,l}$. We will now show that the sets $E_{0,l}$ have exactly the same number of elements - our first important observation about the structure of our toric codes. It may be useful to refer to Fig. 7.3, which provides a graphical representation of the result for the classic code, whilst reading the section.

To show that the $E_{0,l}$ are all the same size, we will show that they all have the same number of elements as $E_{0,0}$ - the set of elements of E_0 that introduce no logical error. To see this, take element $e_1 \in E_{0,l}$ and $e_2 \in E_0$. We claim that

$$e_2 \in E_{0,l} \Leftrightarrow e_1 e_2 \in E_{0,0}, \quad \forall e_1 \in E_{0,l}. \quad (7.11)$$

The proof of the claim follows from the fact that all logical operators $l \in L$ are

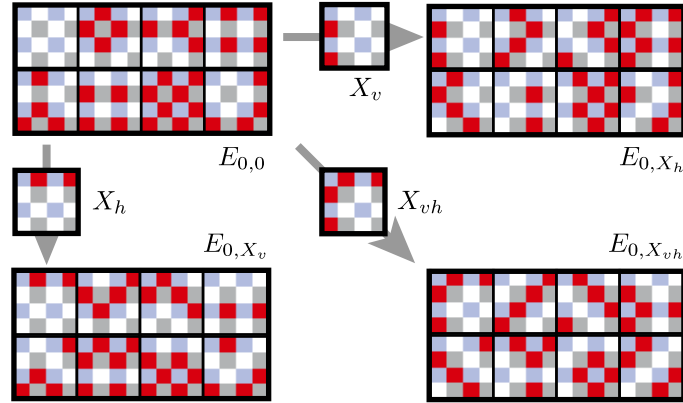


Figure 7.3: E_0 for the classic toric code. The red squares represent physical Z -errors. The set $E_{0,0}$ combined with the logical errors $\{X_v, X_h, X_{vh}\}$ generate the $E_{0,l}$.

products of individual qubit operators, so that $l^2 = \mathbf{1}$: by applying the same logical error twice we undo it. If by applying e_1 after e_2 we have no logical error, they must be in the same error class, and the converse is also true. We now consider the set

$$e_1 E_{0,0} = \{e_1 e : e \in E_{0,0}\} \quad (7.12)$$

and claim that, given $e_1 \in E_{0,l}$, we must have $E_{0,l} = e_1 E_{0,0}$. This follows as,

$$e_2 = e_1 e \Leftrightarrow e_1 e_2 = e, \quad (7.13)$$

where we have used that $e_1^2 = \mathbf{1}$. Therefore we can use e_1 to establish a bijection between $E_{0,l}$ and $E_{0,0}$ and so the sets must have the same number of elements.

We now move on to the sets of errors, E_a , corresponding to a general syndrome, $a \in A$. As we have taken A to be the set of obtainable syndromes, it follows that there must be at least one element in each set E_a . It is useful to assume that we have chosen an arbitrary member from E_a . We call this a *matching* for the syndrome, and denote our specific choice of matching $m^*(a)$. In practice there are many ways to construct a specific matching for each syndrome a , for example see Fig. 7.4. If

we observe the syndrome a and apply the matching $m^*(a)$ we are guaranteed to be back in the codespace.

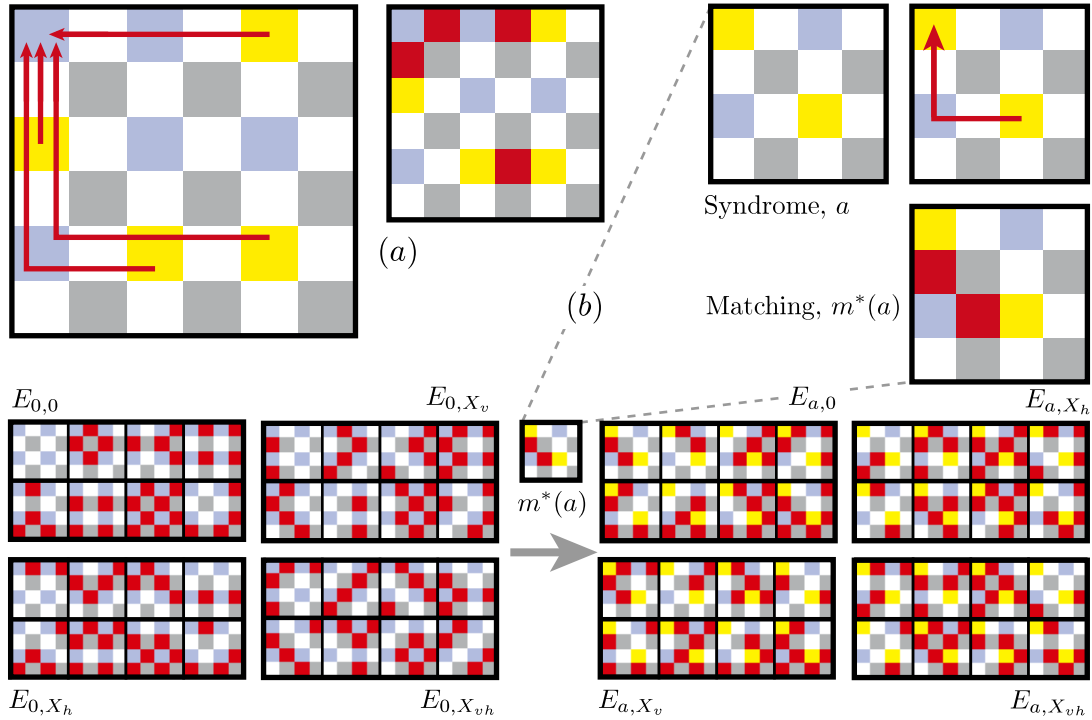


Figure 7.4: Part (a) shows the method we use for constructing a matching from a syndrome: all firing stabilisers are ‘pushed’ to the left, then to the top. A Z -operation is performed on any qubit that has been passed over an odd number of times. Part (b) shows how to use a matching $m^*(a)$ for a syndrome a to generate the set E_a from the set E_0 .

Following a similar procedure to before we can show that $E_a = m^*(a)E_0$, and therefore each of the sets E_a have the same number of elements. Furthermore we can split the set E_a up into a set of classes

$$E_{a,l} = m^*(a)E_{0,l}. \quad (7.14)$$

The set $E_{a,l}$ can be interpreted as the set of errors that when corrected by $m^*(a)$ induce the logical error l on the encoded qubits. All the sets $E_{a,l}$ have the same number of elements as $E_{0,0}$.

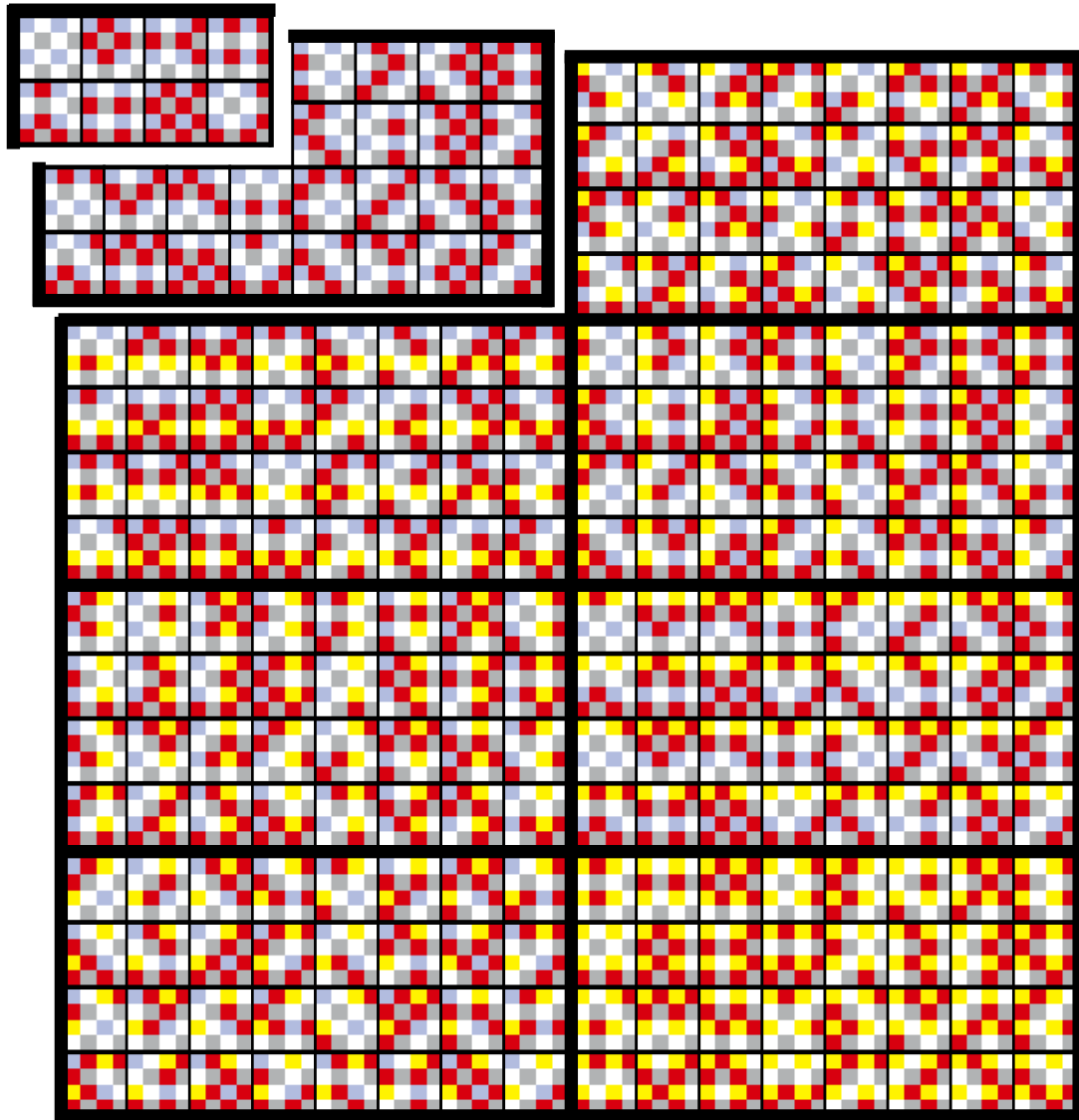


Figure 7.5: Full set of errors, E , for the classical 4-code. $E_{0,0}$ and E_0 have been separated from the rest to highlight their role in generating the complete set E .

In the preceding paragraphs we have split up the total set of errors E into identically sized subsets $E_{a,l}$ indexed by $a \in A$ and $l \in L$ (Fig. 7.5). It follows immediately that

$$|E| = |A| \cdot |L| \cdot |E_{0,0}|. \quad (7.15)$$

Code	$ E $	$ A $	$ L $	$E_{0,0}$
Classical	2^{2n^2}	2^{n^2-2}	4	2^{n^2-2}
Reduced Quantum	2^{2n^2}	$2^{2n(n-1)}$	4	2^{2n-2}
Full Quantum	4^{2n^2}	2^{2n^2-2}	16	2^{2n^2-2}

Table 7.2: Sizes of the sets involved with our three toric code variants.

One can see that this relationship holds for our three code variations in Table 7.2.

We have shown that given a syndrome always corresponds to multiple logical error classes, of which we can correct only one. We still have to answer the question of which one to correct. In the Shor code case we picked the matching to minimise the probability of introducing a logical error. Ideally that is what we would do here too. This of course depends on the error model, which we have not discussed yet. It is also not straightforward to do. The number of matchings in each class grows exponentially with the size of the grid. No efficient way of calculating the probabilities is known, even for the simplest error model.

The job of picking a matching given a syndrome falls to a decoder. These are often heuristic procedures, designed to balance calculation time with identifying the most likely class as often as possible. Determining a good decoding strategy is currently a very active area of research and there are a number of different approaches [67, 200, 69]. It is not only important that a decoder maximises the probability of returning to the codespace without inducing an error on the logical qubits, but also that the decoder can run in a reasonable amount of time.

7.6 Error Model

We consider depolarising noise distributed uniformly over the lattice with a given, constant probability:

$$D(\rho) = p_x X \rho X + p_z Z \rho Z + p_y Y \rho Y + (1 - p_x - p_y - p_z) \rho. \quad (7.16)$$

The values of p_x , p_y and p_z vary over our different code variants accordingly

1. Classical case: $p_x = p$, $p_y = p_z = 0$
2. Reduced quantum case: $p_y = p$, $p_x = p_z = 0$
3. Full quantum case: $p_x = p_y = p_z = p/3$.

We also consider the effect of stabiliser sites mis-reporting the stabiliser measurement outcomes: that with some probability, q , the stabiliser outcome is reported as a $+1$ when it was -1 , or a -1 when it was $+1$.

In the literature, faulty stabiliser evaluations are often dealt with by extending the code into a third dimension. This treats the case when multiple rounds of faulty stabiliser evaluations are performed, where there is benefit to considering the history of the stabiliser outcomes as well as the current value. Here we consider only one round of stabiliser evaluations, so instead aim to identify and correct the most likely true stabiliser result given the outcome we observed. Even in the multiple evaluation round case, the last stage would involve a procedure similar to ours, so our results provide an upper bound on the decoding probability: you would not use this approach on each stage of a multi-round scheme, but those previous rounds certainly will not increase your probability of a successful decode in the last step.

7.7 A Precomputed Decoder

We begin by looking at the probability of getting a particular logical error, l , given that syndrome, a , occurs and we attempt to correct it using our chosen matching method by applying $m^*(a)$:

$$p(l|a) = \sum_{e \in E_{a,l}} \frac{p(e)}{p(a)}. \quad (7.17)$$

For each stabiliser outcome a we identify the most likely logical error l_a , such that $p(l_a|a)$ obtains a maximum¹. We may then correct our earlier attempt by applying the operator l_a , so that the total correction operation on the state will be $l_a m^*(a)$. The overall successful decoding probability from following this procedure is

$$P_d = \sum_{a \in A} p(l_a|a) p(a) \quad (7.18)$$

$$= \sum_{a \in A} \max_{l \in L} \left\{ \sum_{e \in E_{a,l}} \frac{p(e)}{p(a)} \right\} p(a) \quad (7.19)$$

$$= \sum_{a \in A} \max_{l \in L} \left\{ \sum_{e \in E_{a,l}} p(e) \right\}. \quad (7.20)$$

When considering mis-reported stabiliser outcomes we can no longer assume that the syndrome we observe will be in A . We let A' be the set of all possible stabiliser outcomes $A' = \{0, 1\}^{\otimes n^2}$. If we are to successfully decode a syndrome a' , we must first identify the correct syndrome a , on which to perform the arbitrary matching, and then identify the most likely logical error l_a to correct. If we identify the wrong a , the final state will not even be in the code space. Given a' we must pick a and l to provide the maximum probability of a successful decoding in the case of

¹In cases where the most likely logical error is not unique we pick arbitrarily between the candidates.

mis-reporting stabiliser outcomes:

$$P'_d = \sum_{a' \in A'} p(\text{success}|a')p(a') \quad (7.21)$$

$$= \sum_{a' \in A'} \max_{a \in A} \{p(l_a|a)p(a|a')\} p(a') \quad (7.22)$$

$$= \sum_{a' \in A'} \max_{a \in A} \left\{ \max_{l \in L} \left\{ \sum_{e \in E_{a,l}} \frac{p(e)}{p(a)} \right\} p(a \cap a') \right\} \quad (7.23)$$

$$= \sum_{a' \in A'} \max_{a \in A} \left\{ \max_{l \in L} \left\{ \sum_{e \in E_{a,l}} p(e) \right\} p(a'|a) \right\}. \quad (7.24)$$

While equations (7.20) and (7.24) are conceptually simple, calculations are beset by difficulties due to the rapid growth in the size of the sets $E_{a,l}$, A , and A' : in the single noise channel case for the $2n$ -code $|E_{a,l}| = |A| = 2^{n^2-1}$; for the full noise channel $2n$ -code $|E_{a,l}| = |A| = 2^{2n^2-2}$. For example, the total number of error configurations, $|E|$, for the 6-code is 2^{36} , which would require $\sim 200\text{GB}$ of storage space.

Thankfully, we do not need the complete set of error configurations to compute the value of p_{success} in Eq. (7.20). For each configuration $e \in E$ the probability is

$$p(e) = (1-p)^{2n^2-n(e)} p^{n(e)} \quad (7.25)$$

where $n(e)$ counts the number of errors in error configuration $e \in E$. When summing over the errors consistent with a given logical error and syndrome we get

$$\sum_{e \in E_{a,l}} p(e) = \sum_{e \in E_{a,l}} (1-p)^{2n^2-n(e)} p^{n(e)} \quad (7.26)$$

$$= (1-p)^{n^2} \sum_{i=0}^{2n^2} d_{a,l}^{(i)} \left(\frac{p}{1-p} \right)^i \quad (7.27)$$

$$=: (1-p)^{n^2} \chi_{a,l} \left(\frac{p}{1-p} \right) \quad (7.28)$$

where $d_{a,l}^{(i)} = |\{e \in E_{a,l} : n(e) = i\}|$ and we have used the final line to define the characteristic function $\chi_{a,l}$ of the class $E_{a,l}$. By computing and storing the coefficients $d_{a,l}$ we are able to calculate the success probabilities for a range of values of p .

The full source code used for our calculations, along with the computed tables of characteristic function coefficients, is available online [202].

7.8 Simulation Results

7.8.1 Classical Toric Code

Using the method described, we calculated the success probabilities $P_d(n,p)$, and compared them with $p_{\text{bare}} = (1-p)^2$, the probability that two non-encoded qubits would remain error-free (Fig. 7.6).

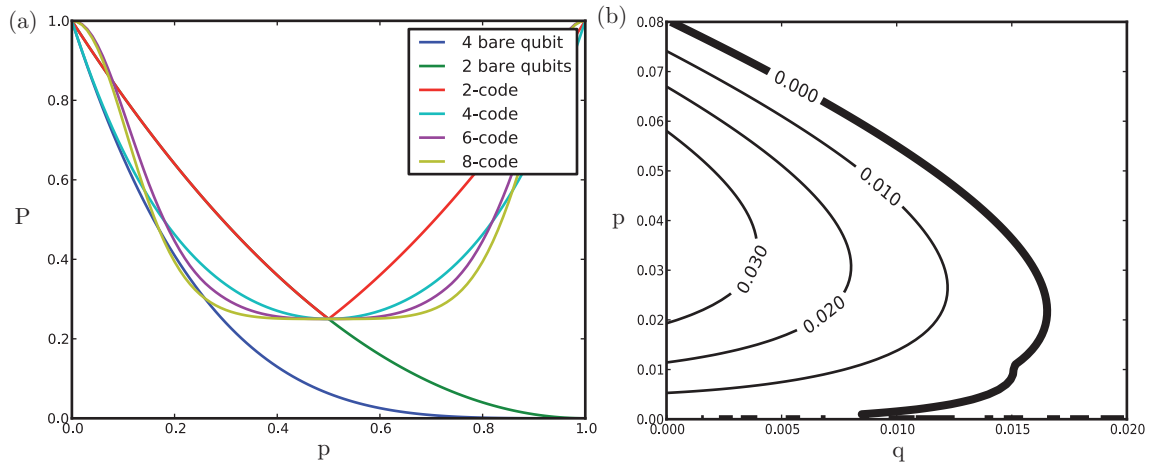


Figure 7.6: Success probabilities for classical toric code: (a) shows the success probability, P , for ideal version of the code vs. the error rate, p , with two and four unprotected qubits for comparison; (b) shows the power of the 6-code in the case when stabiliser outcomes are misreported with probability q .

The 2-code performs exactly the same as the bare qubits. This is not surprising, as the 2-code has 2 physical code qubits and no error detect capacity - there is

only one possible syndrome. For this reason, in future plots we omit p_{bare} , instead performing the comparison with the 2-code. The 4-code performs worse than the bare qubits. Although the 4-code has error-detect capacity, it has no error correct capacity. This can be seen by considering the case when a single error occurs - due to the translational symmetry of the lattice, the syndrome can give us no information about whether our correction introduced a logical error or not. For the 4-code to be successful there must be no errors on the 4 qubits that X_h and X_v measure, an event with probability approximately equal to $(1 - p)^4$ for small p .

The 6-code is the smallest code that exhibits encoding power for some values of p . Provided that $p < 0.08$ the 6-code outperforms the bare qubits. The 8-code appears to offer roughly the same performance as the 6-code. We were not able to go beyond $2n = 8$ with the computing resources available, but we expect that as n increases the curves would tend towards a step function at the one-channel threshold. We looked at the mis-reported stabiliser outcome case for the 6-code. There is a small region with positive encoding power, that requires stabiliser fidelity in the region of 1%.

7.8.2 Reduced Quantum Code

For the reduced quantum code, we find that the 4-code is the first code to offer encoding power in this scenario (Fig. 7.7). As before the 2-code has no error detect capacity. Unlike before, the 4-code is able to detect and correct errors, as it can use both X - and Z -stabiliser information to break the symmetry and pinpoint the error.

We investigated the case of mis-reported stabiliser measurement outcomes for the 4-code. We obtain positive encoding power for mis-reporting rates of up to 10%. Overall the reduced quantum code shows remarkable encoding power, even for small

codes. In using the full stabiliser information to detect a reduced set of errors, we have managed to hugely reduce the size of each error class (Fig. 7.2).

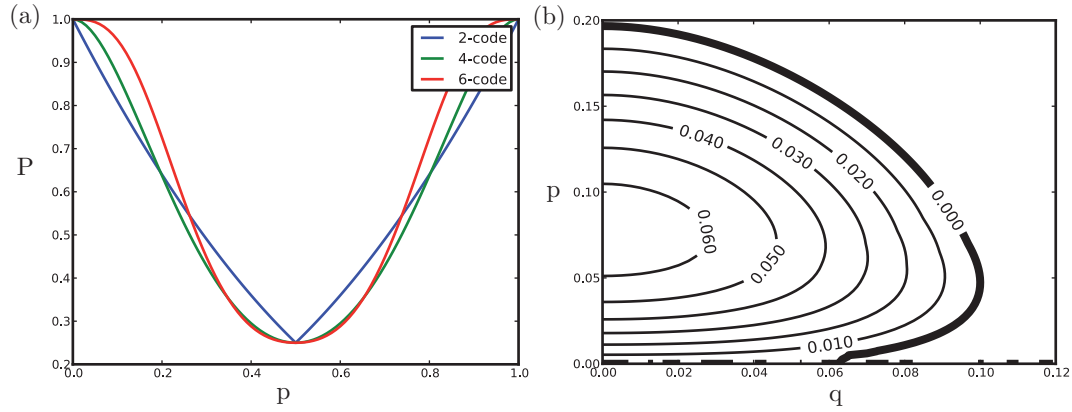


Figure 7.7: Success probabilities for reduced quantum toric code: (a) shows the success probability, P , for ideal version of the code vs. the error rate, p , with two and four unprotected qubits for comparison; (b) shows the power of the 4-code in the case when stabiliser outcomes are misreported with probability q .

The circumstances that could justify the assumptions of the reduced quantum code are not unrealistic: we envisage a system with a single dominant error channel. In picking this to be the Y channel, we exploit the lack of symmetry in our code effectively tailoring our code to be effective against the dominant error channel.

7.8.3 Full Quantum Code

Finally we look at the full code, protecting against full depolarizing noise, taking $p_x = p_y = p_z$ in equation (7.16).

The 6-code is the first code to offer encoding power (Fig. 7.8). We looked at mis-reported stabiliser outcomes for the 6-code. Due to computational constraints we were only able to find a lower bound for $P'_d(p, q)$. This was obtained by modifying

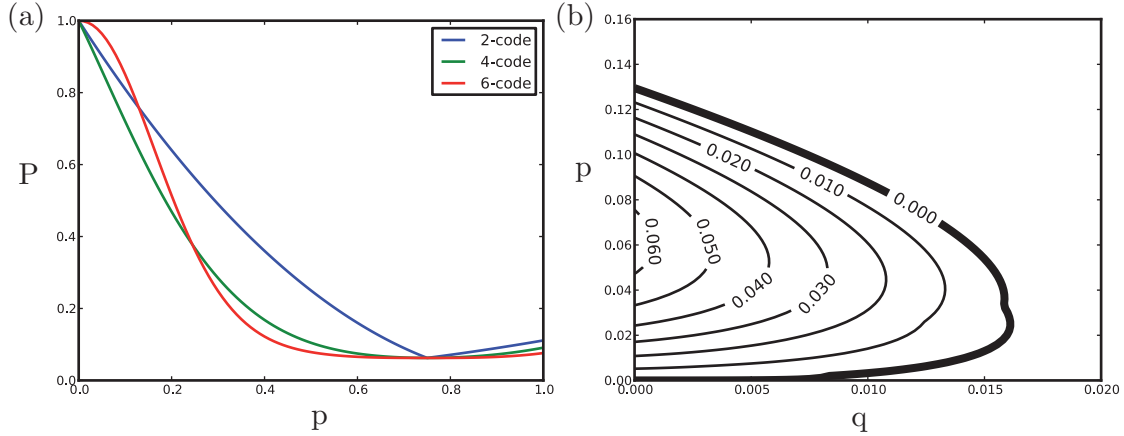


Figure 7.8: Success probabilities for full quantum code: (a) shows the success probability, P , for ideal version of the code vs. the error rate, p , with two and four unprotected qubits for comparison. Note that the graph has a minimum at $p = 0.75$ when the probability of each error is equal to the probability of no error. (b) shows the power of the 6-code in the case when stabiliser outcomes are misreported with probability q .

equation (7.24) to maximise only over a close to a' :

$$P'_d = \sum_{a' \in A'} \max_{a \in N(a', x)} \left\{ \max_{l \in L} \left\{ \sum_{e \in E_{a, l}} p(e) \right\} p(a'|a) \right\} \quad (7.29)$$

where $N(a', x) = \{a \in A : d(a', a) \leq x\}$ with $d(a', a)$ the number of stabilisers where a' differs from a . We took $x = 2$ to produce a rough region, and then used $x = 4$ to refine the boundary.

7.9 An Experimental Suggestion

Our aim in this section is to provide a criterion which an experimentalist can use to verify whether a given candidate toric code set-up is providing protection.

Our criterion is based on the observation that the 2-code is essentially equivalent to two unprotected qubits: the syndrome outcome is always +1 so we are unable to even detect errors and the logical operations reduce to single qubit operations. By

comparing the performance of the candidate code system against that of the 2-code we are able to say whether the candidate system is exhibiting protective power.

We do not specify the decoder that the experimentalist must use for the larger code (decoding is trivial in the 2-code), but our precomputed decoder will give optimal results. In our analysis we assumed that the stabiliser mis-reporting and physical qubit errors are independent events. A round of stabilisers is permitted to introduce physical qubit errors, but these must be sprinkled evenly over the lattice and not be correlated with mis-reporting sites. If strong correlations were to exist a modified decoder would give a better chance of satisfying the criterion.

We assume that an experimentalist has the ability to perform all X - and Z -stabiliser measurement operations and the logical measurements. In a large code the logical operations are potentially tricky, given their non-local nature. Here, due to the size of the codes considered, the logical operations actually involve fewer qubits than the stabilisers, and so are likely to be less technically demanding.

Our experimental proposal is as follows:

1. Measure X_v , X_h , and the stabilisers to find initial syndrome a'_i and logical qubit states (x_i^v, x_i^h) .
2. Wait. Manually introduce noise if required.
3. Measure X_v , X_h , and the stabilisers to find final syndrome a'_f and logical qubit states (x_f^v, x_f^h) .
4. Decode the calculated syndrome, $a' = a'_i \text{ XOR } a'_f$, to find matching m .
5. Modify (x_f^v, x_f^h) to reflect what the outcomes would have been if we had applied m before measurement to find (x_m^v, x_m^h) .
6. If $(x_i^v, x_i^h) = (x_m^v, x_m^h)$ count the round as a success; if not, count the round as a failure.

7. Repeat steps 1 to 6 many times to calculate an experimental successful decoding probability P_d^{expt} .

The procedure is then repeated for initial measurements of $X_v Z_v$, $X_h Z_h$ and $Z_h Z_v$. We then repeat this procedure for the 2-code and compare the results: if the larger system outperforms the 2-code protection is provided.

7.10 Conclusion and Further Work

We have provided a protocol and pre-computed decoder for demonstrating toric encoding size at minimal scale. The fewest qubits with which one could implement the $2n$ -code is $2n^2 + 1$, and in that case the ‘extra’ qubit must be capable of performing gate operations with all others. For the 4-code this is a requirement of 9 qubits and for the 6-code the requirement is 19 qubits. The error rates provided are not unrealistic for current experimental systems.

As further work, a natural extension would be to apply the procedure described here to other surface codes. The smallest planar code can be constructed with fewer qubits than the smallest toric code, so could provide an easy experimental realisation of the class of surface codes. It is unclear whether the lower degree of symmetry in planar codes would improve the successful decoding probabilities that we calculate or not.

We also believe that the reduced quantum case is particularly interesting and merits further investigation. The figures given in Table 7.2 show an imbalance between the sizes of A and $E_{0,0}$ not present in the other codes, which seem to be the source of the codes high tolerance both to physical qubit errors and to mis-reported stabiliser outcomes. The structure of the code is also highly specialised, to an extent that it may be possible to calculate the characteristic functions for the classes $E_{a,l}$ without resorting to a full space search. This would allow far larger sizes of code

to be investigated. The reduced quantum code model could also be experimentally appropriate for systems where one error channel is heavily dominant.

Bibliography

- [1] Feynman, R. (1982) Simulating physics with computers. *Int. J. Theor. Phys.*, **21**, 467–488.
- [2] Deutsch, D. (1985) Quantum theory, the Church-Turing principle and the universal quantum computer. *Proc. R. Soc. A*, **400**, 97–117.
- [3] Deutsch, D. and Jozsa, R. (1992) Rapid solution of problems by quantum computation. *Proceedings: Mathematical and Physical Sciences*, **439**, 553–558.
- [4] Simon, D. R. (1994) On the power of quantum computation. *Siam J. Comput.*, **26**, 116–123.
- [5] Grover, L. K. (1996) A fast quantum mechanical algorithm for database search. *Proceedings, 28th Annual ACM Symposium on the Theory of Computing (STOC)*, pp. 212–219.
- [6] Shor, P. (1997) Polynomial-time algorithms for prime factorization and discrete logarithms on a quantum computer. *Siam J. Comput.*, **26**, 1484–1509.
- [7] Rivest, R., Shamir, A., and Adleman, L. (1978) A method for obtaining digital signatures and public-key cryptosystems. *Communications of the ACM*, **21**, 120–126.
- [8] Landauer, R. (1996) The physical nature of information. *Phys. Lett. A*, **217**, 188–193.
- [9] Ladd, T. D., Jelezko, F., Laflamme, R., Nakamura, Y., Monroe, C., and O’Brien, J. L. (2010) Quantum computers. *Nature*, **464**, 45–53.
- [10] Shor, P. W. (1995) Scheme for reducing decoherence in quantum computer memory. *Phys. Rev. A*, **52**, 2493–2496.
- [11] Steane, A. (1996) Error correcting codes in quantum theory. *Phys. Rev. Lett.*, **77**, 793–797.
- [12] Steane, A. (1996) Multiple-particle interference and quantum error correction. *Proc. R. Soc. A*, **452**, 2551–2577.

-
- [13] Laflamme, R., Miquel, C., Paz, J. P., and Zurek, W. H. (1996) Perfect quantum error correcting code. *Phys. Rev. Lett.*, **77**, 198–201.
- [14] Aharonov, D. and Ben-Or, M. (1997) Fault-tolerant quantum computation with constant error. *Proc. 29th ann. ACM symp. Th. comp.*, pp. 176–188.
- [15] Knill, E. (2005) Quantum computing with realistically noisy devices. *Nature*, **434**, 39–44.
- [16] Singh, S. (1999) *The Code Book: The Secret History of Codes and Code-breaking*. Doubleday.
- [17] Bennett, C. and Brassard, G. (1984) Quantum cryptography: Public key distribution and coin tossing. *Proceedings of IEEE International Conference on Computers, Systems and Signal Processing*, **175**.
- [18] Wootters, W. K. and Zurek, W. H. (1982) A single quantum cannot be cloned. *Nature*, **299**, 802–803.
- [19] Ekert, A. K. (1991) Quantum cryptography based on Bell’s theorem. *Phys. Rev. Lett.*, **67**, 661–663.
- [20] Bell, J. (1964) On the Einstein-Podolsky-Rosen paradox. *Physics*, **1**, 195–200.
- [21] Gisin, N., Ribordy, G., Tittel, W., and Zbinden, H. (2002) Quantum cryptography. *Rev. Mod. Phys.*, **74**, 145–195.
- [22] World premiere: Bank transfer via quantum cryptography based on entangled photons. ”http://www.secoqc.net/downloads/pressrelease/Banktransfer_english.pdf”.
- [23] Id quantique. <http://www.idquantique.com/>.
- [24] Quantum key distribution system (q-box). <http://www.magiqtech.com/MagIQ/Products.html>.
- [25] Peev, M., et al. (2009) The SECOQC quantum key distribution network in vienna. *New J. Phys.*, **11**, 075001.
- [26] Sasaki, M., et al. (2011) Field test of quantum key distribution in the tokyo qkd network. *Opt. Express*, **19**, 10387–10409.
- [27] Brassard, G., Lutkenhaus, N., Mor, T., and Sanders, B. (2000) Limitations on practical quantum cryptography. *Phys. Rev. Lett.*, **85**, 1330–1333.
- [28] Hwang, W.-Y. (2003) Quantum key distribution with high loss: Toward global secure communication. *Phys. Rev. Lett.*, **91**, 057901.

- [29] Lydersen, L., Wiechers, C., Wittmann, C., Elser, D., Skaar, J., and Makarov, V. (2010) Hacking commercial quantum cryptography systems by tailored bright illumination. *Nat. Photon.*, **4**, 686–689.
- [30] Tanaka, A., et al. (2008) Ultra fast quantum key distribution over a 97 km installed telecom fiber with wavelength division multiplexing clock synchronization. *Opt. Express*, **16**, 11354–11360.
- [31] Schmitt-Manderbach, T., et al. (2007) Experimental demonstration of free-space decoy-state quantum key distribution over 144 km. *Phys. Rev. Lett.*, **98**, 010504.
- [32] Patel, K. A., Dynes, J. F., Choi, I., Sharpe, A. W., Dixon, A. R., Yuan, Z. L., Pentz, R. V., and Shields, A. J. (2012) Coexistence of high-bit-rate quantum key distribution and data on optical fiber. *Phys. Rev. X*, **2**, 041010.
- [33] Nauerth, S., Moll, F., Rau, M., Fuchs, C., Horwath, J., Frick, S., and Weinfurter, H. (2013) Air-to-ground quantum communication. *Nat. Photon.*, pp. –.
- [34] Lloyd, S. (1996) Universal quantum simulators. *Science*, **273**, 1073–1078.
- [35] Blatt, R. and Roos, C. F. (2012) Quantum simulations with trapped ions. *Nat. Phys.*, **8**, 277–284.
- [36] Buluta, I. and Nori, F. (2009) Quantum simulators. *Science*, **326**, 108–111.
- [37] Aspuru-Guzik, A. and Walther, P. (2012) Photonic quantum simulators. *Nat. Phys.*, **8**, 285–291.
- [38] of Energy, U. D. (2010), National energy research supercomputing center annual report. <http://www.nersc.gov/assets/Annual-Reports/annrep2010.pdf>.
- [39] Abrams, D. S. and Lloyd, S. (1999) Quantum algorithm providing exponential speed increase for finding eigenvalues and eigenvectors. *Phys. Rev. Lett.*, **83**, 5162–5165.
- [40] Abrams, D. S. and Lloyd, S. (1997) Simulation of many-body fermi systems on a universal quantum computer. *Phys. Rev. Lett.*, **79**, 2586–2589.
- [41] Aspuru-Guzik, A., Dutoi, A. D., Love, P. J., and Head-Gordon, M. (2005) Simulated quantum computation of molecular energies. *Science*, **309**, 1704–1707.
- [42] Whitfield, J. D., Biamonte, J., and Aspuru-Guzik, A. (2011) Simulation of electronic structure hamiltonians using quantum computers. *Molecular Physics*, **109**, 735–750.

- [43] Farhi, E. and Gutmann, S. (1998) Quantum computation and decision trees. *Phys. Rev. A*, **58**, 915–928.
- [44] Perets, H. B., Lahini, Y., Pozzi, F., Sorel, M., Morandotti, R., and Silberberg, Y. (2008) Realization of quantum walks with negligible decoherence in waveguide lattices. *Phys. Rev. Lett.*, **100**, 170506.
- [45] Engel, G. S., Calhoun, T. R., Read, E. L., Ahn, T.-K., Mancal, T., Cheng, Y.-C., Blankenship, R. E., and Fleming, G. R. (2007) Evidence for wavelike energy transfer through quantum coherence in photosynthetic systems. *Nature*, **446**, 782–786.
- [46] Collini, E., Wong, C. Y., Wilk, K. E., Curmi, P. M. G., Brumer, P., and Scholes, G. D. (2010) Coherently wired light-harvesting in photosynthetic marine algae at ambient temperature. *Nature*, **463**, 644–647.
- [47] Panitchayangkoon, G., Hayes, D., Fransted, K. A., Caram, J. R., Harel, E., Wen, J., Blankenship, R. E., and Engel, G. S. (2010) Long-lived quantum coherence in photosynthetic complexes at physiological temperature. *Proceedings of the National Academy of Sciences*, **107**, 12766–12770.
- [48] Ma, X.-s., Dakic, B., Naylor, W., Zeilinger, A., and Walther, P. (2011) Quantum simulation of the wavefunction to probe frustrated heisenberg spin systems. *Nat. Phys.*, **7**, 399–405.
- [49] DiVincenzo, D. P. (1995) 2-bit gates are universal for quantum computation. *Phys. Rev. A*, **51**, 1015–1022.
- [50] DiVincenzo, D. P. (2000) The physical implementation of quantum computation. *Fortschritte der Physik*, **48**, 771–783.
- [51] Farhi, E., Goldstone, J., Gutmann, S., and Sipser, M. (2000) Quantum computation by adiabatic evolution. *arXiv:quant-ph/0001106*.
- [52] Mizel, A., Lidar, D. A., and Mitchell, M. (2007) Simple proof of equivalence between adiabatic quantum computation and the circuit model. *Phys. Rev. Lett.*, **99**, 070502.
- [53] Biamonte, J. D. and Love, P. J. (2008) Realizable hamiltonians for universal adiabatic quantum computers. *Phys. Rev. A*, **78**, 012352.
- [54] Jozsa, R. (2005) An introduction to measurement based quantum computation. *arXiv:quant-ph/0508124*.
- [55] Raussendorf, R. and Briegel, H. (2001) A one-way quantum computer. *Phys. Rev. Lett.*, **86**, 5188–5191.
- [56] Daniel Gottesman, I. L. C. (1999) Quantum teleportation is a universal computational primitive. *Nature*, **402**, 390–393.

- [57] Raussendorf, R., Browne, D. E., and Briegel, H. J. (2003) Measurement-based quantum computation on cluster states. *Phys. Rev. A*, **68**, 022312.
- [58] den Nest, M. V., Duer, W., Miyake, A., and Briegel, H. J. (2007) Fundamentals of universality in one-way quantum computation. *New J. Phys.*, **9**, 204.
- [59] Kitaev, A. (2003) Fault-tolerant quantum computation by anyons. *Annals of Physics*, **303**, 2–30.
- [60] Kitaev, A. Y. (1997) Quantum computations: algorithms and error correction. *Russian Math. Surveys*, **52**, 1191–1249.
- [61] Bravyi, S. B. and Kitaev, A. Y. (1998) Quantum codes on a lattice with boundary. *arXiv:quant-ph/9811052*.
- [62] Freedman, M. H. and Meyer, D. A. (2001) Projective plane and planar quantum codes. *Foundations of Computational Mathematics*, **1**, 325–332.
- [63] Wang, C., Harrington, J., and Preskill, J. (2003) Confinement-higgs transition in a disordered gauge theory and the accuracy threshold for quantum memory. *Annals of Physics*, **303**, 31–58.
- [64] Raussendorf, R. and Harrington, J. (2007) Fault-tolerant quantum computation with high threshold in two dimensions. *Phys. Rev. Lett.*, **98**, 190504.
- [65] Raussendorf, R., Harrington, J., and Goyal, K. (2007) Topological fault-tolerance in cluster state quantum computation. *New J. Phys.*, **9**, 199.
- [66] Fowler, A. G., Whiteside, A. C., McInnes, A. L., and Rabbani, A. (2012) Topological code autotune. *Phys. Rev. X*, **2**, 041003.
- [67] Duclos-Cianci, G. and Poulin, D. (2010) Fast decoders for topological quantum codes. *Phys. Rev. Lett.*, **104**, 050504.
- [68] Duclos-Cianci, G. and Poulin, D. (2010) A renormalization group decoding algorithm for topological quantum codes. *Information Theory Workshop (ITW), 2010 IEEE*, pp. 1–5.
- [69] Wootton, J. R. and Loss, D. (2012) High threshold error correction for the surface code. *Phys. Rev. Lett.*, **109**, 160503.
- [70] Einstein, A., Podolsky, B., and Rosen, N. (1935) Can quantum-mechanical description of physical reality be considered complete? *Phys. Rev.*, **47**, 777–780.
- [71] Bennett, C. H., Bernstein, H. J., Popescu, S., and Schumacher, B. (1996) Concentrating partial entanglement by local operations. *Phys. Rev. A*, **53**, 2046–2052.

- [72] Denchev, V. S. and Pandurangan, G. (2008) Distributed quantum computing: a new frontier in distributed systems or science fiction? *SIGACT News*, **39**, 77–95.
- [73] Cabrillo, C., Cirac, J., Garcia-Fernandez, P., and Zoller, P. (1999) Creation of entangled states of distant atoms by interference. *Phys. Rev. A*, **59**, 1025–1033.
- [74] Duan, L.-M. and Kimble, H. J. (2003) Efficient engineering of multiatom entanglement through single-photon detections. *Phys. Rev. Lett.*, **90**, 253601.
- [75] Feng, X.-L., Zhang, Z.-M., Li, X.-D., Gong, S.-Q., and Xu, Z.-Z. (2003) Entangling distant atoms by interference of polarized photons. *Phys. Rev. Lett.*, **90**, 217902.
- [76] Barrett, S. D. and Kok, P. (2005) Efficient high-fidelity quantum computation using matter qubits and linear optics. *Phys. Rev. A*, **71**, 060310.
- [77] Lim, Y. L., Beige, A., and Kwek, L. C. (2005) Repeat-until-success linear optics distributed quantum computing. *Phys. Rev. Lett.*, **95**, 030505.
- [78] Moehring, D. L., Maunz, P., Olmschenk, S., Young, K. C., Matsukevich, D. N., Duan, L.-M., and Monroe, C. (2007) Entanglement of single-atom quantum bits at a distance. *Nature*, **449**, 68–71.
- [79] Pfaff, W., Taminiau, T. H., Robledo, L., Bernien, H., Markham, M., Twitchen, D. J., and Hanson, R. (2013) Demonstration of entanglement-by-measurement of solid-state qubits. *Nat. Phys.*, **9**, 29–33.
- [80] Benjamin, S. C., Browne, D. E., Fitzsimons, J., and Morton, J. J. L. (2006) Brokered graph-state quantum computation. *New J. Phys.*, **8**, 141.
- [81] Gershenfeld, N. A. and Chuang, I. L. (1997) Bulk spin-resonance quantum computation. *Science*, **275**, 350–356.
- [82] Chuang, I., Vandersypen, L., Zhou, X., Leung, D., and Lloyd, S. (1998) Experimental realization of a quantum algorithm. *Nature*, **393**, 143–146.
- [83] Vandersypen, L., Steffen, M., Breyta, G., Yannoni, C., Sherwood, M., and Chuang, I. (2001) Experimental realization of Shor’s quantum factoring algorithm using nuclear magnetic resonance. *Nature*, **414**, 883–887.
- [84] Braunstein, S., Caves, C., Jozsa, R., Linden, N., Popescu, S., and Schack, R. (1999) Separability of very noisy mixed states and implications for NMR quantum computing. *Phys. Rev. Lett.*, **83**, 1054–1057.
- [85] Xu, N., Zhu, J., Lu, D., Zhou, X., Peng, X., and Du, J. (2012) Quantum factorization of 143 on a dipolar-coupling nuclear magnetic resonance system. *Phys. Rev. Lett.*, **108**, 130501.

- [86] Kane, B. E. (1998) A silicon-based nuclear spin quantum computer. *Nature*, **393**, 133–137.
- [87] Simmons, S., Brown, R., Riemann, H., Abrosimov, N., Becker, P., Pohl, H., Thewalt, M., Itoh, K., and Morton, J. (2011) Entanglement in a solid-state spin ensemble. *Nature*, **470**, 69–72.
- [88] Morello, A., et al. (2010) Single-shot readout of an electron spin in silicon. *Nature*, **467**, 687–691.
- [89] Pla, J. J., Tan, K. Y., Dehollain, J. P., Lim, W. H., Morton, J. J. L., Jamieson, D. N., Dzurak, A. S., and Morello, A. (2012) A single-atom electron spin qubit in silicon. *Nature*, **489**, 541–545.
- [90] Tyryshkin, A. M., et al. (2012) Electron spin coherence exceeding seconds in high-purity silicon. *Nat. Mater.*, **11**, 143–147.
- [91] Cirac, J. I. and Zoller, P. (1995) Quantum computations with cold trapped ions. *Phys. Rev. Lett.*, **74**, 4091–4094.
- [92] Monroe, C., Meekhof, D. M., King, B. E., Itano, W. M., and Wineland, D. J. (1995) Demonstration of a fundamental quantum logic gate. *Phys. Rev. Lett.*, **75**, 4714–4717.
- [93] Wineland, D., Monroe, C., Itano, W. M., Leibfried, D., King, B. E., and Meekhof, D. M. (1998) Experimental issues in coherent quantum-state manipulation of trapped atomic ions. *J. Res. Natl. Inst. Stand. Technol.*, **103**, 259–328.
- [94] Gulde, S., Riebe, M., Lancaster, G., Becher, C., Eschner, J., Haffner, H., Schmidt-Kaler, F., Chuang, I., and Blatt, R. (2003) Implementation of the deutsch-jozsa algorithm on an ion-trap quantum computer. *Nature*, **421**, 48–50.
- [95] Leibfried, D., et al. (2002) Trapped-ion quantum simulator: Experimental application to nonlinear interferometers. *Phys. Rev. Lett.*, **89**, 247901.
- [96] Monz, T., Schindler, P., Barreiro, J. T., Chwalla, M., Nigg, D., Coish, W. A., Harlander, M., Hänsel, W., Hennrich, M., and Blatt, R. (2011) 14-qubit entanglement: Creation and coherence. *Phys. Rev. Lett.*, **106**, 130506.
- [97] Lanyon, B. P., et al. (2011) Universal digital quantum simulation with trapped ions. *Science*, **334**, 57–61.
- [98] Barreiro, J. T., Muller, M., Schindler, P., Nigg, D., Monz, T., Chwalla, M., Hennrich, M., Roos, C. F., Zoller, P., and Blatt, R. (2011) An open-system quantum simulator with trapped ions. *Nature*, **470**, 486–491.

- [99] Stick, D., Hensinger, W., Olmschenk, S., Madsen, M., Schwab, K., and Monroe, C. (2006) Ion trap in a semiconductor chip. *Nat. Phys.*, **2**, 36–39.
- [100] Britton, J. W., Sawyer, B. C., Keith, A. C., Wang, C. C. J., Freericks, J. K., Uys, H., Biercuk, M. J., and Bollinger, J. J. (2012) Engineered two-dimensional ising interactions in a trapped-ion quantum simulator with hundreds of spins. *Nature*, **484**, 489–492.
- [101] Kroutvar, M., Ducommun, Y., Heiss, D., Bichler, M., Schuh, D., Abstreiter, G., and Finley, J. (2004) Optically programmable electron spin memory using semiconductor quantum dots. *Nature*, **432**, 81–84.
- [102] Greilich, A., Yakovlev, D. R., Shabaev, A., Efros, A. L., Yugova, I. A., Oulton, R., Stavarache, V., Reuter, D., Wieck, A., and Bayer, M. (2006) Mode locking of electron spin coherences in singly charged quantum dots. *Science*, **313**, 341–345.
- [103] Burkard, G., Loss, D., and DiVincenzo, D. (1999) Coupled quantum dots as quantum gates. *Phys. Rev. B*, **59**, 2070–2078.
- [104] Li, X., Wu, Y., Steel, D., Gammon, D., Stievater, T., Katzer, D., Park, D., Piermarocchi, C., and Sham, L. (2003) An all-optical quantum gate in a semiconductor quantum dot. *Science*, **301**, 809–811.
- [105] Calarco, T., Datta, A., Fedichev, P., Pazy, E., and Zoller, P. (2003) Spin-based all-optical quantum computation with quantum dots: Understanding and suppressing decoherence. *Phys. Rev. A*, **68**, 012310.
- [106] Chen, G., Bonadeo, N., Steel, D., Gammon, D., Katzer, D., Park, D., and Sham, L. (2000) Optically induced entanglement of excitons in a single quantum dot. *Science*, **289**, 1906–1909.
- [107] Yokoi, T., Adachi, S., Sasakura, H., Muto, S., Song, H., Usuki, T., and Hirose, S. (2005) Polarization-dependent shift in excitonic Zeeman splitting of self-assembled In_{0.75}Al_{0.25}As/Al_{0.3}Ga_{0.7}As quantum dots. *Phys. Rev. B*, **71**, 041307.
- [108] Atatüre, M., Dreiser, J., Badolato, A., Högele, A., Karrai, K., and Imamoglu, A. (2006) Quantum-dot spin-state preparation with near-unity fidelity. *Science*, **312**, 551–553.
- [109] Gerardot, B. D., Brunner, D., Dalgarno, P. A., Ohberg, P., Seidl, S., Kroner, M., Karrai, K., Stoltz, N. G., Petroff, P. M., and Warburton, R. J. (2008) Optical pumping of a single hole spin in a quantum dot. *Nature*, **451**, 441–444.

- [110] Press, D., Ladd, T. D., Zhang, B., and Yamamoto, Y. (2008) Complete quantum control of a single quantum dot spin using ultrafast optical pulses. *Nature*, **456**, 218–221.
- [111] Berezovsky, J., Mikkelsen, M. H., Gywat, O., Stoltz, N. G., Coldren, L. A., and Awschalom, D. D. (2006) Nondestructive optical measurements of a single electron spin in a quantum dot. *Science*, **314**, 1916–1920.
- [112] Hu, Y., Kuemmeth, F., Lieber, C. M., and Marcus, C. M. (2012) Hole spin relaxation in ge-si core-shell nanowire qubits. *Nat. Nano.*, **7**, 47–50.
- [113] Kok, P., Munro, W. J., Nemoto, K., Ralph, T. C., Dowling, J. P., and Milburn, G. J. (2007) Linear optical quantum computing with photonic qubits. *Rev. Mod. Phys.*, **79**, 797.
- [114] Fox, A. M. (2006) *Quantum Optics: An Introduction*. Oxford University Press.
- [115] Walls, D. and Milburn, G. (2008) *Quantum Optics*. Springer, 2 edn.
- [116] Shapiro, J. H. (2006) Single-photon Kerr nonlinearities do not help quantum computation. *Phys. Rev. A*, **73**, 062305.
- [117] Knill, E., Laflamme, R., and Milburn, G. (2001) A scheme for efficient quantum computation with linear optics. *Nature*, **409**, 46–52.
- [118] O’Brien, J. L. (2007) Optical quantum computing. *Science*, **318**, 1567–1570.
- [119] Politi, A., Matthews, J. C. F., and O’Brien, J. L. (2009) Shor’s quantum factoring algorithm on a photonic chip. *Science*, **325**, 1221.
- [120] Martin-Lopez, E., Laing, A., Lawson, T., Alvarez, R., Zhou, X.-Q., and O’Brien, J. L. (2012) Experimental realization of Shor’s quantum factoring algorithm using qubit recycling. *Nat. Photon.*, **6**, 773–776.
- [121] Hadfield, R. H. (2009) Single-photon detectors for optical quantum information applications. *Nat. Photon.*, **3**, 696–705.
- [122] Grangier, P., Sanders, B., and Vuckovic, J. (2004) Focus on single photons on demand. *New J. Phys.*, **6**.
- [123] Kok, P. and Lovett, B. W. (2006) Materials science - qubits in the pink. *Nature*, **444**, 49–49.
- [124] Jelezko, F., Gaebel, T., Popa, I., Gruber, A., and Wrachtrup, J. (2004) Observation of coherent oscillations in a single electron spin. *Phys. Rev. Lett.*, **92**, 076401.

- [125] van der Sar, T., Wang, Z. H., Blok, M. S., Bernien, H., Taminiau, T. H., Toyli, D. M., Lidar, D. A., Awschalom, D. D., Hanson, R., and Dobrovitski, V. V. (2012) Decoherence-protected quantum gates for a hybrid solid-state spin register. *Nature*, **484**, 82–86.
- [126] Dolde, F., Jakobi, I., Naydenov, B., Zhao, N., Pezzagna, S., Trautmann, C., Meijer, J., Neumann, P., Jelezko, F., and Wrachtrup, J. (2013) Room-temperature entanglement between single defect spins in diamond. *Nat. Phys.*, **9**, 139–143.
- [127] Bernien, H., et al. (2012) Heralded entanglement between solid-state qubits separated by 3 meters. *arXiv:1212.6136*.
- [128] Steffen, M. (2011) Superconducting qubits are getting serious. *Physics*, **4**, 103.
- [129] Josephson, B. D. (1974) The discovery of tunnelling supercurrents. *Rev. Mod. Phys.*, **46**, 251–254.
- [130] Nakamura, Y., Pashkin, Y. A., and Tsai, J. S. (1999) Coherent control of macroscopic quantum states in a single-cooper-pair box. *Nature*, **398**, 786–788.
- [131] Chiorescu, I., Nakamura, Y., Harmans, C. J. P. M., and Mooij, J. E. (2003) Coherent quantum dynamics of a superconducting flux qubit. *Science*, **299**, 1869–1871.
- [132] Ansmann, M., et al. (2009) Violation of Bell’s inequality in Josephson phase qubits. *Nature*, **461**, 504–506.
- [133] DiCarlo, L., Reed, M. D., Sun, L., Johnson, B. R., Chow, J. M., Gambetta, J. M., Frunzio, L., Girvin, S. M., Devoret, M. H., and Schoelkopf, R. J. (2010) Preparation and measurement of three-qubit entanglement in a superconducting circuit. *Nature*, **467**, 574–578.
- [134] DiCarlo, L., et al. (2009) Demonstration of two-qubit algorithms with a superconducting quantum processor. *Nature*, **460**, 240–244.
- [135] Paik, H., et al. (2011) Observation of high coherence in Josephson junction qubits measured in a three-dimensional circuit qed architecture. *Phys. Rev. Lett.*, **107**, 240501.
- [136] Johnson, M. W., et al. (2011) Quantum annealing with manufactured spins. *Nature*, **473**, 194–198.
- [137] Nielsen, M. A. and Chuang, I. L. (2000) *Quantum Computation and Quantum Information*. Cambridge University Press.
- [138] Peres, A. (1990) Neumark’s theorem and quantum inseparability. *Foundations of Physics*, **20**, 1441–1453.

-
- [139] Lindblad, G. (1976) On the generators of quantum dynamical semigroups. *Commun. Math. Phys.*, **48**, 119–130.
- [140] Brun, T. (2002) A simple model of quantum trajectories. *Am. J. Phys.*, **70**, 719–737.
- [141] Kok, P. and Lovett, B. W. (2010) *Introduction to Optical Quantum Information Processing*. Cambridge University Press.
- [142] Breuer, H. P. and Petruccione, F. (2002) *The Theory of Open Quantum Systems*. Oxford University Press.
- [143] Einstein, A. (1905) Über einen die erzeugung und verwandlung des liches betreffenden heuristischen gesichtspunkt. *Annalen der Physik*, **322**, 132–148.
- [144] Planck, M. (1901) Ueber das gesetz der energieverteilung im normalspectrum. *Annalen der Physik*, **309**, 553–563.
- [145] Dirac, P. A. M. (1927) The quantum theory of the emission and absorption of radiation. *Proc. R. Soc. A*, **114**, 243–265.
- [146] Garrison, J. and Chiao, R. (2008) *Quantum Optics*. Oxford University Press.
- [147] Mahan, G. D. (2000) *Many Particle Physics (Physics of Solids and Liquids)*. Springer, 3rd edn.
- [148] Gardiner, C. and Zoller, P. (2004) *Quantum Noise: A Handbook of Markovian and Non-Markovian Quantum Stochastic Methods with Applications to Quantum Optics*. Springer.
- [149] Pazy, E. (2002) Calculation of pure dephasing for excitons in quantum dots. *Semiconductor Science and Technology*, **17**, 1172.
- [150] P., C., Wernsdorfer W., Bouchiat V., Ondarcuhu T., and Monthieux M. (2006) Carbon nanotube superconducting quantum interference device. *Nat. Nano.*, **1**, 53–59.
- [151] Neumann, P., Beck, J., Steiner, M., Rempp, F., Fedder, H., Hemmer, P. R., Wrachtrup, J., and Jelezko, F. (2010) Single-shot readout of a single nuclear spin. *Science*, **329**, 542–544.
- [152] Vamivakas, A. N., Lu, C. Y., Matthiesen, C., Zhao, Y., Falt, S., Badolato, A., and Atatüre, M. (2010) Observation of spin-dependent quantum jumps via quantum dot resonance fluorescence. *Nature*, **467**, 297–300.
- [153] Berezovsky, J., Mikkelsen, M. H., Stoltz, N. G., Coldren, L. A., and Awschalom, D. D. (2008) Picosecond coherent optical manipulation of a single electron spin in a quantum dot. *Science*, **320**, 349–352.

-
- [154] Leibfried, D., Blatt, R., Monroe, C., and Wineland, D. (2003) Quantum dynamics of single trapped ions. *Rev. Mod. Phys.*, **75**, 281–324.
- [155] Hanson, R., Kouwenhoven, L. P., Petta, J. R., Tarucha, S., and Vandersypen, L. M. K. (2007) Spins in few-electron quantum dots. *Rev. Mod. Phys.*, **79**, 1217–1265.
- [156] Morton, J. J. L. and Lovett, B. W. (2011) Hybrid solid-state qubits: The powerful role of electron spins. *Annual Review of Condensed Matter Physics*, **2**, 189–212.
- [157] Lee, J.-S. and Khitrin, A. (2005) Stimulated wave of polarization in a one-dimensional ising chain. *Phys. Rev. A*, **71**, 062338.
- [158] Perez-Delgado, C. A., Mosca, M., Cappellaro, P., and Cory, D. G. (2006) Single spin measurement using cellular automata techniques. *Phys. Rev. Lett.*, **97**, 100501.
- [159] Stanley, R. P. (1975) Fibonacci lattice. *Fibonacci Quart*, **13**, 215–232.
- [160] Sagan, B. (2001) The symmetric group: representations, combinatorial algorithms, and symmetric functions. *Springer*, pp. 191–197.
- [161] Fitzsimons, J. and Twamley, J. (2005) Superballistic diffusion of entanglement in disordered spin chains. *Phys. Rev. A*, **72**, 050301.
- [162] Farhi, E. and Gutmann, S. (1998) Quantum computation and decision trees. *Phys. Rev. A*, **58**, 915–928.
- [163] Knill, E., Laflamme, R., and Milburn, G. J. (2001) A scheme for efficient quantum computation with linear optics. *Nature*, **409**, 46–52.
- [164] Kok, P., Munro, W. J., Nemoto, K., Ralph, T. C., Dowling, J. P., and Milburn, G. J. (2007) Linear optical quantum computing with photonic qubits. *Rev. Mod. Phys.*, **79**, 797.
- [165] Kok, P. and Lovett, B. W. (2010) *Introduction to Optical Quantum Information Processing*. Cambridge University Press.
- [166] Bose, S., Knight, P. L., Plenio, M. B., and Vedral, V. (1999) Proposal for teleportation of an atomic state via cavity decay. *Phys. Rev. Lett.*, **83**, 5158.
- [167] Simon, C. and Irvine, W. T. M. (2003) Robust long-distance entanglement and a loophole-free bell test with ions and photons. *Phys. Rev. Lett.*, **91**, 110405.
- [168] Lim, Y. L., Beige, A., and Kwek, L. C. (2005) Repeat-until-success quantum computing. *Phys. Rev. Lett.*, **95**, 030505.

- [169] Raussendorf, R. and Briegel, H. J. (2001) A one-way quantum computer. *Phys. Rev. Lett.*, **86**, 5188.
- [170] Hong, C. K., Ou, Z. Y., and Mandel, L. (1987) Measurement of subpicosecond time intervals between two photons by interference. *Phys. Rev. Lett.*, **59**, 2044–2046.
- [171] Lounis, B. and Orrit, M. (2005) Single photon sources. *Rep. Prog. Phys.*, **68**, 1129.
- [172] Kuhn, A., Hennrich, M., and Rempe, G. (2002) Deterministic single-photon source for distributed quantum networking. *Phys. Rev. Lett.*, **89**, 067901.
- [173] McKeever, J., Boca, A., Boozer, A. D., Miller, R., Buck, J. R., Kuzmich, A., and Kimble, H. J. (2004) Deterministic generation of single photons from one atom trapped in a cavity. *Science*, **303**, 1992–1994.
- [174] Darquie, B., Jones, M. P. A., Dingjan, J., Beugnon, J., Bergamini, S., Sortais, Y., Messin, G., Browaeys, A., and Grangier, P. (2005) Controlled single-photon emission from a single trapped two-level atom. *Science*, **309**, 454–456.
- [175] Hijlkema, M., Weber, B., Specht, H. P., Webster, S. C., Kuhn, A., and Rempe, G. (2007) A single-photon server with just one atom. *Nat. Phys.*, **3**, 253–255.
- [176] Kako, S., Santori, C., Hoshino, K., Gotzinger, S., Yamamoto, Y., and Arakawa, Y. (2006) A gallium nitride single-photon source operating at 200 k. *Nat. Mater.*, **5**, 887–892.
- [177] Hennessy, K., Badolato, A., Winger, M., Gerace, D., Atature, M., Gulde, S., Falt, S., Hu, E. L., and Imamoglu, A. (2007) Quantum nature of a strongly coupled single quantum dot-cavity system. *Nature*, **445**, 896–899.
- [178] Wu, E., Rabeau, J. R., Roger, G., Treussart, F., Zeng, H., Grangier, P., Praver, S., and Roch, J.-F. (2007) Room temperature triggered single-photon source in the near infrared. *New J. Phys.*, **9**, 434.
- [179] Bernien, H., Childress, L., Robledo, L., Markham, M., Twitchen, D., and Hanson, R. (2012) Two-photon quantum interference from separate nitrogen vacancy centers in diamond. *Phys. Rev. Lett.*, **108**, 043604.
- [180] Sipahigil, A., Goldman, M. L., Togan, E., Chu, Y., Markham, M., Twitchen, D. J., Zibrov, A. S., Kubanek, A., and Lukin, M. D. (2012) Quantum interference of single photons from remote nitrogen-vacancy centers in diamond. *Phys. Rev. Lett.*, **108**, 143601.
- [181] Flagg, E. B., Muller, A., Polyakov, S. V., Ling, A., Migdall, A., and Solomon, G. S. (2010) Interference of single photons from two separate semiconductor quantum dots. *Phys. Rev. Lett.*, **104**, 137401.

- [182] Patel, R. B., Bennett, A. J., Farrer, I., Nicoll, C. A., Ritchie, D. A., and Shields, A. J. (2010) Two-photon interference of the emission from electrically tunable remote quantum dots. *Nat. Photon.*, **4**, 632–635.
- [183] Su, C.-H., Greentree, A. D., and Hollenberg, L. C. L. (2008) Towards a picosecond transform-limited nitrogen-vacancy based single photon source. *Opt. Express*, **16**, 6240–6250.
- [184] Kiraz, A., Atatüre, M., and Imamoglu, A. (2004) Quantum-dot single-photon sources: Prospects for applications in linear optics quantum-information processing. *Phys. Rev. A*, **69**, 032305.
- [185] Santori, C., Fattal, D., Fu, K.-M. C., Barclay, P. E., and Beausoleil, R. G. (2009) On the indistinguishability of raman photons. *New J. Phys.*, **11**, 123009.
- [186] Nazir, A. and Barrett, S. D. (2009) Overcoming non-markovian dephasing in single-photon sources through postselection. *Phys. Rev. A*, **79**, 011804.
- [187] Purcell, E. M. (1946) Long lived coherence in self-assembled quantum dots. *Phys. Rev.*, **69**, 681.
- [188] Englund, D., Fattal, D., Waks, E., Solomon, G., Zhang, B., Nakaoka, T., Arakawa, Y., Yamamoto, Y., and Vučković, J. (2005) Controlling the spontaneous emission rate of single quantum dots in a two-dimensional photonic crystal. *Phys. Rev. Lett.*, **95**, 013904.
- [189] Auffèves, A., Gerace, D., Gérard, J.-M., Santos, M. F. m. c., Andreani, L. C., and Poizat, J.-P. (2010) Controlling the dynamics of a coupled atom-cavity system by pure dephasing. *Phys. Rev. B*, **81**, 245419.
- [190] Ramsay, A. J., Gopal, A. V., Gauger, E. M., Nazir, A., Lovett, B. W., Fox, A. M., and Skolnick, M. S. (2010) Damping of exciton rabi rotations by acoustic phonons in optically excited InGaAs/GaAs quantum dots. *Phys. Rev. Lett.*, **104**, 017402.
- [191] Mahan, G. D. (2000) *Many Particle Physics (Physics of Solids and Liquids)*. Springer, 3rd edn.
- [192] Gauger, E. M., Benjamin, S. C., Nazir, A., and Lovett, B. W. (2008) High-fidelity all-optical control of quantum dot spins: Detailed study of the adiabatic approach. *Phys. Rev. B*, **77**, 115322.
- [193] Gauger, E. M. and Wabnig, J. (2010) Heat pumping with optically driven excitons. *Phys. Rev. B*, **82**, 1–4.
- [194] Breuer, H. P. and Petruccione, F. (2002) *The Theory of Open Quantum Systems*. Oxford University.

-
- [195] Ramsay, A. J., Godden, T., Boyle, S. J., Gauger, E. M., Nazir, A., Lovett, B. W., Fox, A. M., and Skolnick, M. S. (2010) Phonon-Induced Rabi-Frequency Renormalization of Optically Driven Single InGaAs/GaAs Quantum Dots. *Phys. Rev. Lett.*, **105**, 177402.
- [196] Kaer, P., Lodahl, P., Jauho, A.-P., and Mork, J. (2012) Microscopic theory of indistinguishable single-photon emission from a quantum dot coupled to a cavity: The role of non-markovian phonon-induced decoherence. <http://arxiv.org/abs/1203.6268>.
- [197] Tian, L. and Carmichael, H. J. (1992) Quantum trajectory simulations of two-state behavior in an optical cavity containing one atom. *Phys. Rev. A*, **46**, R6801–R6804.
- [198] Majumdar, A., Englund, D., Bajcsy, M., and Vučković, J. (2012) Nonlinear temporal dynamics of a strongly coupled quantum-dot-cavity system. *Phys. Rev. A*, **85**, 033802.
- [199] Wang, D. S., Fowler, A. G., and Hollenberg, L. C. L. (2011) Surface code quantum computing with error rates over 10^2 to 10^3 .
- [200] Fowler, A. G., Whiteside, A. C., and Hollenberg, L. C. L. (2012) Towards practical classical processing for the surface code. *Phys. Rev. Lett.*, **108**, 180501.
- [201] Svore, K. M., Divincenzo, D. P., and Terhal, B. M. (2007) Noise threshold for a fault-tolerant two-dimensional lattice architecture. *Quantum Info. Comput.*, **7**, 297–318.
- [202] http://github.com/TomClose/mcmc_code.